A M A Z O N I A

CREAR

CREAR AMAZONÍA

Center for Research and Education of the Amazonian Rainforest www.crearamazonia.org

MODELACION NUMERICA DEL TRANSPORTE DE SEDIMENTOS → MORFOLOGIA

Jorge D. Abad[1] & Alejandro Mendoza

[1]*Assistant Professor*
http://www.pitt.edu/~jabad/

Director for Research and Education, CREAR
Dept. of Civil and Environmental Engineering (CEE)
Dept. of Geology and Planetary Science (GPS)
University of Pittsburgh, USA

Collaborators:
@ University of Pittsburgh:
- *Center for Latin American Studies (CLAS)*
- *Alejandro Mendoza (Postdoc)*
- *Christian Frias, Ronald Gutierrez, Kristin Dauer (G)*
- *Adrian Garcia, Brian Hone, Collin Ortals (UG)*

IV SEMINARIO INTERNACIONAL DE POTAMOLOGÍA "JOSÉ ANTONIO MAZA ÁLVAREZ"

Σ ([1] + [2] + [3] +[4]+...) = RIVER DYNAMICS

[1]PLANFORM DYNAMICS

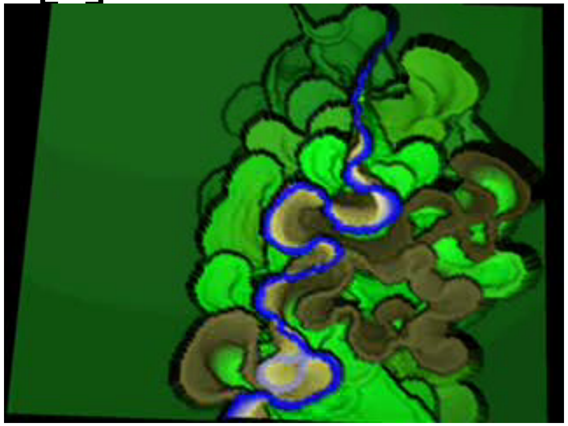

[2]BED MORPHOLOGY

[3]SEDIMENT TRANSPORT

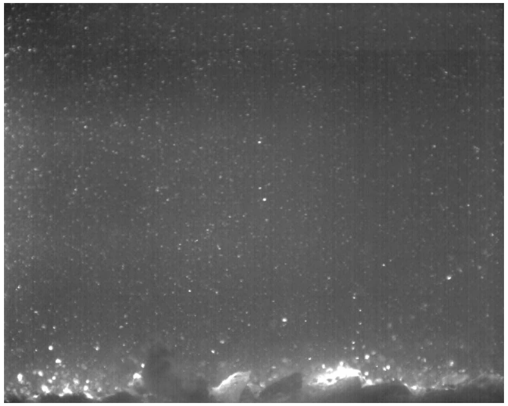

[4]FLUID MOTION

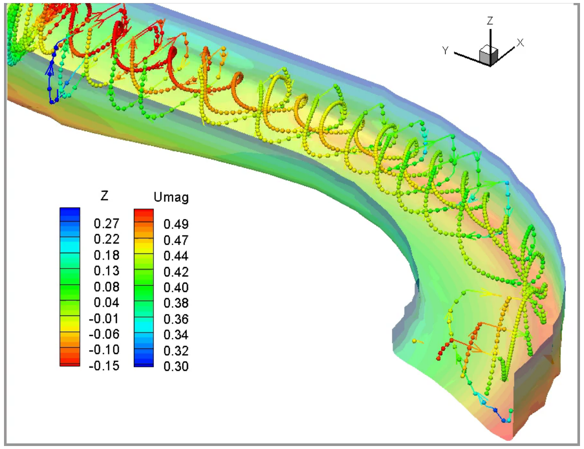

Mean and fluctuating velocities

- **Turbulence originates from the instability of laminar flows**
- **The parameter that plays the most important role in this process is the Reynolds number**

$$\mathrm{Re} = \frac{U\,H}{\nu}$$

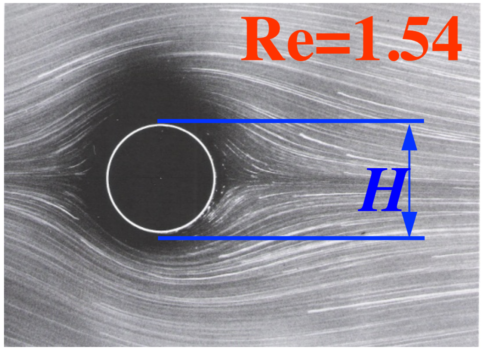

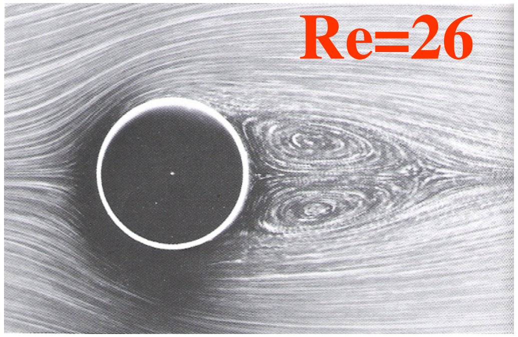

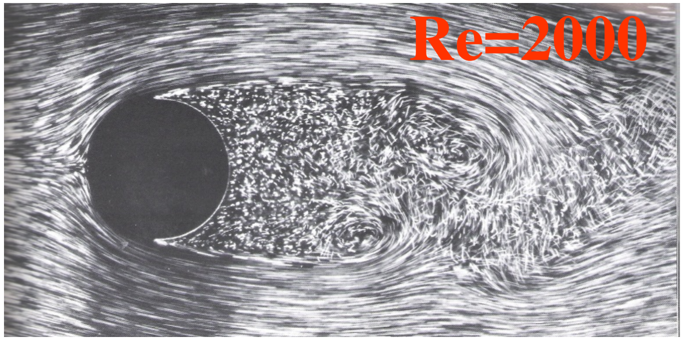

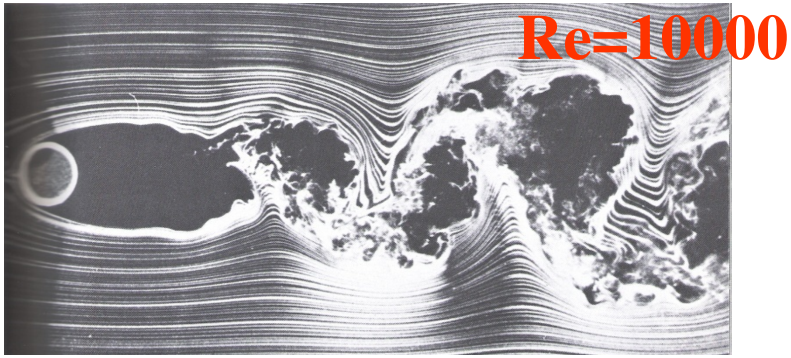

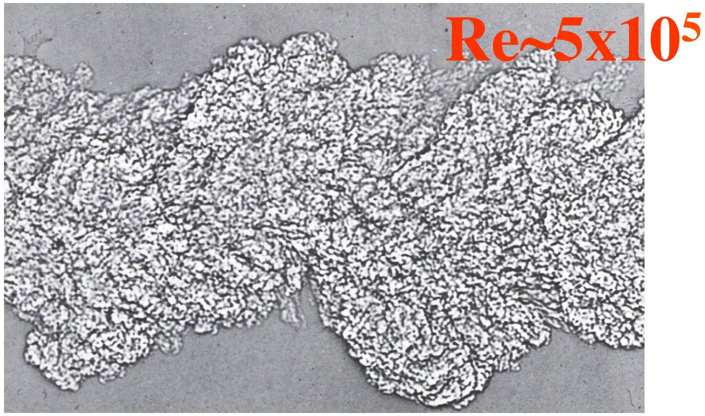

Turbulence modeling

- **We can think of turbulence as a**
  - Collection of eddies flowing
  - Largest eddies of size *L* and smallest eddies of size h
  - Eddies interact in a very complex manner
  - This interaction happens in a self-similar way

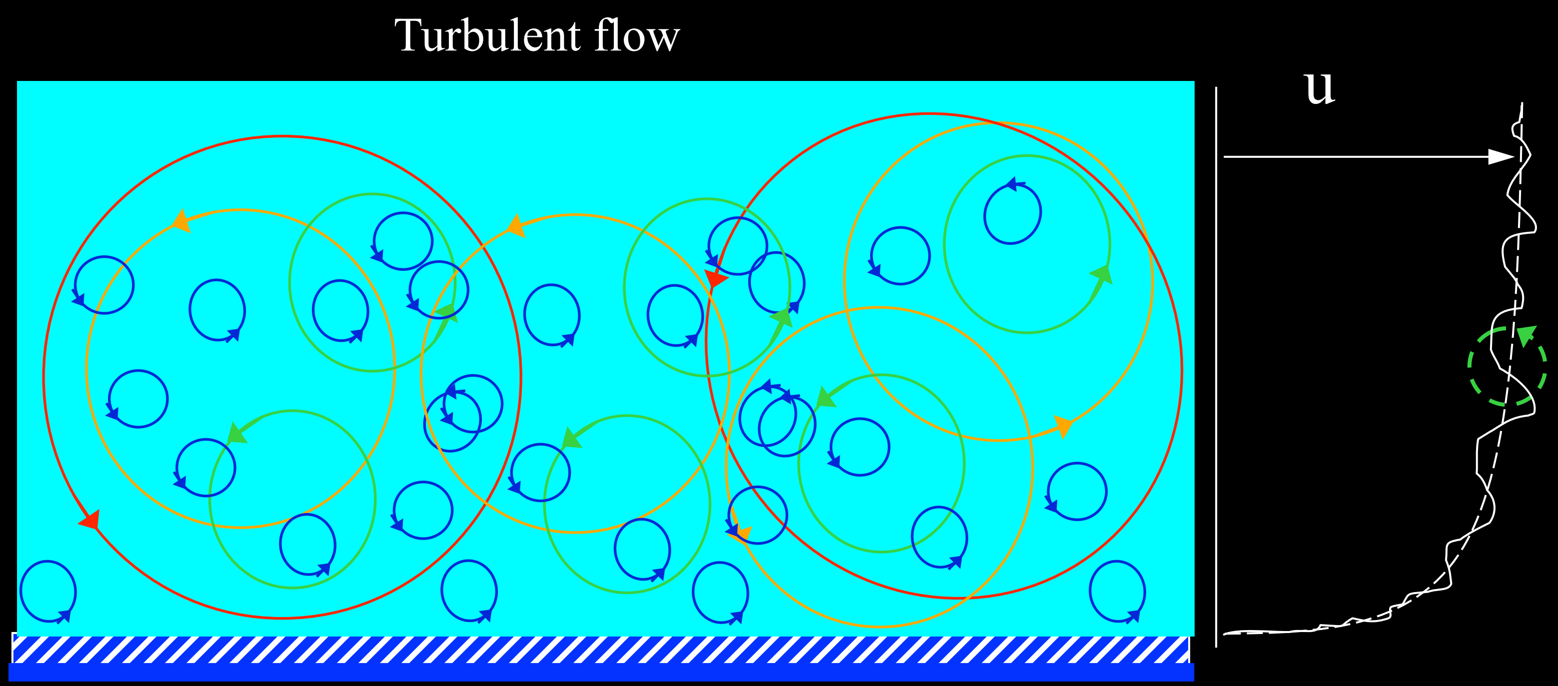

Measuring mean and turbulent flow

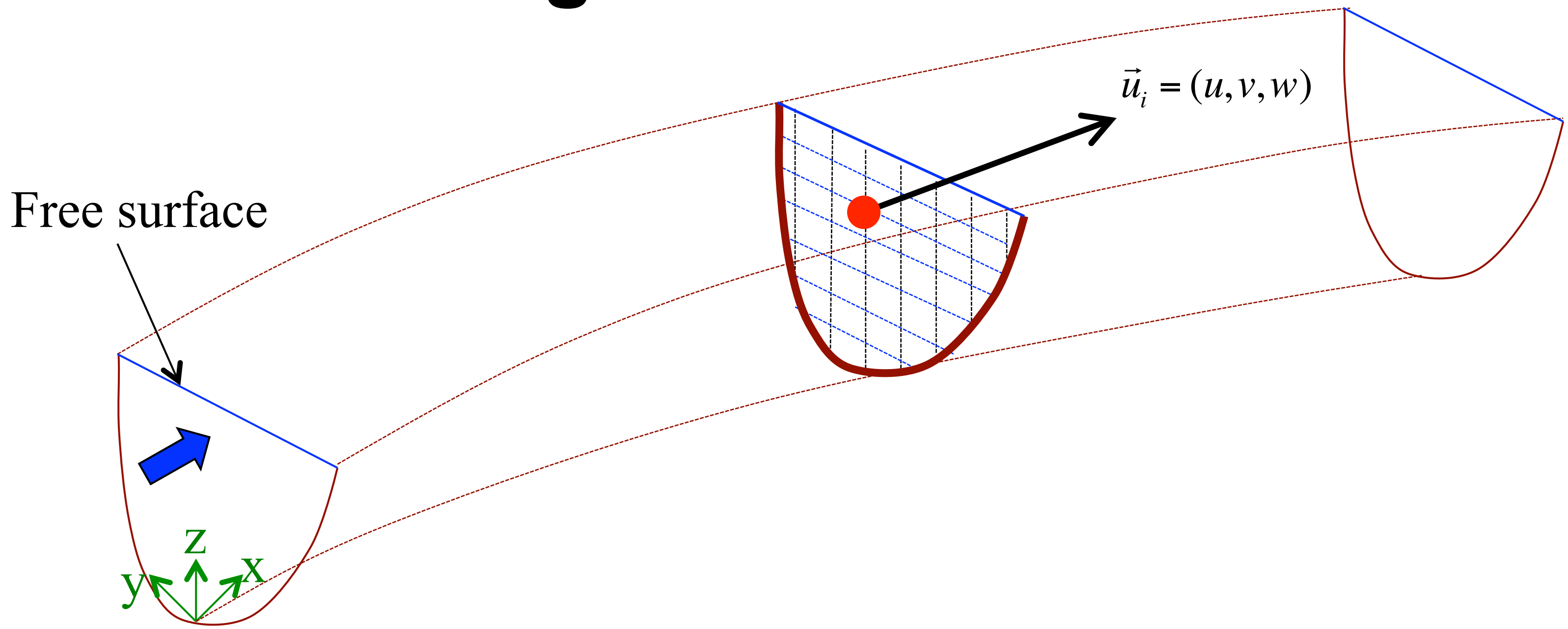

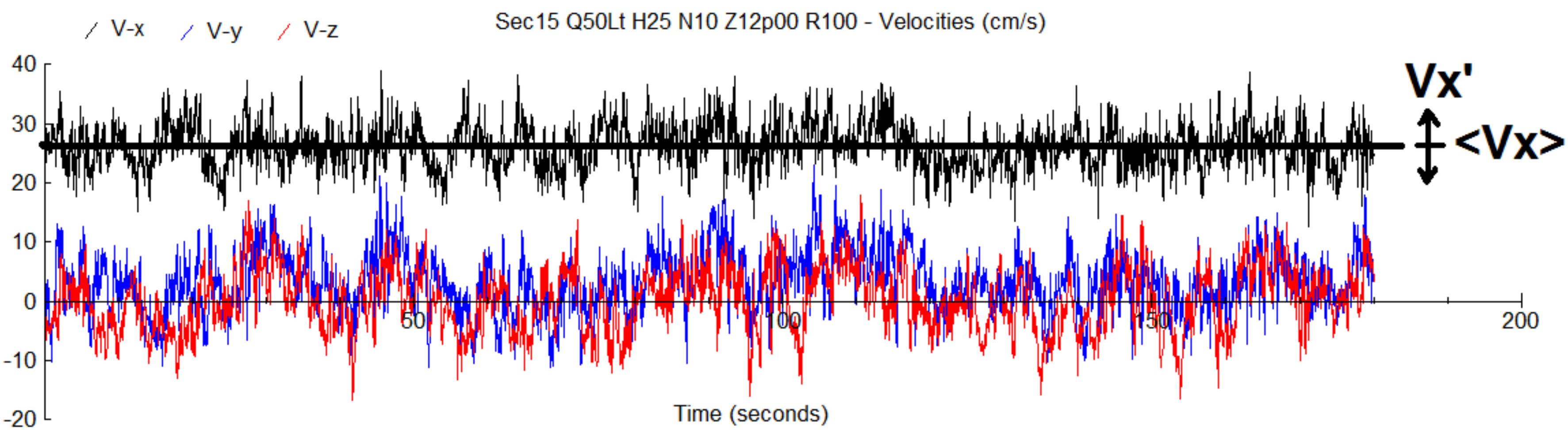

$$u_i = \overline{u_i} + u_i'$$

Measuring mean and turbulent flow

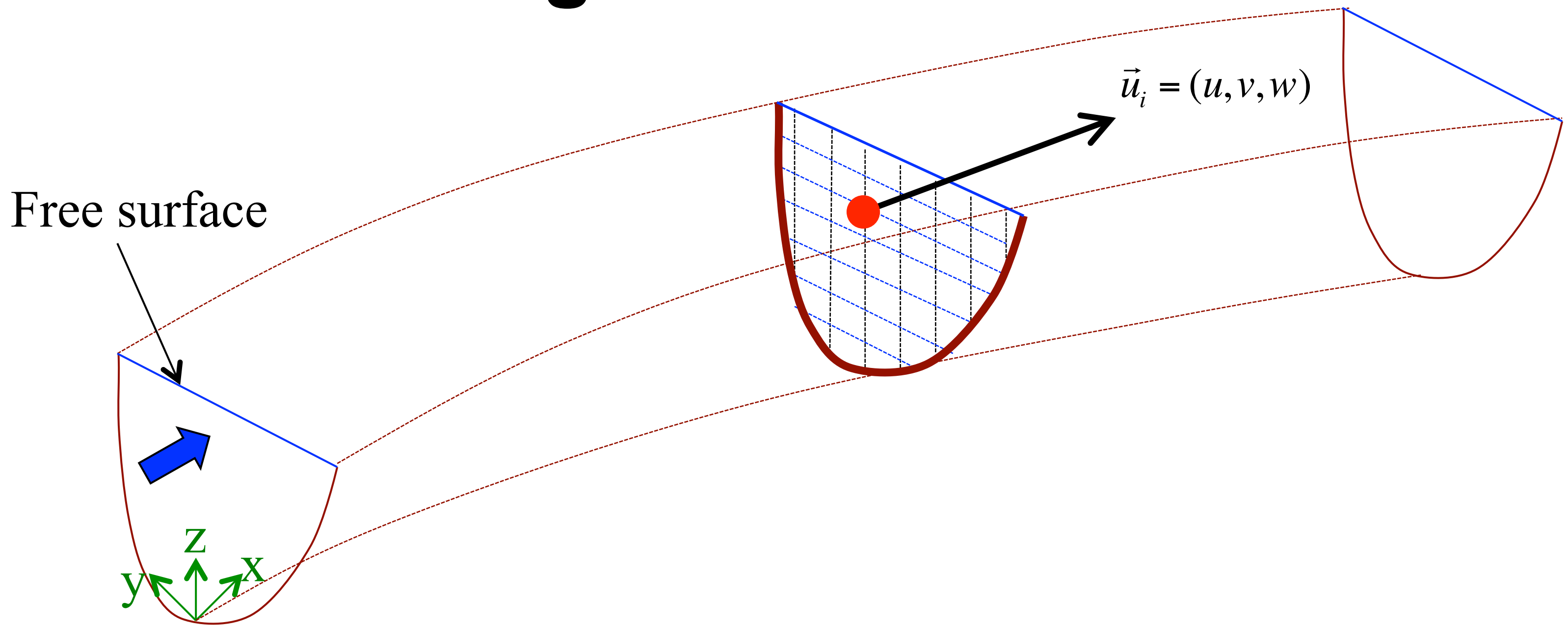

Instantaneous flow equations

$$\frac{\partial \rho}{\partial t} + \frac{\partial (\rho u)}{\partial x} + \frac{\partial (\rho v)}{\partial y} + \frac{\partial (\rho w)}{\partial z} = 0$$

$$\frac{\partial (\rho u)}{\partial t} + \frac{\partial (\rho u^2)}{\partial x} + \frac{\partial (\rho u v)}{\partial y} + \frac{\partial (\rho u w)}{\partial z} = \rho f v - \frac{\partial p}{\partial x} + \frac{\partial \tau_{xx}}{\partial x} + \frac{\partial \tau_{xy}}{\partial y} + \frac{\partial \tau_{xz}}{\partial z}$$

$$\frac{\partial (\rho v)}{\partial t} + \frac{\partial (\rho u v)}{\partial x} + \frac{\partial (\rho v^2)}{\partial y} + \frac{\partial (\rho v w)}{\partial z} = -\rho f u - \frac{\partial p}{\partial y} + \frac{\partial \tau_{yx}}{\partial x} + \frac{\partial \tau_{yy}}{\partial y} + \frac{\partial \tau_{yz}}{\partial z}$$

$$\frac{\partial (\rho w)}{\partial t} + \frac{\partial (\rho u w)}{\partial x} + \frac{\partial (\rho v w)}{\partial y} + \frac{\partial (\rho w^2)}{\partial z} = -\frac{\partial p}{\partial z} - \rho g + \frac{\partial \tau_{zx}}{\partial x} + \frac{\partial \tau_{zy}}{\partial y} + \frac{\partial \tau_{zz}}{\partial z}$$

Different Approaches to Modeling Turbulent Flows

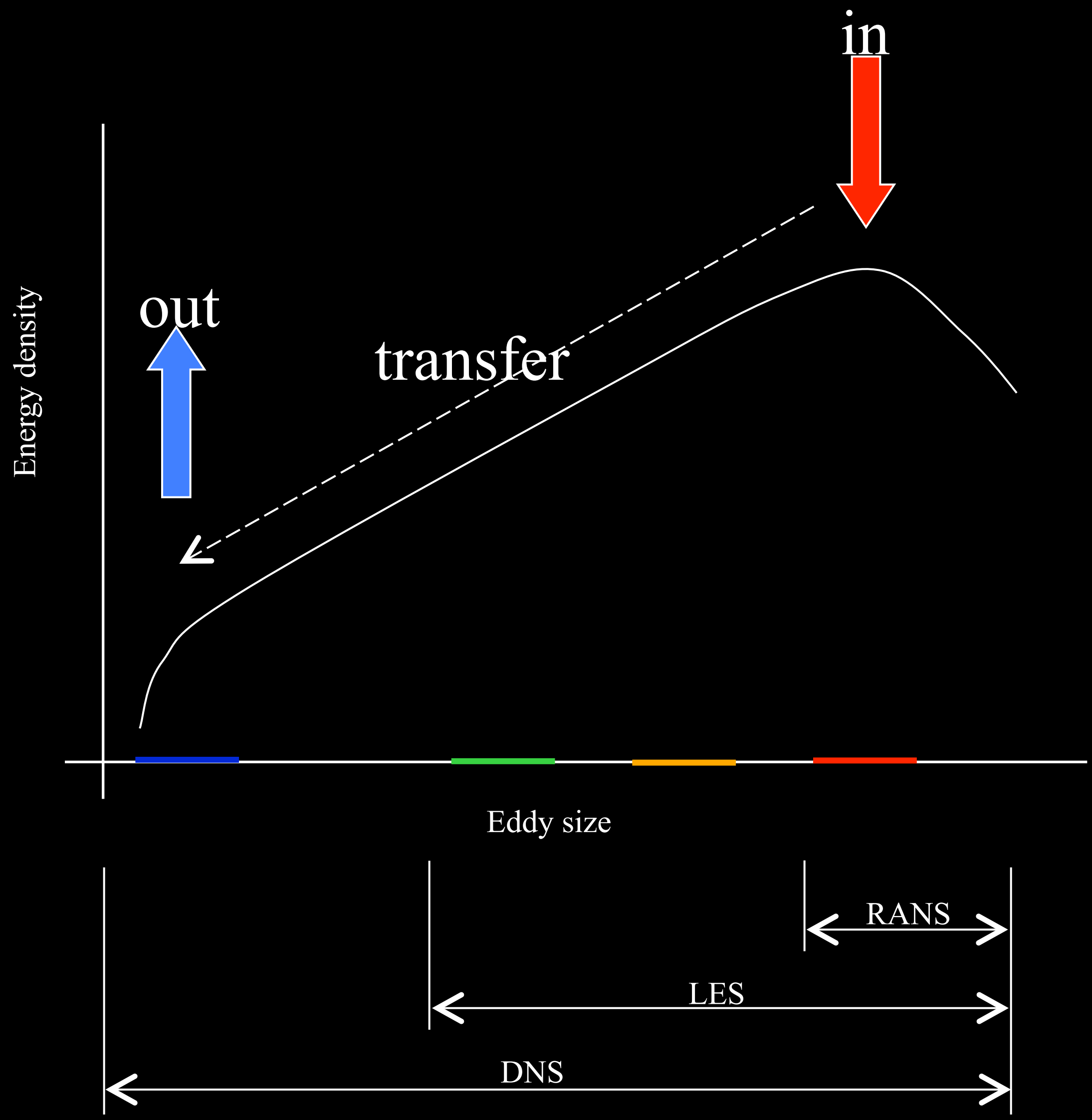

- DNS: direct numerical simulation (resolves all scales)
- LES: Large Eddy Simulation (resolves large and intermediate scales and models small scales)
- RANS: Reynolds Averaged Navier-Stokes (resolves large scales and models intermediate and small scales)

Comparison of Modeling Approaches

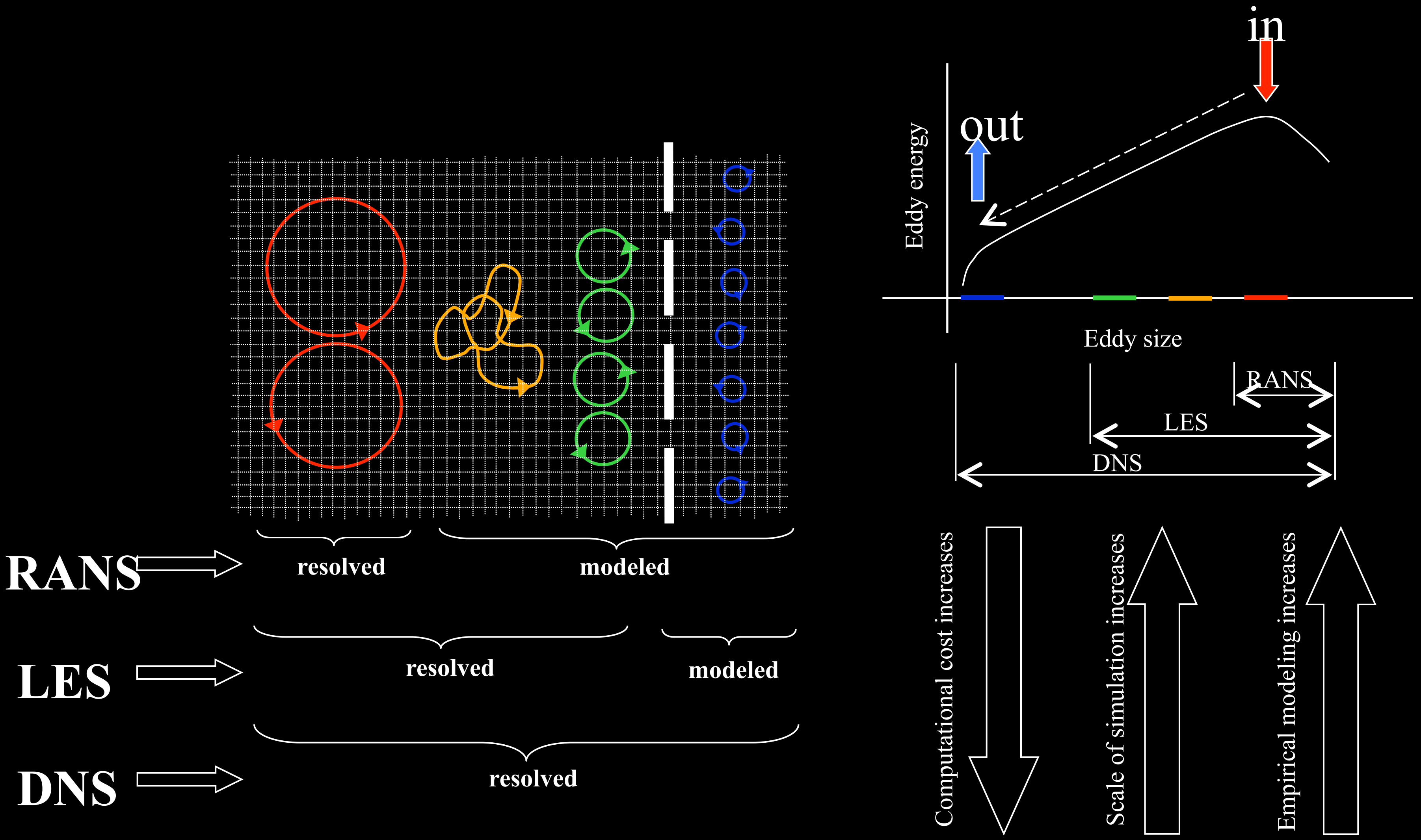

LES (Large Eddy Simulation)

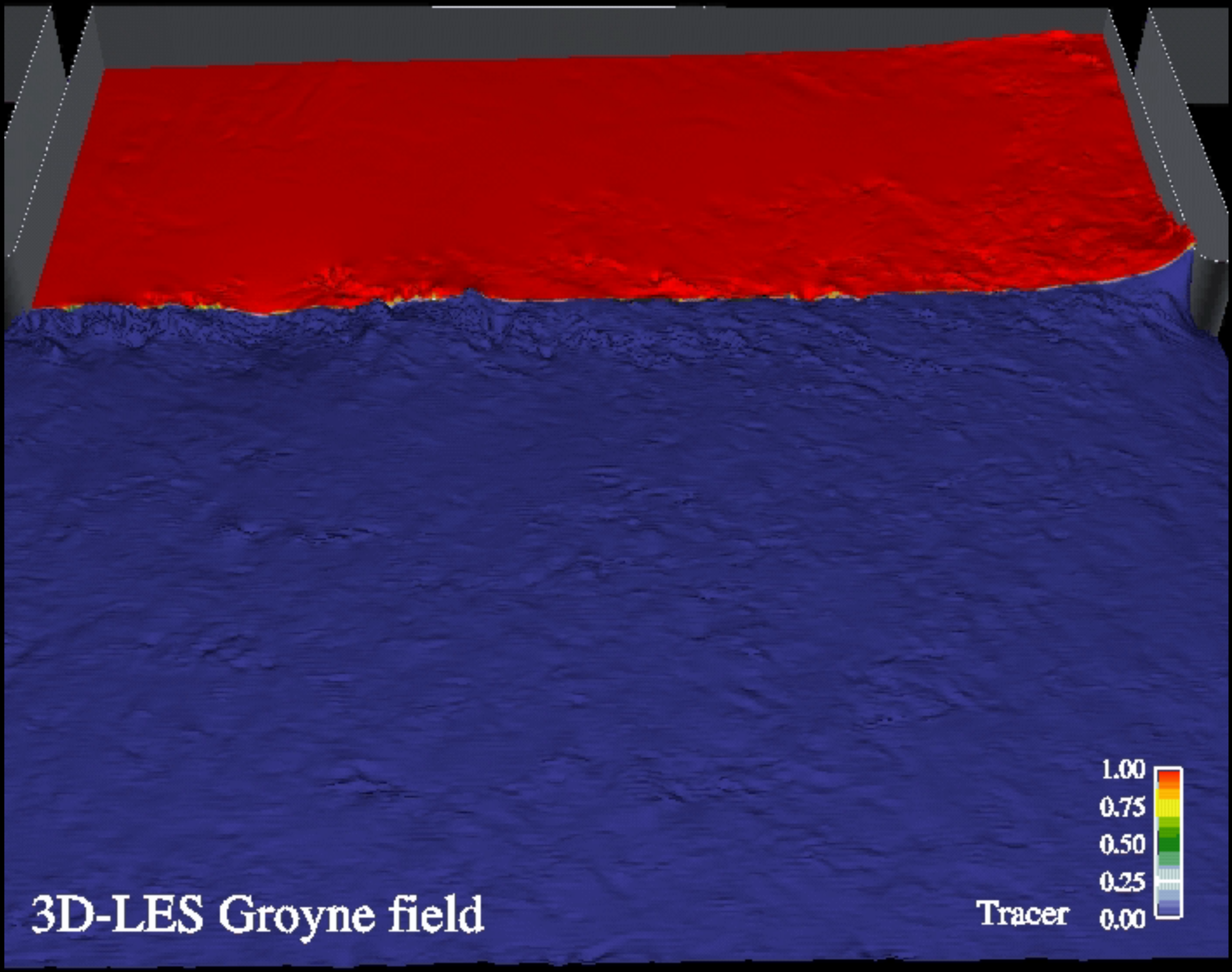

RANS modeling:
KINOSHITA CHANNEL

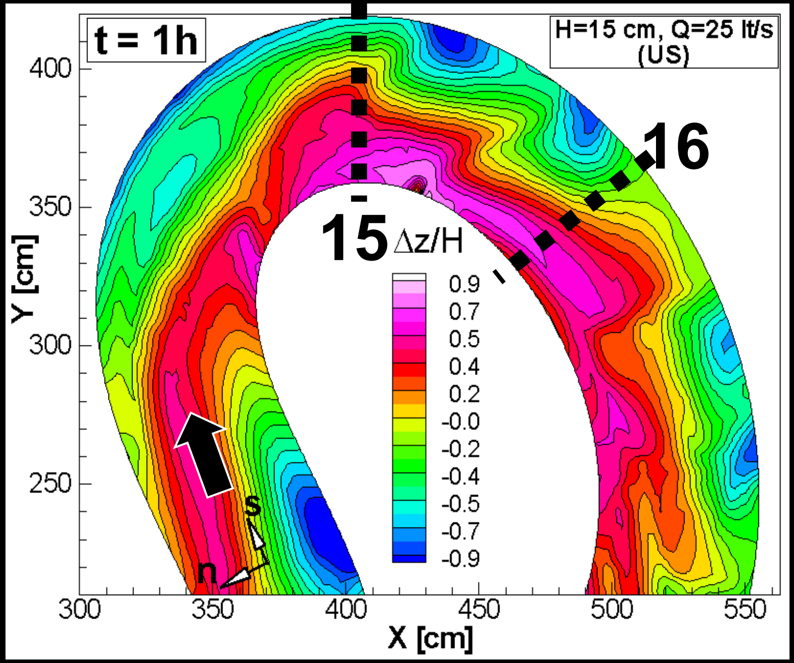

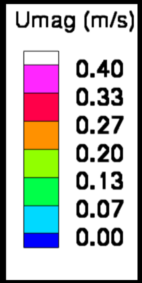

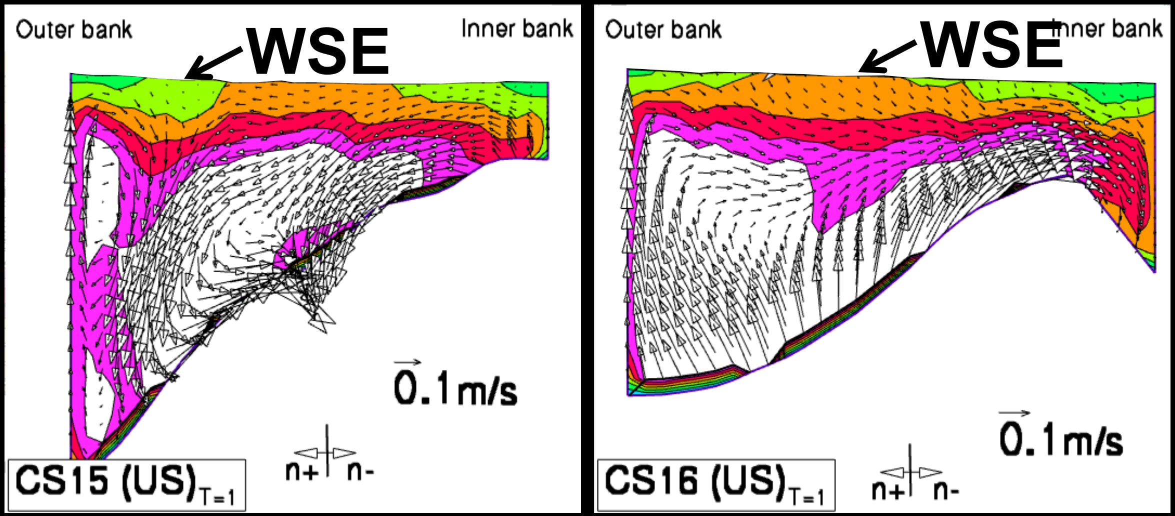

Abad et al. (2013), ESPL

Modeling in river-type systems

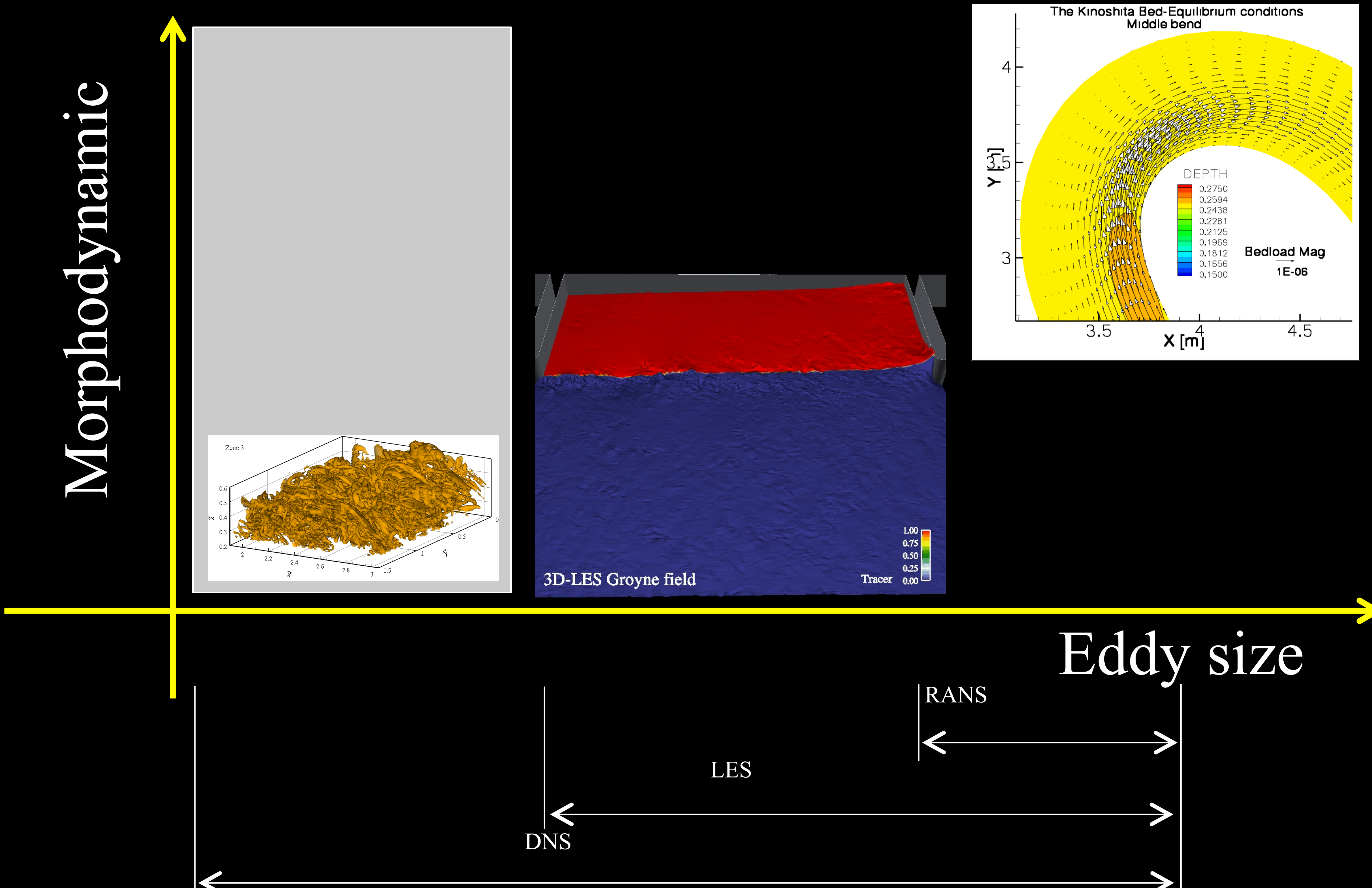

1D, 2D and 3D flow models

3D flow equations

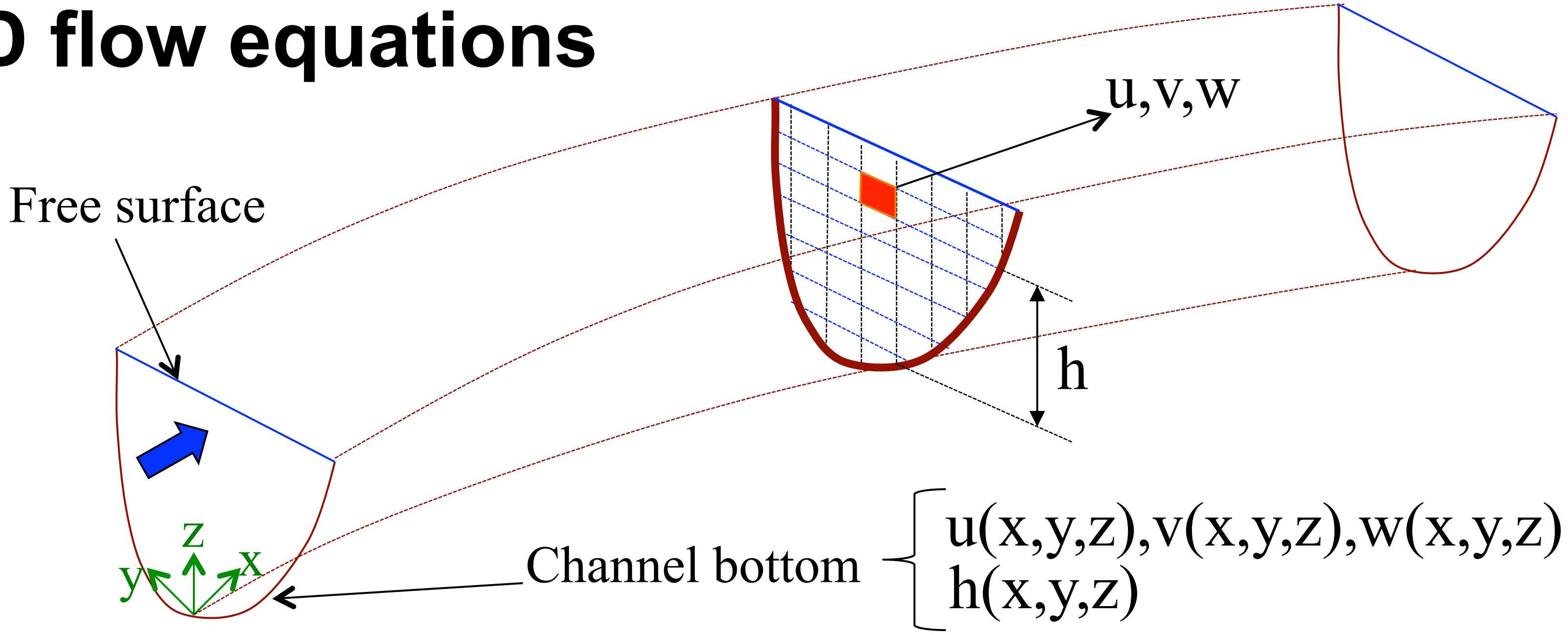

[1] Mass conservation

$$\frac{\partial \rho}{\partial t} + \frac{\partial(\rho \bar{u})}{\partial x} + \frac{\partial(\rho \bar{v})}{\partial y} + \frac{\partial(\rho \bar{w})}{\partial z} = 0$$

[2] x-momentum

$$\frac{\partial(\rho \bar{u})}{\partial t} + \frac{\partial(\rho \bar{u}^2)}{\partial x} + \frac{\partial(\rho \bar{u}\bar{v})}{\partial y} + \frac{\partial(\rho \bar{u}\bar{w})}{\partial z} = \rho f \bar{v} - \frac{\partial \bar{p}}{\partial x} + \frac{\partial \bar{\tau}_{xx}}{\partial x} + \frac{\partial \bar{\tau}_{xy}}{\partial y} + \frac{\partial \bar{\tau}_{xz}}{\partial z}$$

[3] y-momentum

$$\frac{\partial(\rho \bar{v})}{\partial t} + \frac{\partial(\rho \bar{u}\bar{v})}{\partial x} + \frac{\partial(\rho \bar{v}^2)}{\partial y} + \frac{\partial(\rho \bar{v}\bar{w})}{\partial z} = -\rho f \bar{u} - \frac{\partial \bar{p}}{\partial y} + \frac{\partial \bar{\tau}_{yx}}{\partial x} + \frac{\partial \bar{\tau}_{yy}}{\partial y} + \frac{\partial \bar{\tau}_{yz}}{\partial z}$$

[4] z-momentum

$$\frac{\partial(\rho \bar{w})}{\partial t} + \frac{\partial(\rho \bar{u}\bar{w})}{\partial x} + \frac{\partial(\rho \bar{v}\bar{w})}{\partial y} + \frac{\partial(\rho \bar{w}^2)}{\partial z} = -\frac{\partial \bar{p}}{\partial z} - \rho g + \frac{\partial \bar{\tau}_{zx}}{\partial x} + \frac{\partial \bar{\tau}_{zy}}{\partial y} + \frac{\partial \bar{\tau}_{zz}}{\partial z}$$

$$\bar{\tau}_{ij} = \tau_{ij} + \tau^t_{ij} \qquad \bar{\tau}_{ij} = (\nu + \nu_t)\left(\frac{\partial \bar{u}_i}{\partial x_j} + \frac{\partial \bar{u}_j}{\partial x_i}\right)$$

2D flow equations

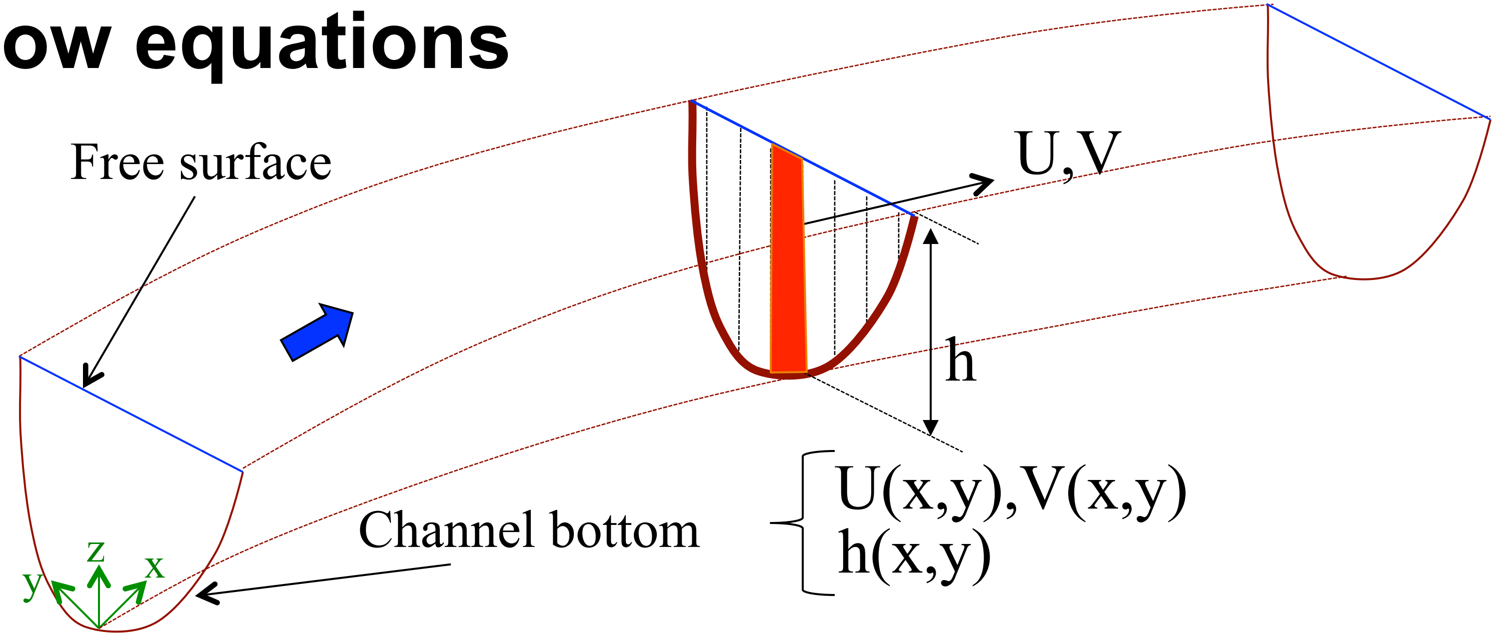

[1] Mass conservation

$$\frac{\partial H}{\partial t} + \frac{\partial (hU)}{\partial x} + \frac{\partial (hV)}{\partial y} = 0$$

[2] x-momentum

$$\frac{\partial (hU)}{\partial t} + \frac{\partial (\beta_x U^2 h)}{\partial x} + \frac{\partial (\beta_{xy} UVh)}{\partial y}$$

$$= fhV - gh\frac{\partial H}{\partial x} - \frac{gh^2}{2\rho_0}\frac{\partial \rho}{\partial x} - \frac{1}{\rho_0}\frac{\partial \bar{p}_a}{\partial x}(H - z_b) + \frac{1}{\rho_0}\tau_{xz}|_H - \frac{1}{\rho_0}\tau_{xz}|_0$$

[3] y-momentum

$$\frac{\partial (hV)}{\partial t} + \frac{\partial (\beta_{xy} UVh)}{\partial x} + \frac{\partial (\beta_y V^2 h)}{\partial y}$$

$$= -fhU - gh\frac{\partial H}{\partial y} - \frac{gh^2}{2\rho_0}\frac{\partial \rho}{\partial y} - \frac{1}{\rho_0}\frac{\partial \bar{p}_a}{\partial y}(H - z_b) + \frac{1}{\rho_0}\tau_{yz}|_H - \frac{1}{\rho_0}\tau_{yz}|_0$$

β_x, $\beta_x y$ and β_z are the Boussinesq coefficients (≈ 1.0) $\quad \tau_{xz}|_0 = \rho g h \left(\frac{Un}{h^{2/3}}\right)^2 \quad \tau_{yz}|_0 = \rho g h \left(\frac{Vn}{h^{2/3}}\right)^2$

1D flow equations

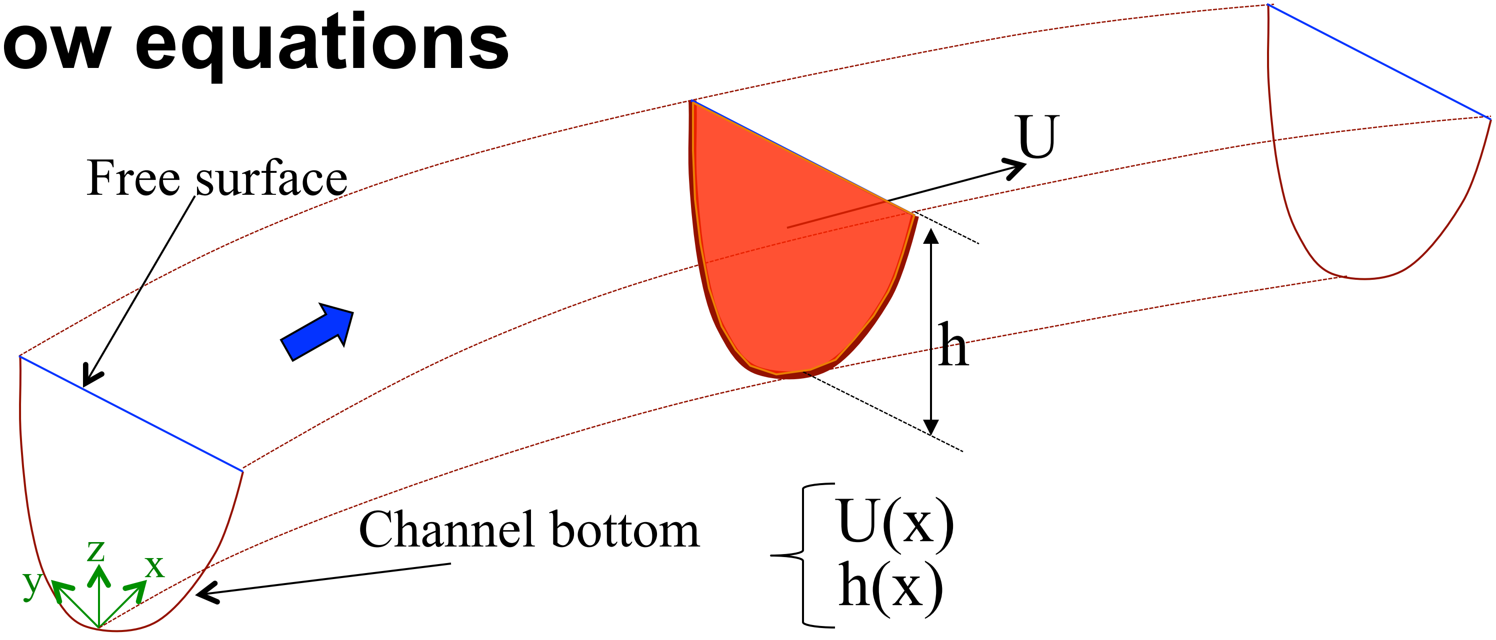

[1] Mass conservation

$$\frac{\partial A}{\partial t} + \frac{\partial Q}{\partial x} = 0$$

[2] x-momentum

$$\frac{\partial Q}{\partial t} + \frac{\partial}{\partial x}(\beta U^2 A) + gA\frac{\partial h}{\partial x} = gA(S_o - S_f)$$

Sediment Transport Processes
And Sediment Conservation Equation (Exner)

Bed load and suspended load

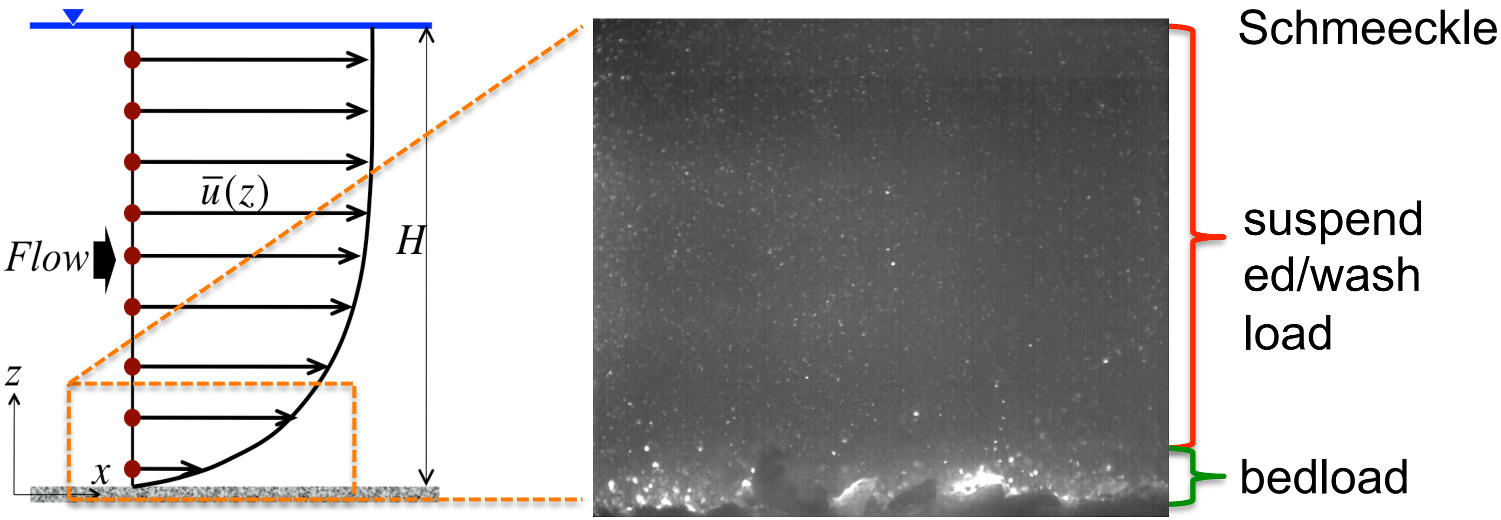

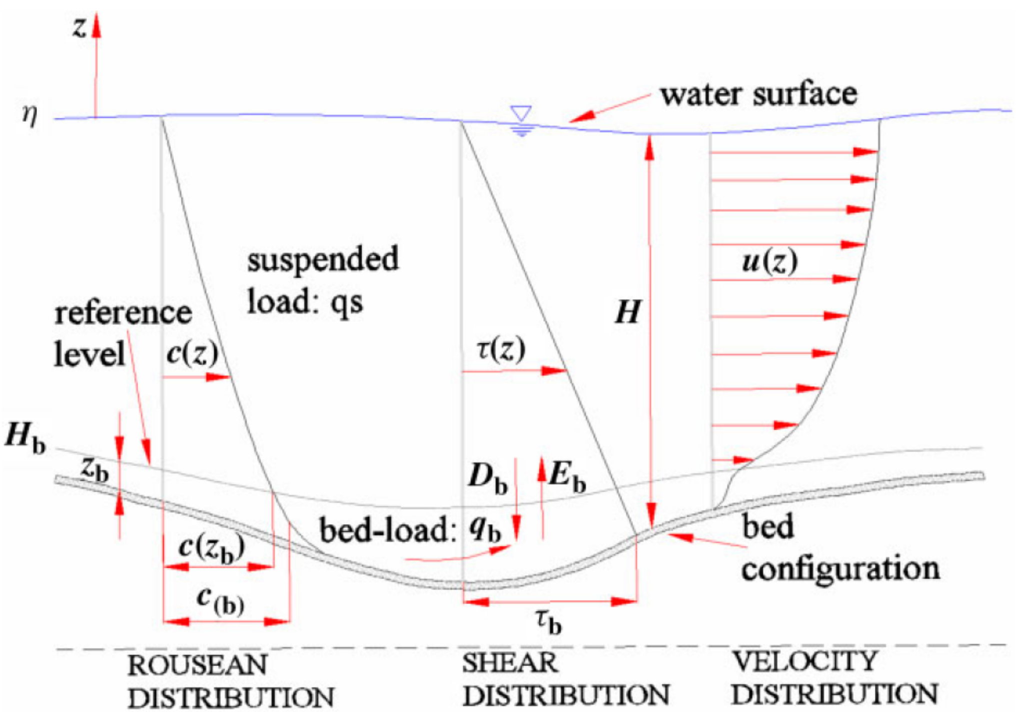

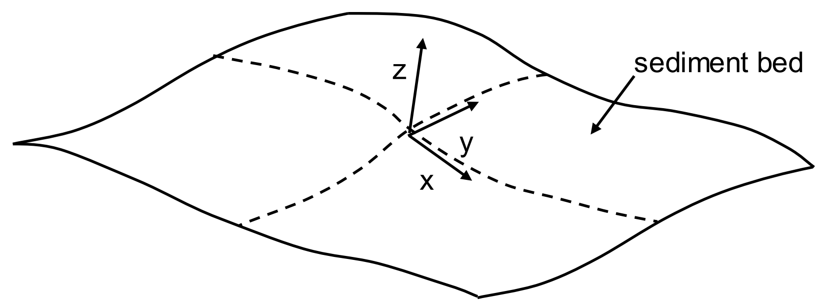

$$\vec{q}_b = q_{bx}\hat{e}_x + q_{by}\hat{e}_y$$

$$(1-\lambda_p)\frac{\partial \eta}{\partial t} = -\vec{\nabla}\cdot\vec{q}_b + v_s\left(\bar{c}_b - E\right)$$

A BEDLOAD TRANSPORT RELATIONS FOR UNIFORM SEDIMENT (Parker's e-book)

$$1-\frac{1}{\sqrt{\pi}}\int_{-(0.143/\tau^*)-2}^{+(0.143/\tau^*)-2} e^{-t^2}\,dt = \frac{43.5q_b^*}{1+43.5q_b^*}$$

Einstein (1950)

$$q_b^* = 17\left(\tau^* - \tau_c^*\right)\left(\sqrt{\tau^*} - \sqrt{\tau_c^*}\right), \quad \tau_c^* = 0.05$$

Ashida & Michiue (1972)

$$q_b^* = 18.74\left(\tau^* - \tau_c^*\right)\left(\sqrt{\tau^*} - 0.7\sqrt{\tau_c^*}\right), \quad \tau_c^* = 0.05$$

Engelund & Fredsoe (1976)

$$q_b^* = 5.7\left(\tau^* - \tau_c^*\right)^{1.5}, \quad \tau_c^* = 0.037 \sim 0.0455$$

Fernandez Luque & van Beek (1976)

$$q_b^* = 11.2\left(\tau^*\right)^{1.5}\left(1-\frac{\tau_c^*}{\tau^*}\right)^{4.5}, \quad \tau_c^* = 0.03$$

Parker (1979) fit to Einstein (1950)

$$q_b^* = q_b^*(\tau^*) \quad \text{or} \quad q_b^* = q_b^*(\tau^* - \tau_c^*)$$

PLOTS OF BEDLOAD TRANSPORT RELATIONS
(Parker's e-book)

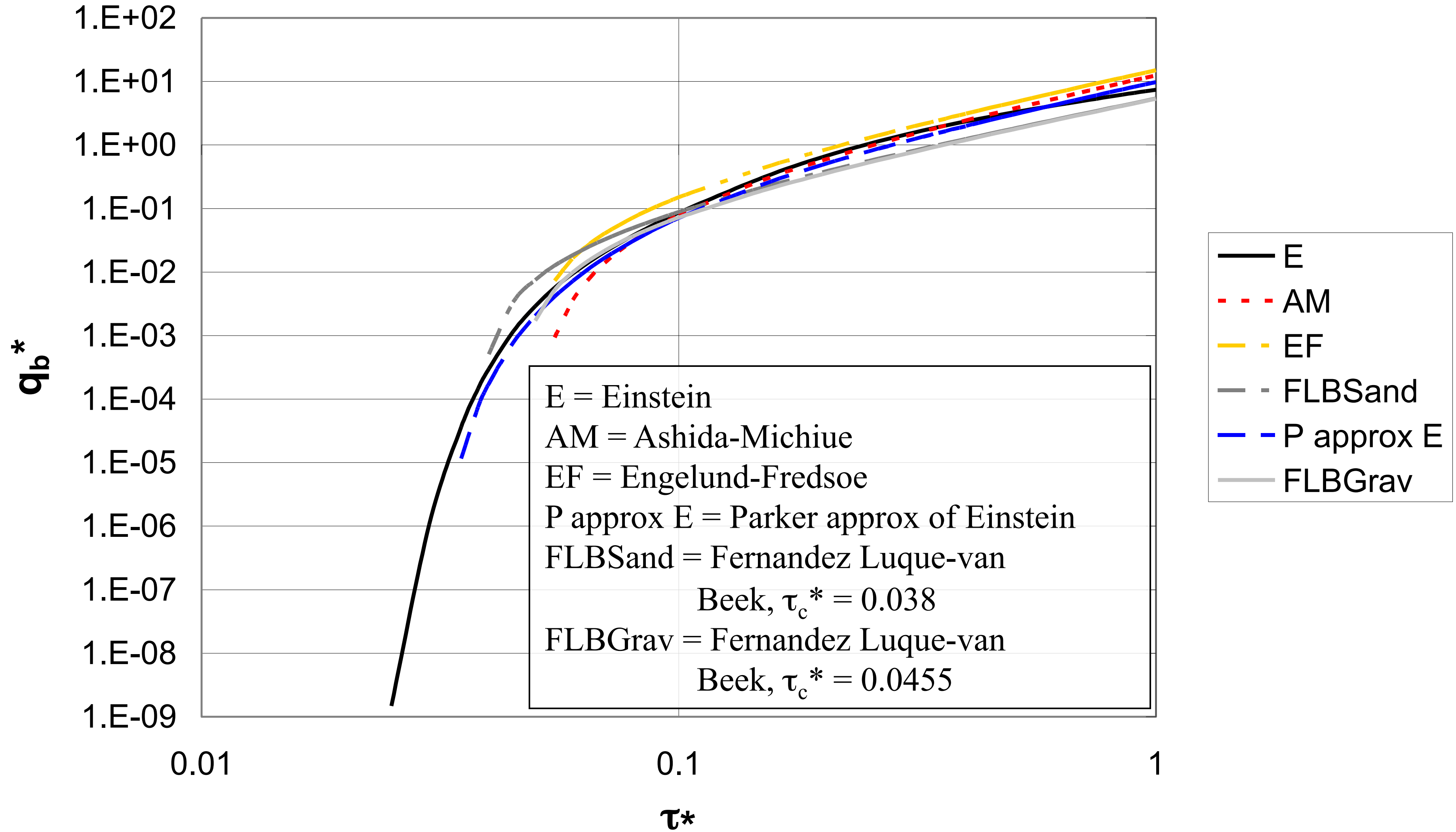

3D simulation - Hydrodynamic

1) EXISTING CONDITION: Lidar (2011)+MBES (2012)

DATA

- Water slope and bed elevation calculation

A slope of 1E-4 from gaging stations Mt. Carmel and New Harmony was calculated.

Using that slope and the elevation of Mt. Carmel on February 2, 2012 a water surface was created for Maier Bend.

Using the water surface and the MBES data the bed elevation surface was obtained.

FIELD MEASUREMENTS – WHAT DO WE NEED TO MEASURE?

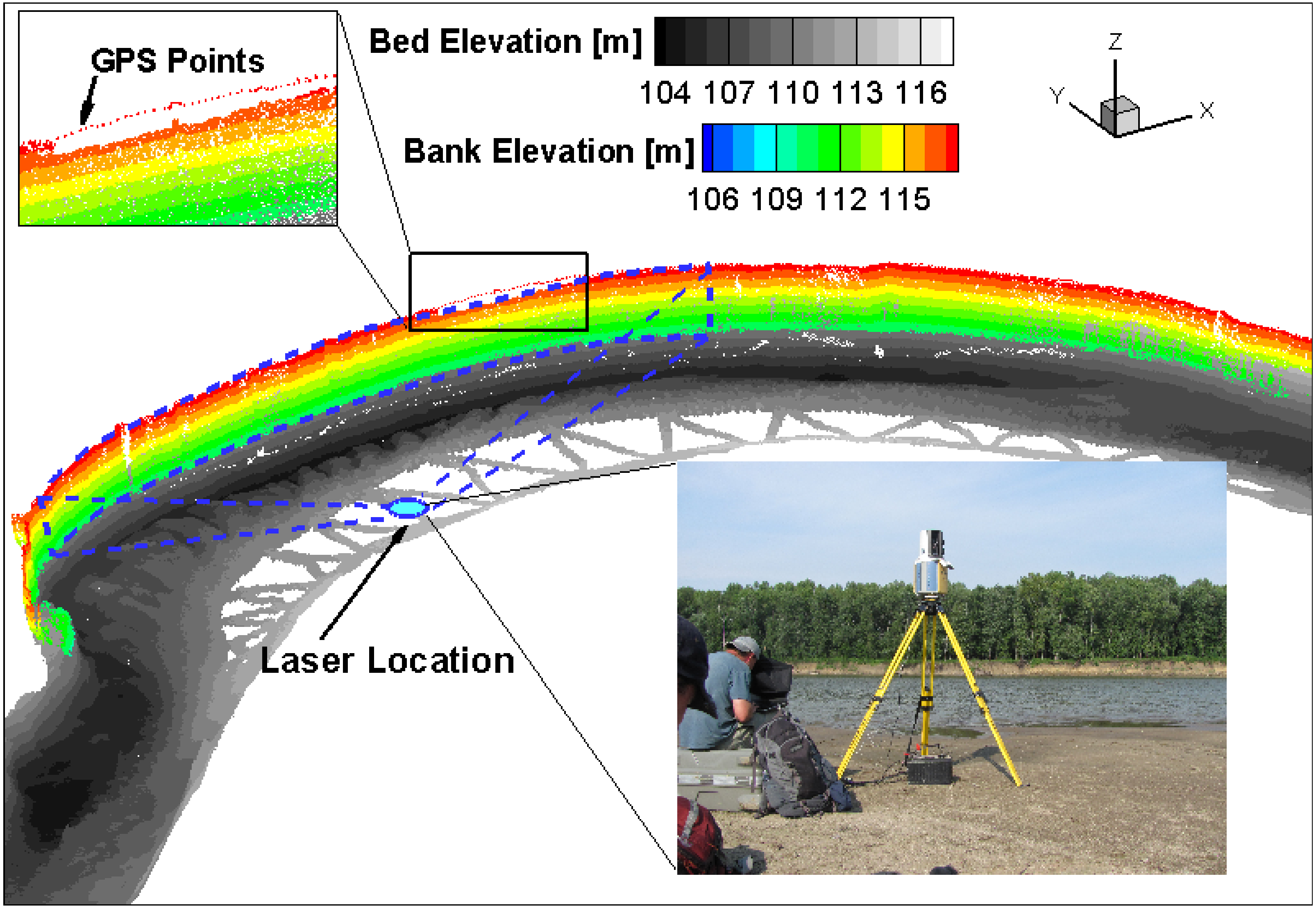

1) Existing condition – Lidar (2011)

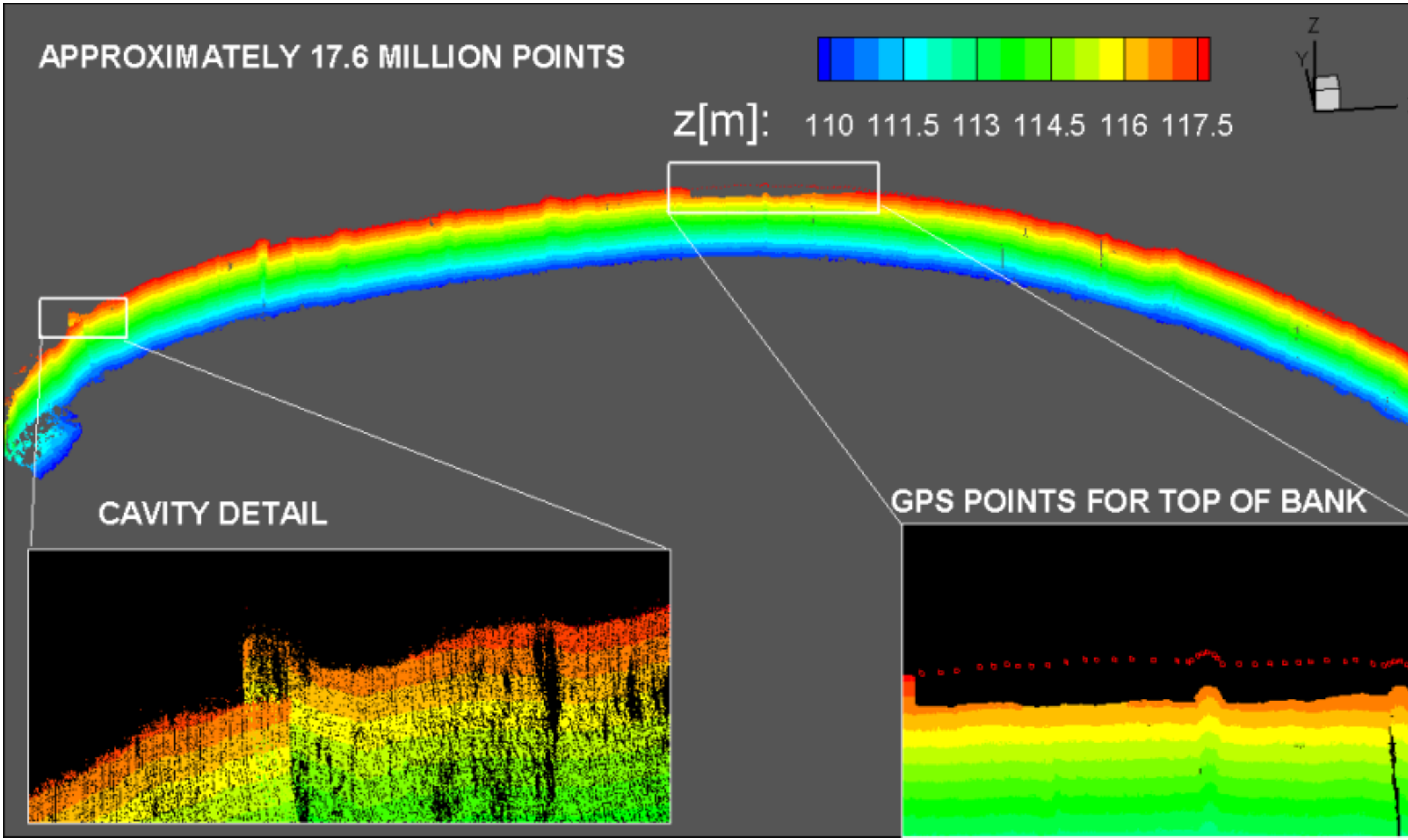

1) Existing condition - MBES (2012)

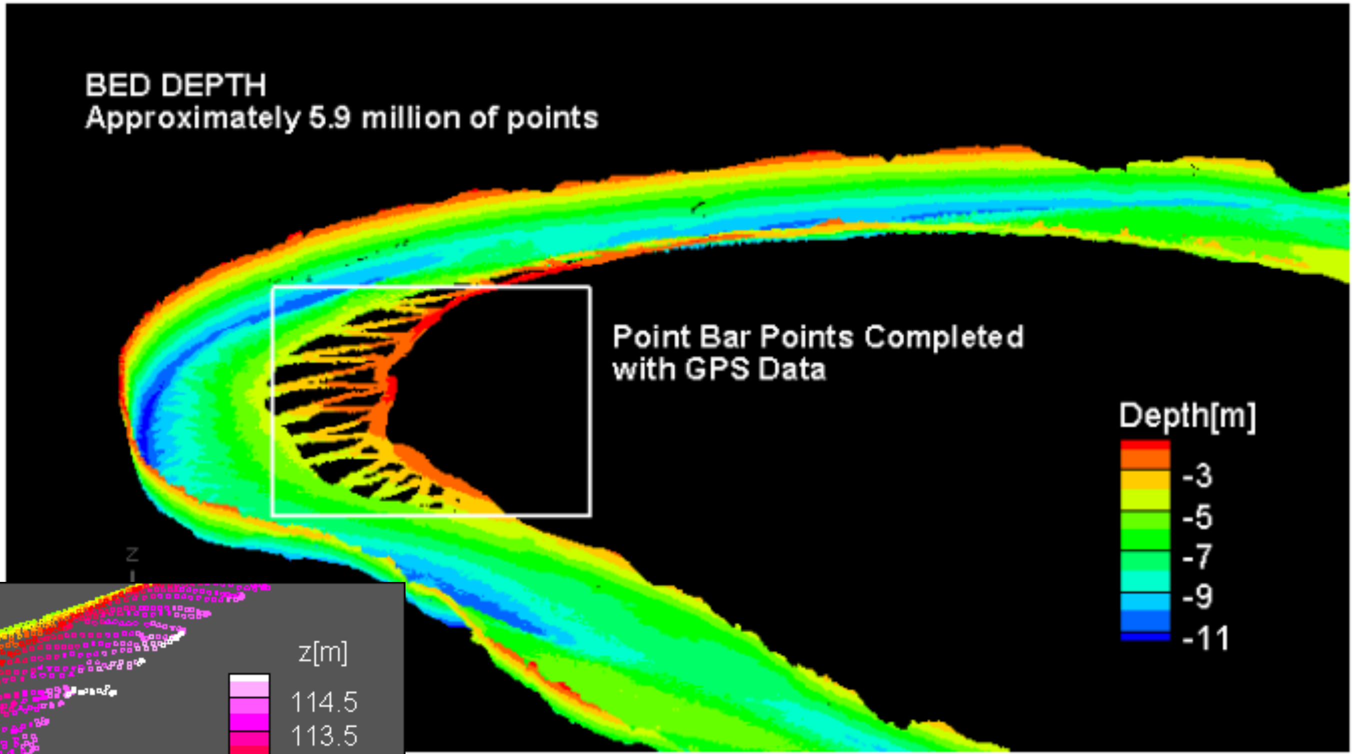

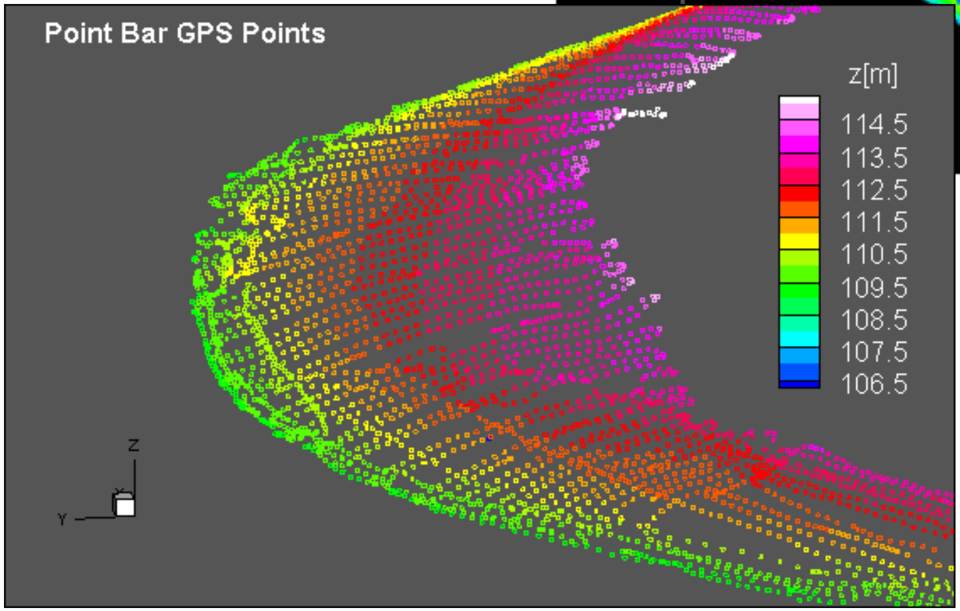

1) EXISTING CONDITION: Lidar (2011)+MBES (2012)

DATA

- <u>Water slope and bed elevation calculation</u>

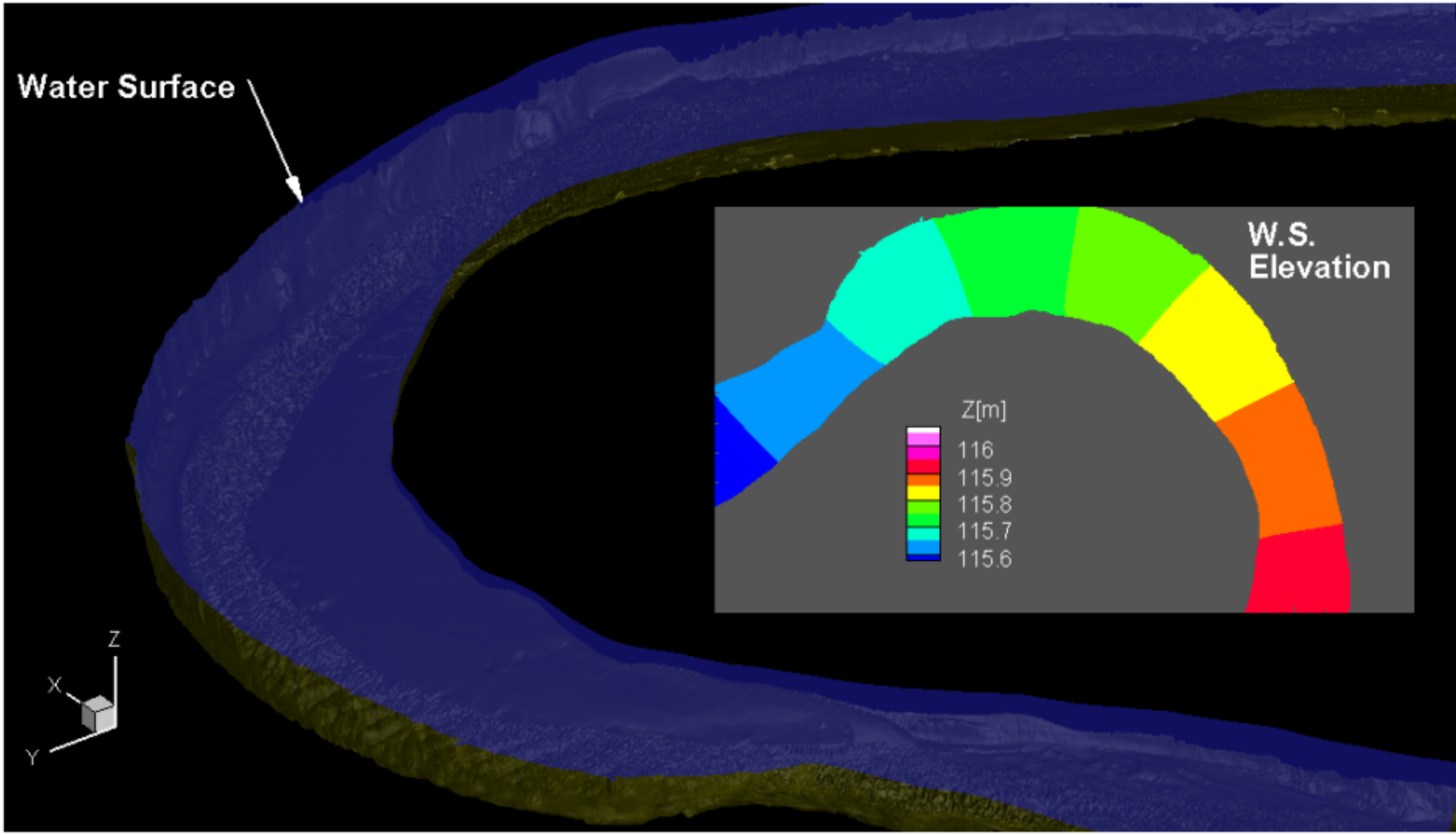

1) EXISTING CONDITION: Lidar (2011)+MBES (2012)

DATA
- <u>MBES + Lidar + point bar (GPS)</u>

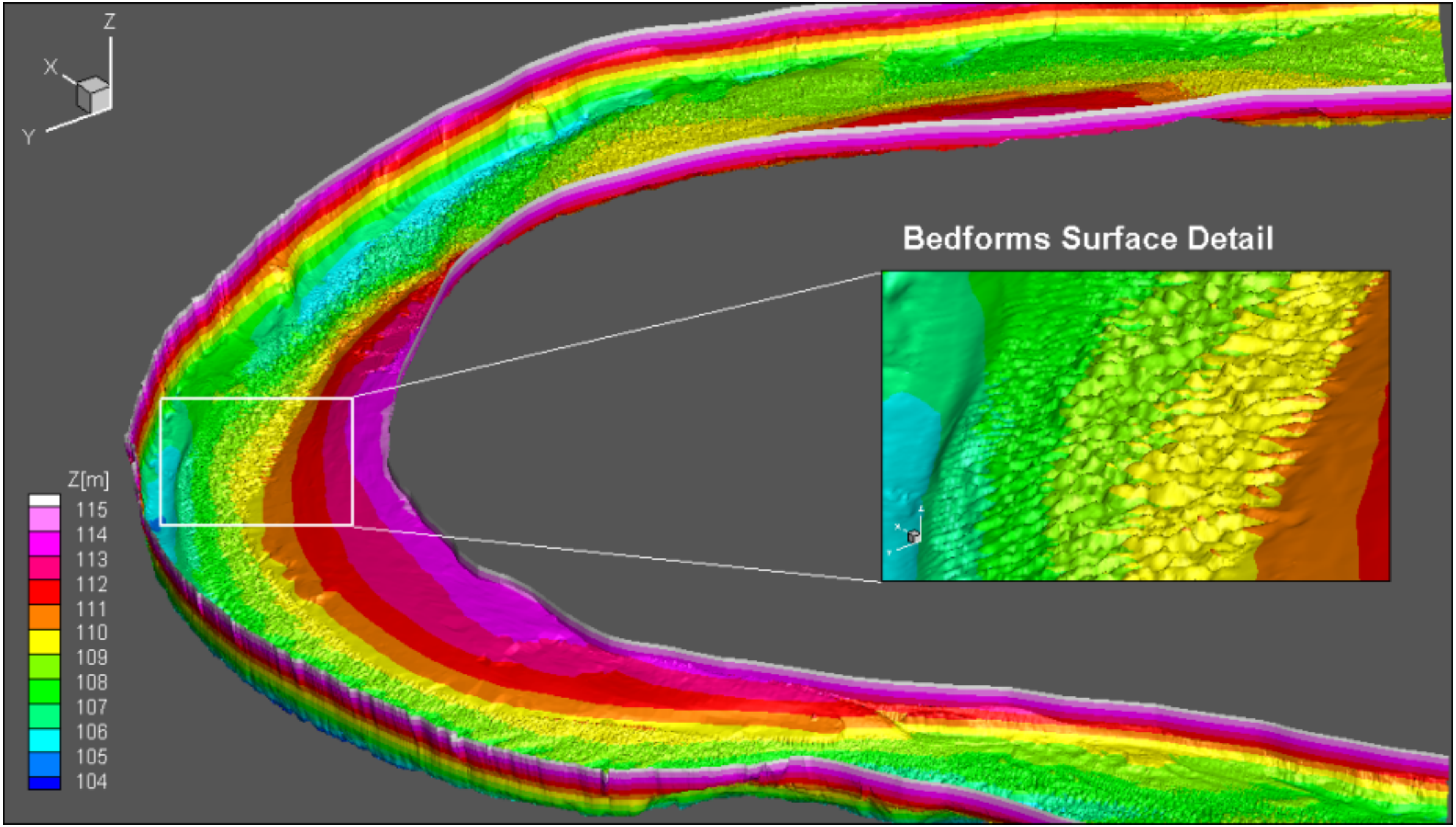

1) EXISTING CONDITION: Lidar (2011)+MBES (2012)

DATA

- aDcp – details of the secondary flows, streamwise velocities and Umag

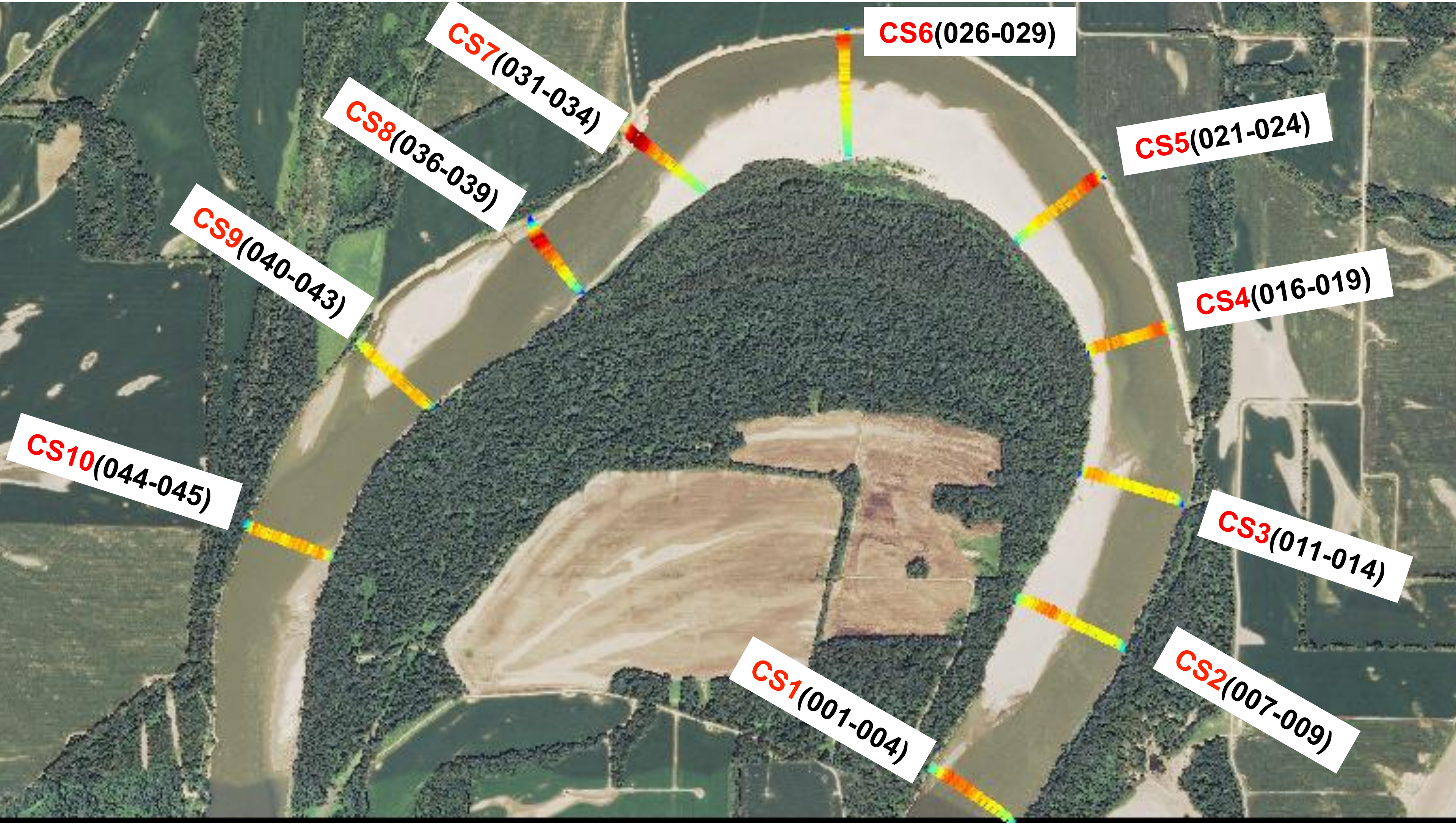

1) EXISTING CONDITION: Lidar (2011)+MBES (2012)

DATA

- aDcp – details of the secondary flows, streamwise velocities and Umag

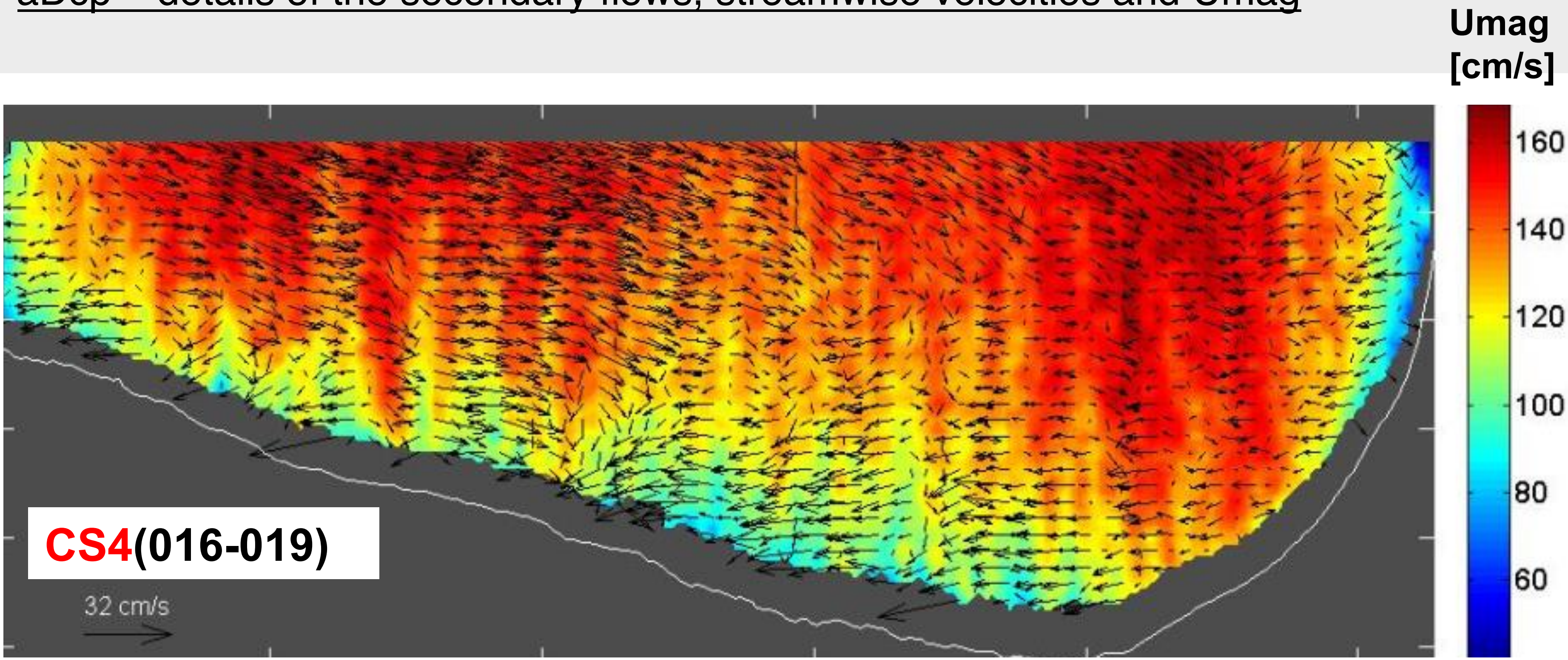

1) EXISTING CONDITION: Lidar (2011)+MBES (2012)

DATA

- <u>aDcp – details of the secondary flows, streamwise velocities and Umag</u>

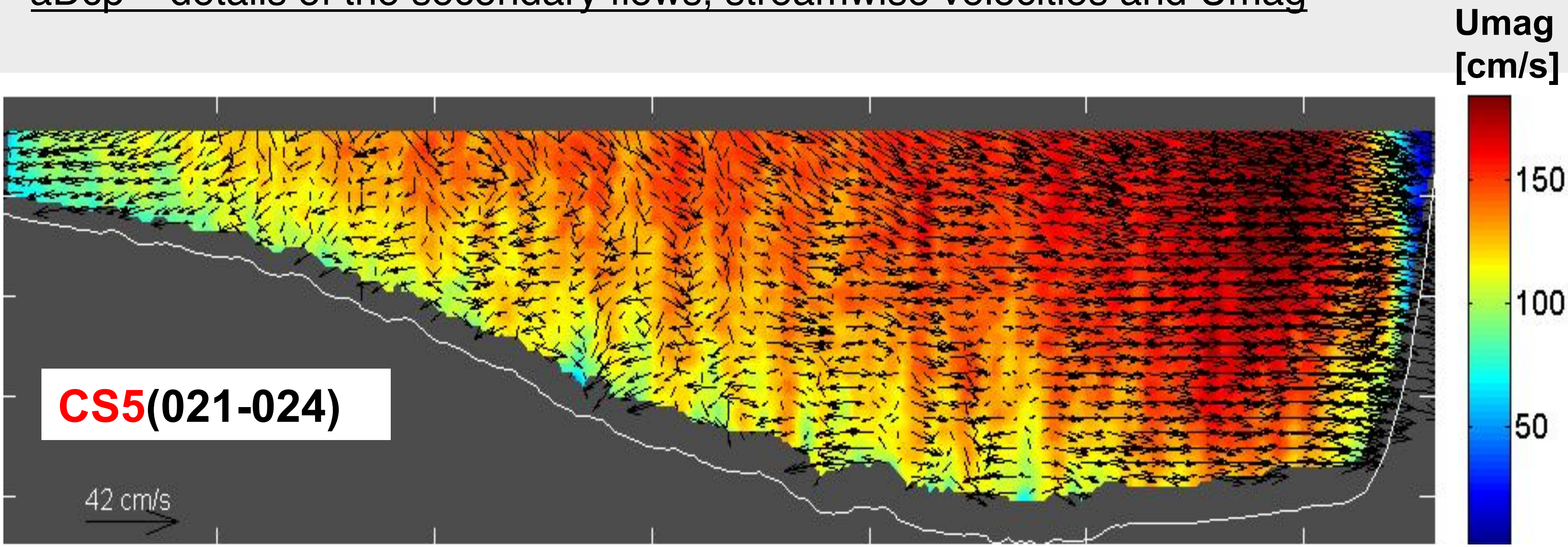

1) EXISTING CONDITION: Lidar (2011)+MBES (2012)

DATA

- <u>aDcp – details of the secondary flows, streamwise velocities and Umag</u>

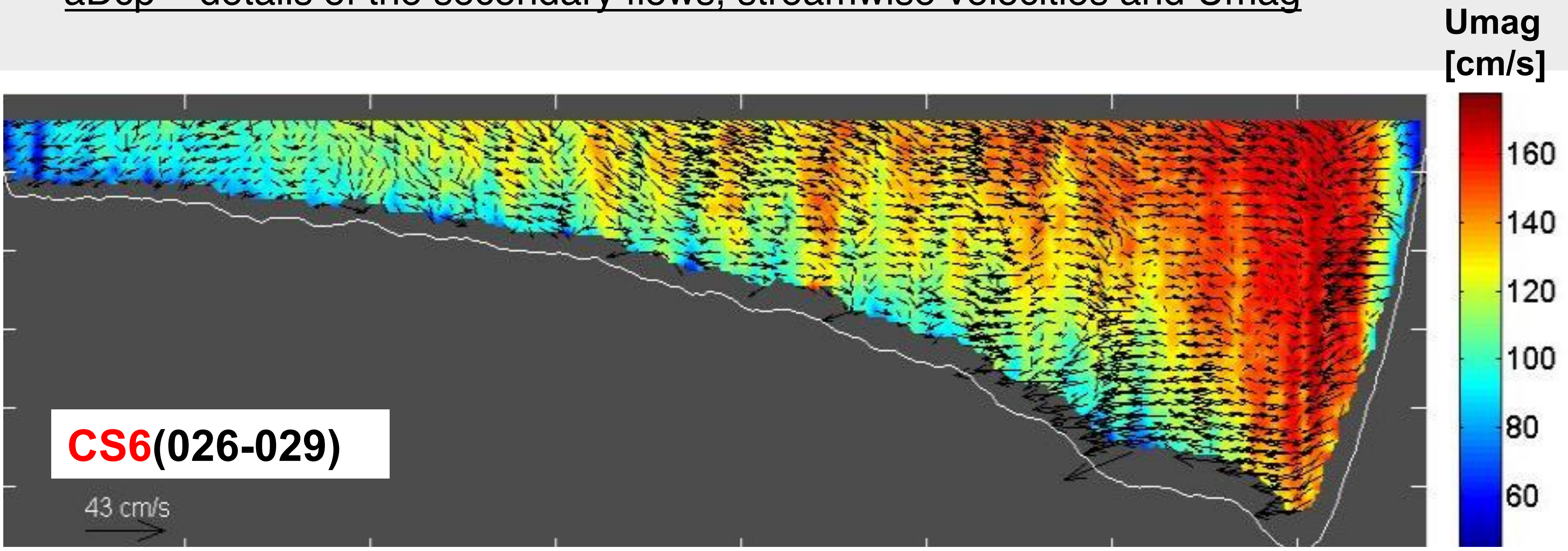

1) EXISTING CONDITION: Lidar (2011)+MBES (2012)

DATA

- aDcp – details of the secondary flows, streamwise velocities and Umag

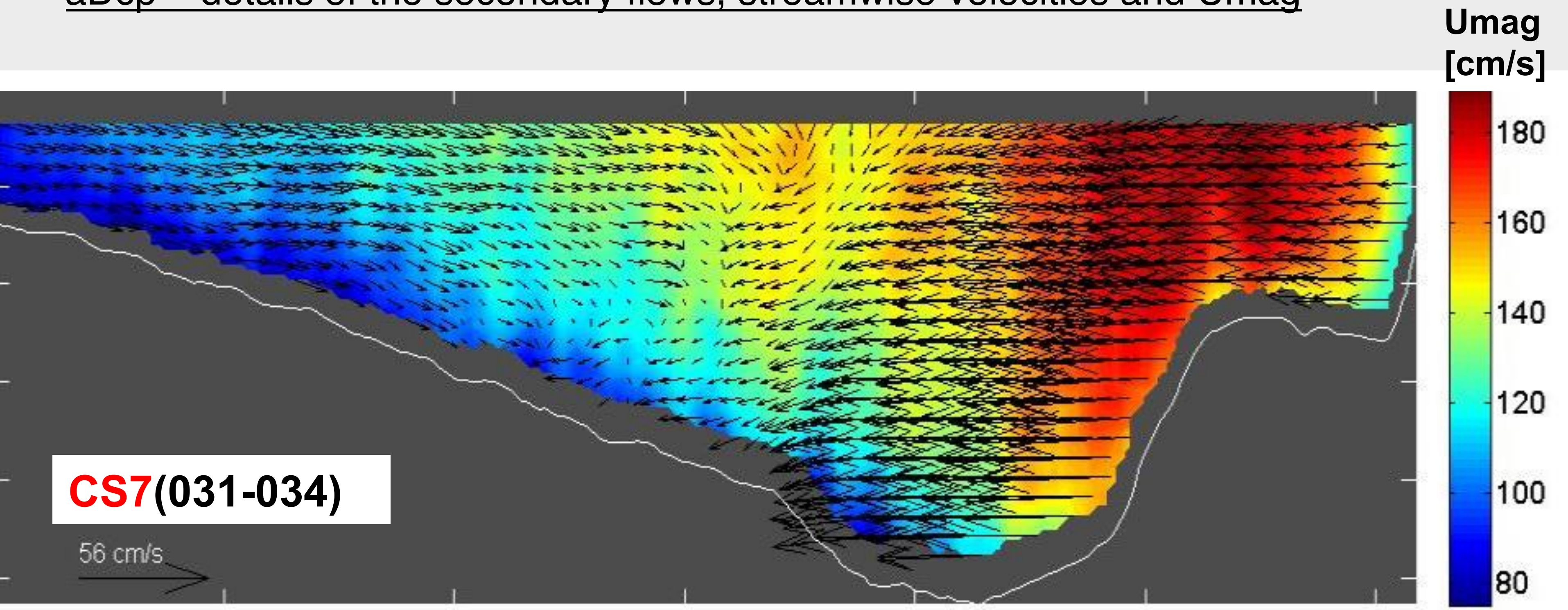

1) EXISTING CONDITION: Lidar (2011)+MBES (2012)

PRE-PROCESSING FOR 3D MODEL

- Details of Mesh generated (unstructured or structured)

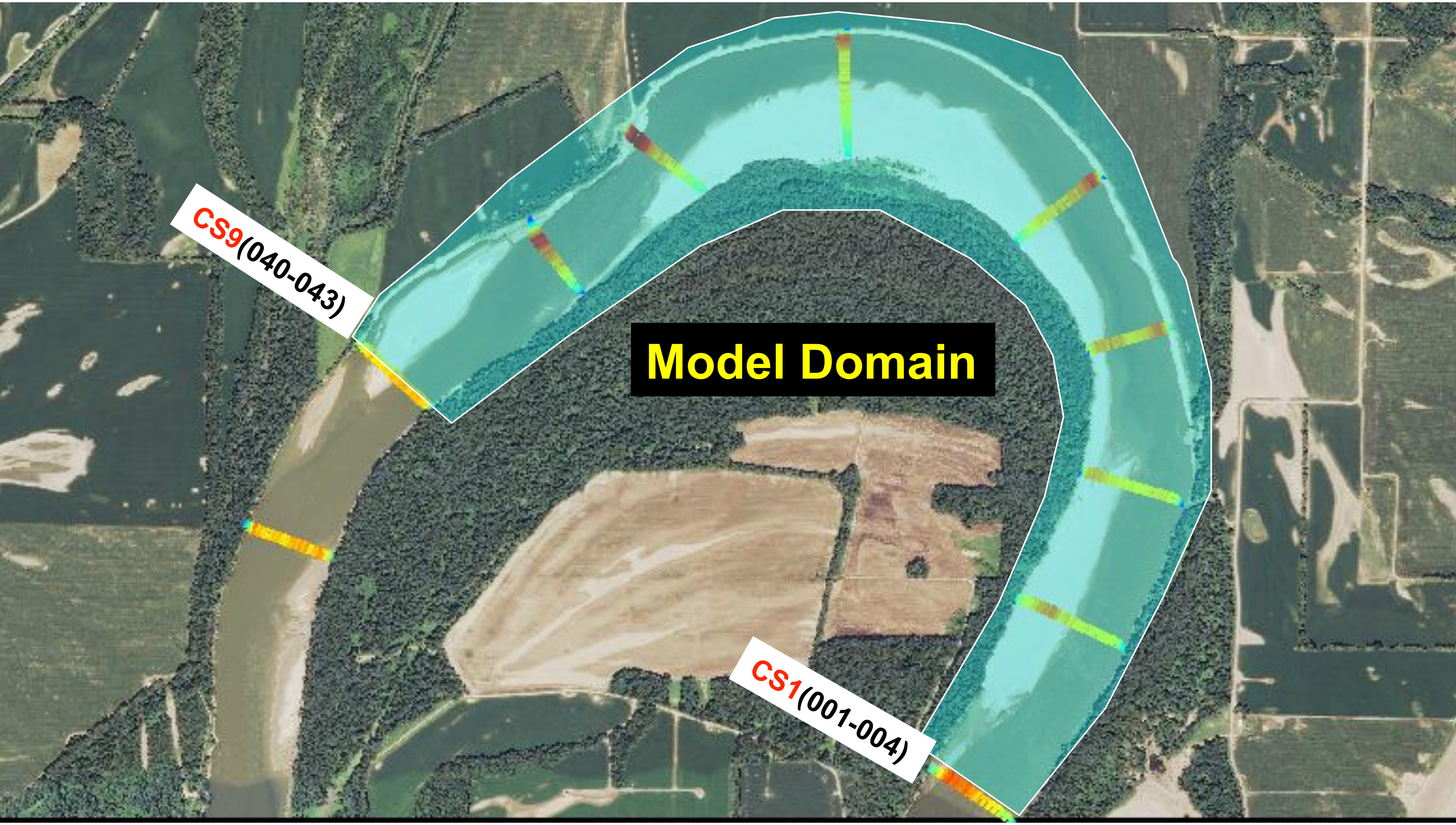

1) EXISTING CONDITION: Lidar (2011)+MBES (2012)

PRE-PROCESSING FOR 3D MODEL

- Details of Mesh generated (unstructured or structured)

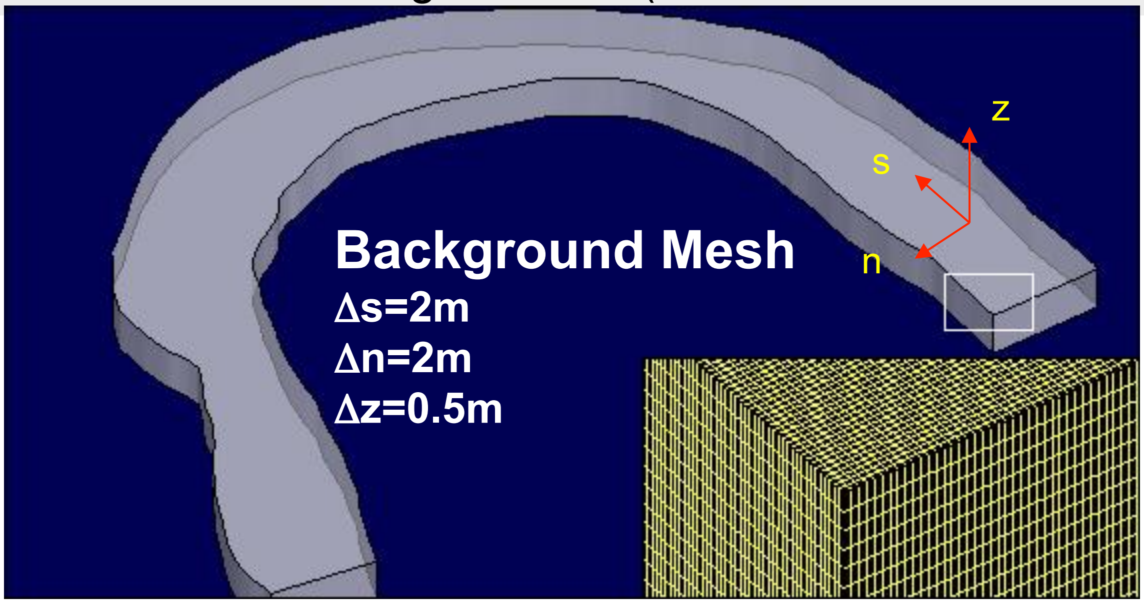

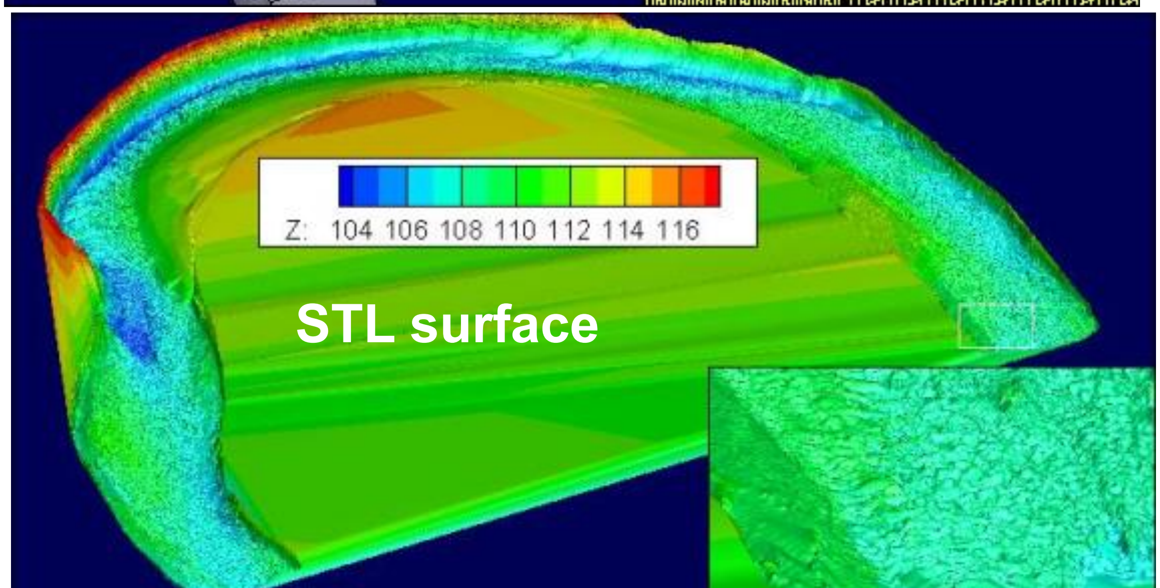

Mesh was generated with OpenFOAM tool snappyHexMesh. It uses a background Hexahedral mesh and an STL surface to create the final mesh.

1) EXISTING CONDITION: Lidar (2011)+MBES (2012)

PRE-PROCESSING FOR 3D MODEL

- Details of Mesh generated (unstructured or structured)

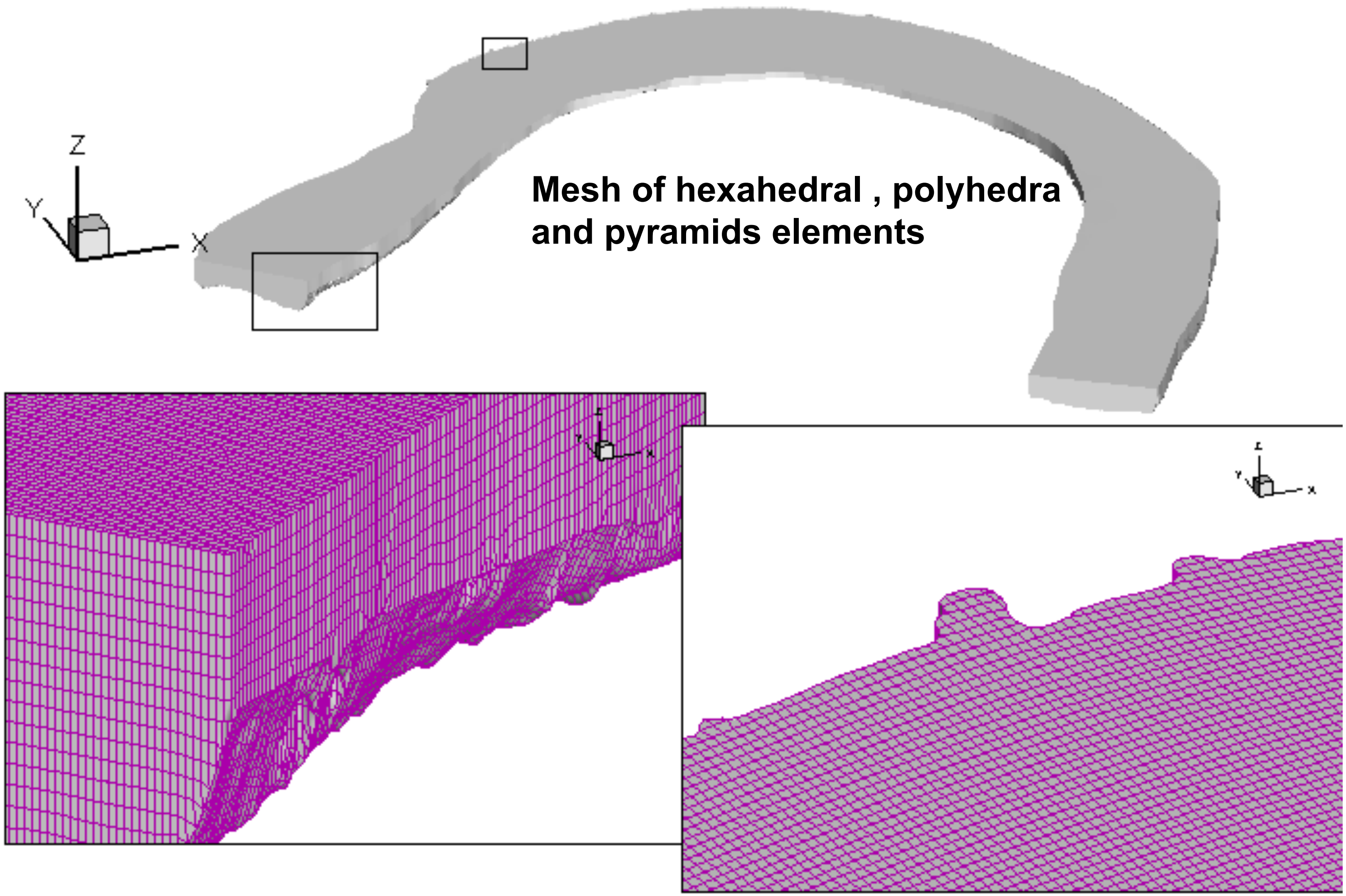

1) EXISTING CONDITION: Lidar (2011)+MBES (2012)

RESULTS

- Flow in 3D visualization (velocities)- cavities

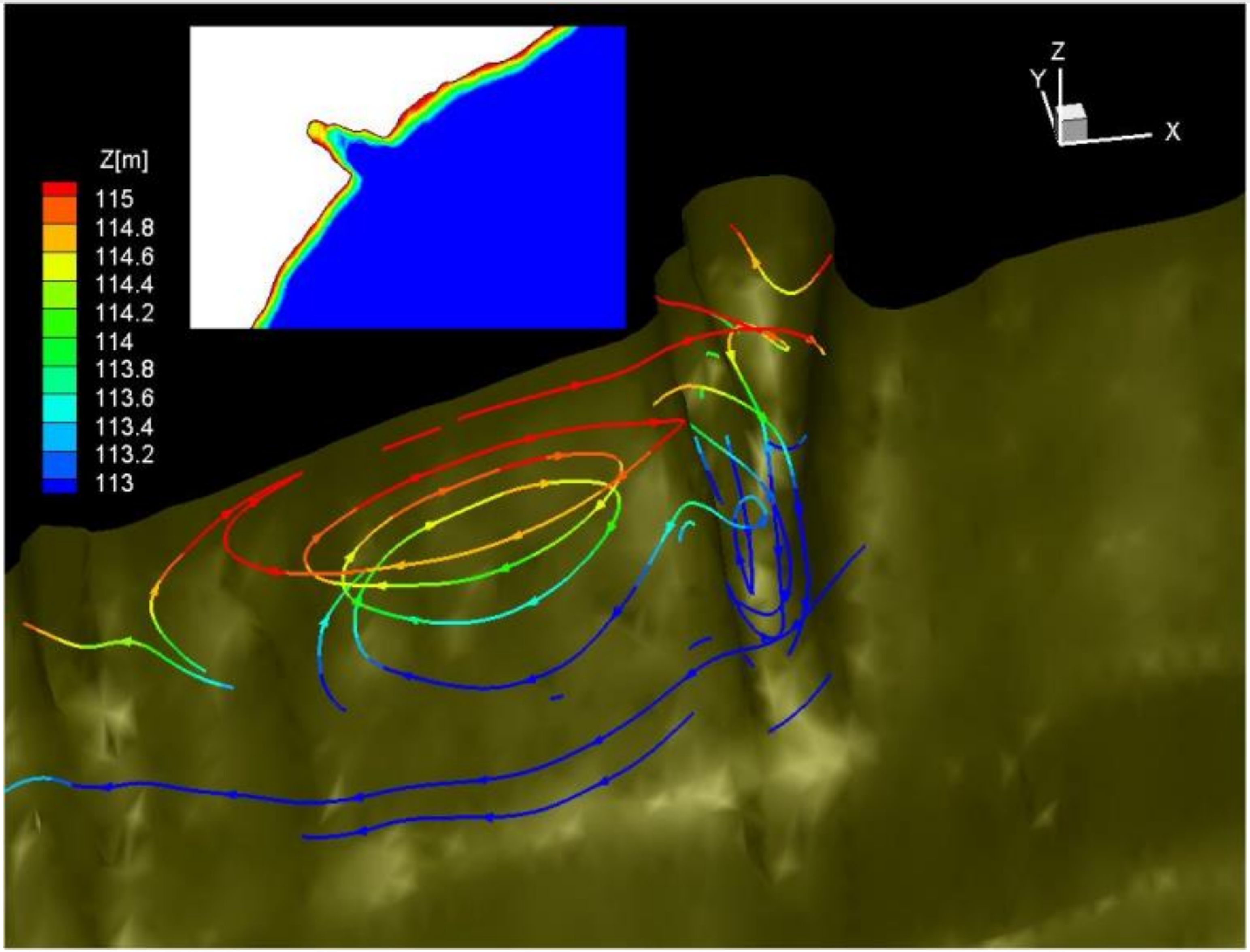

1) EXISTING CONDITION: Lidar (2011)+MBES (2012)

RESULTS

- Comparison between aDcp and Modeled (Umag, secondary flows, etc)

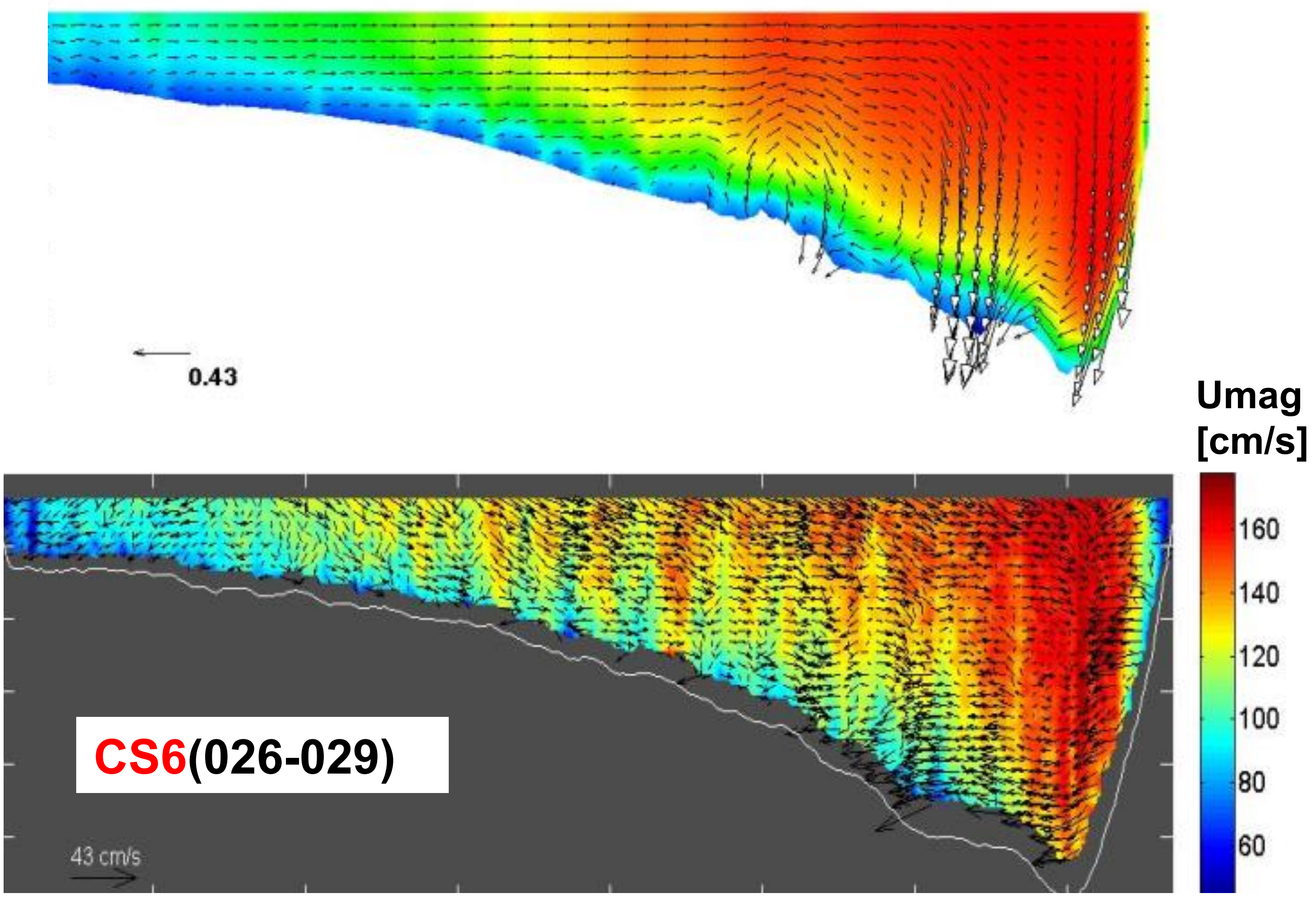

1) EXISTING CONDITION: Lidar (2011)+MBES (2012)

RESULTS

- Comparison between aDcp and Modeled (Umag, secondary flows, etc)

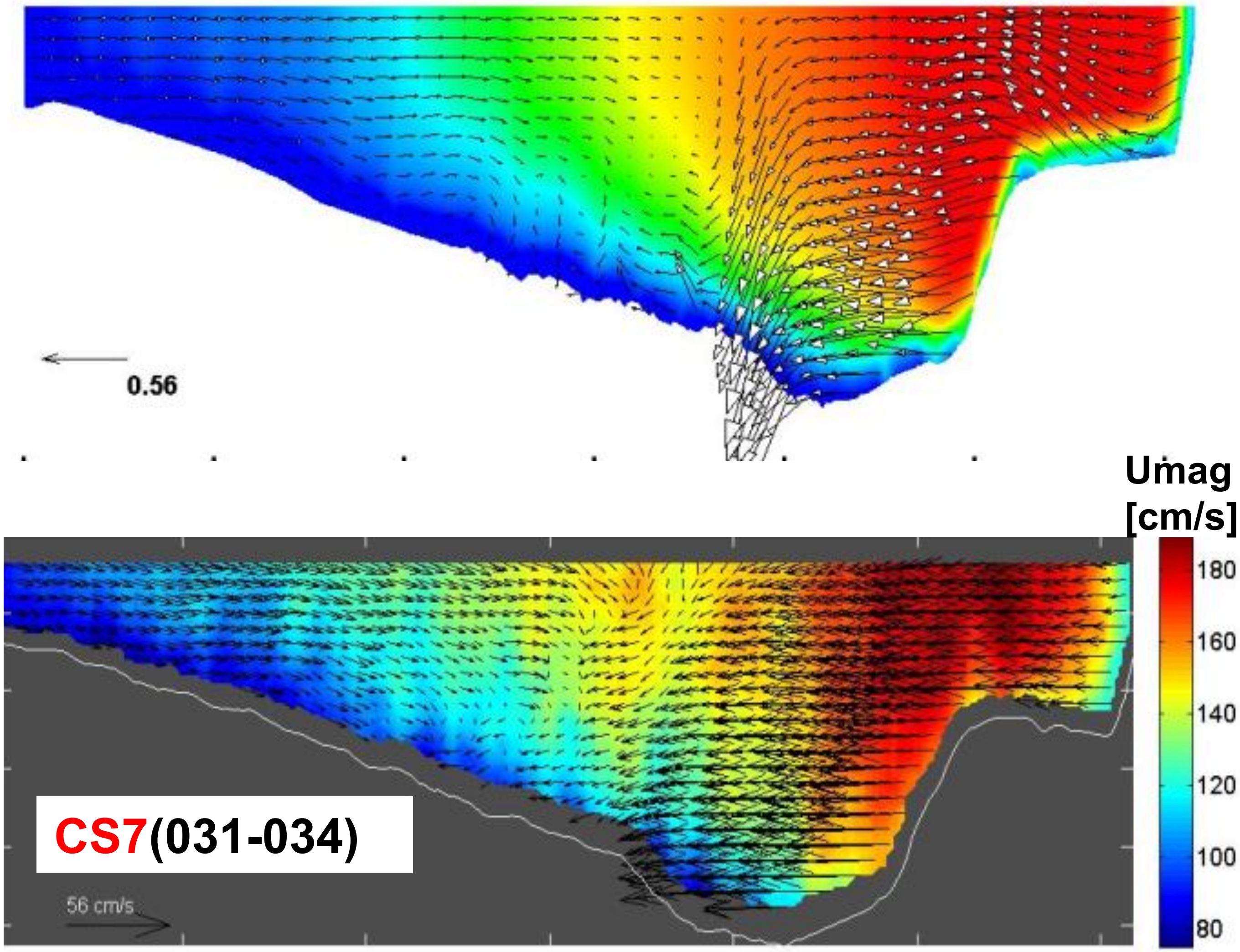

1) EXISTING CONDITION: Lidar (2011)+MBES (2012)

RESULTS

- <u>Comparison between aDcp and Modeled (Umag, secondary flows, etc)</u>

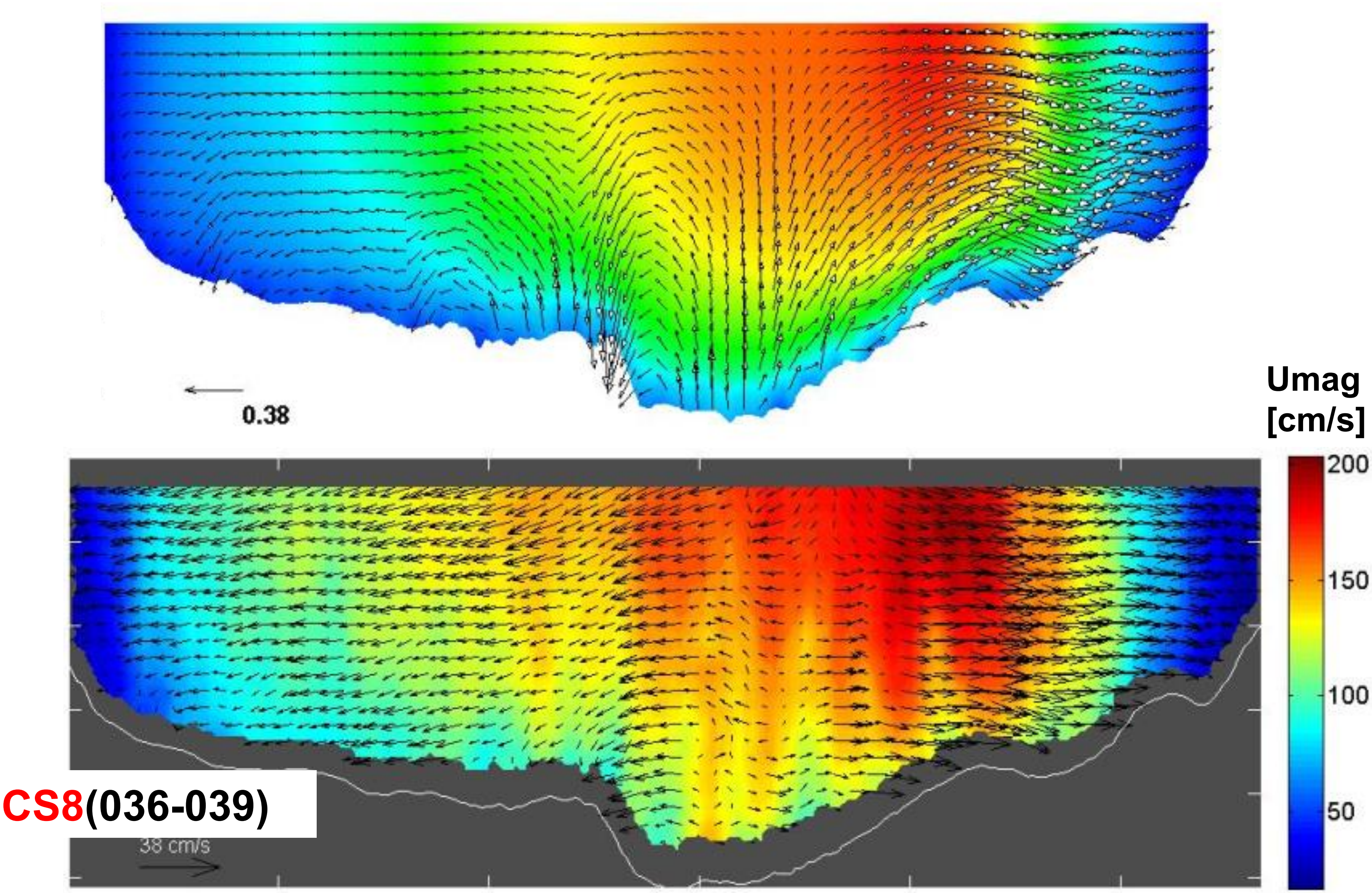

1) EXISTING CONDITION: Lidar (2011)+MBES (2012)

RESULTS

- Prediction of bed and bank shear stresses

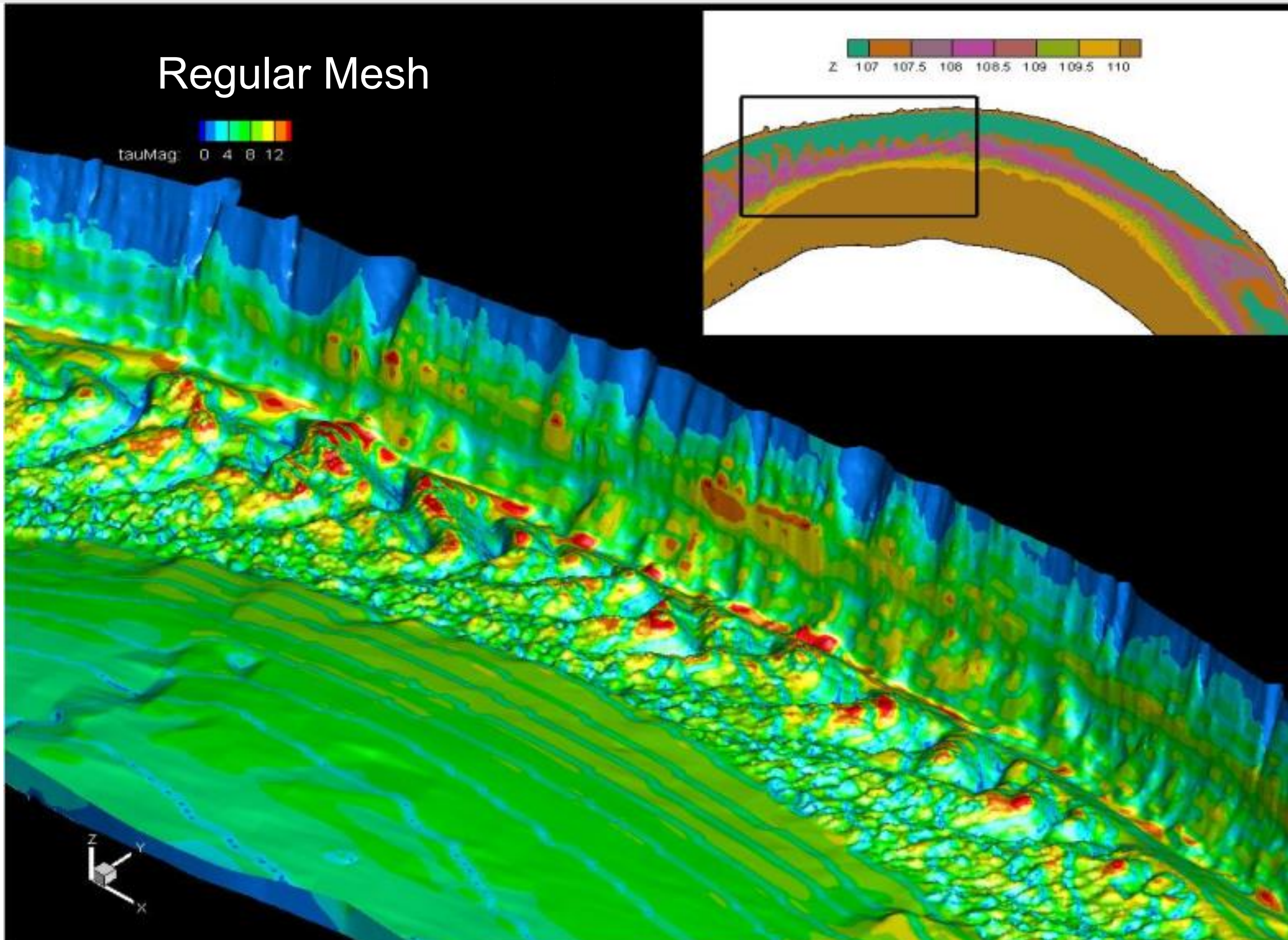

1) EXISTING CONDITION: Lidar (2011)+MBES (2012)

RESULTS

- Prediction of bed and bank shear stresses

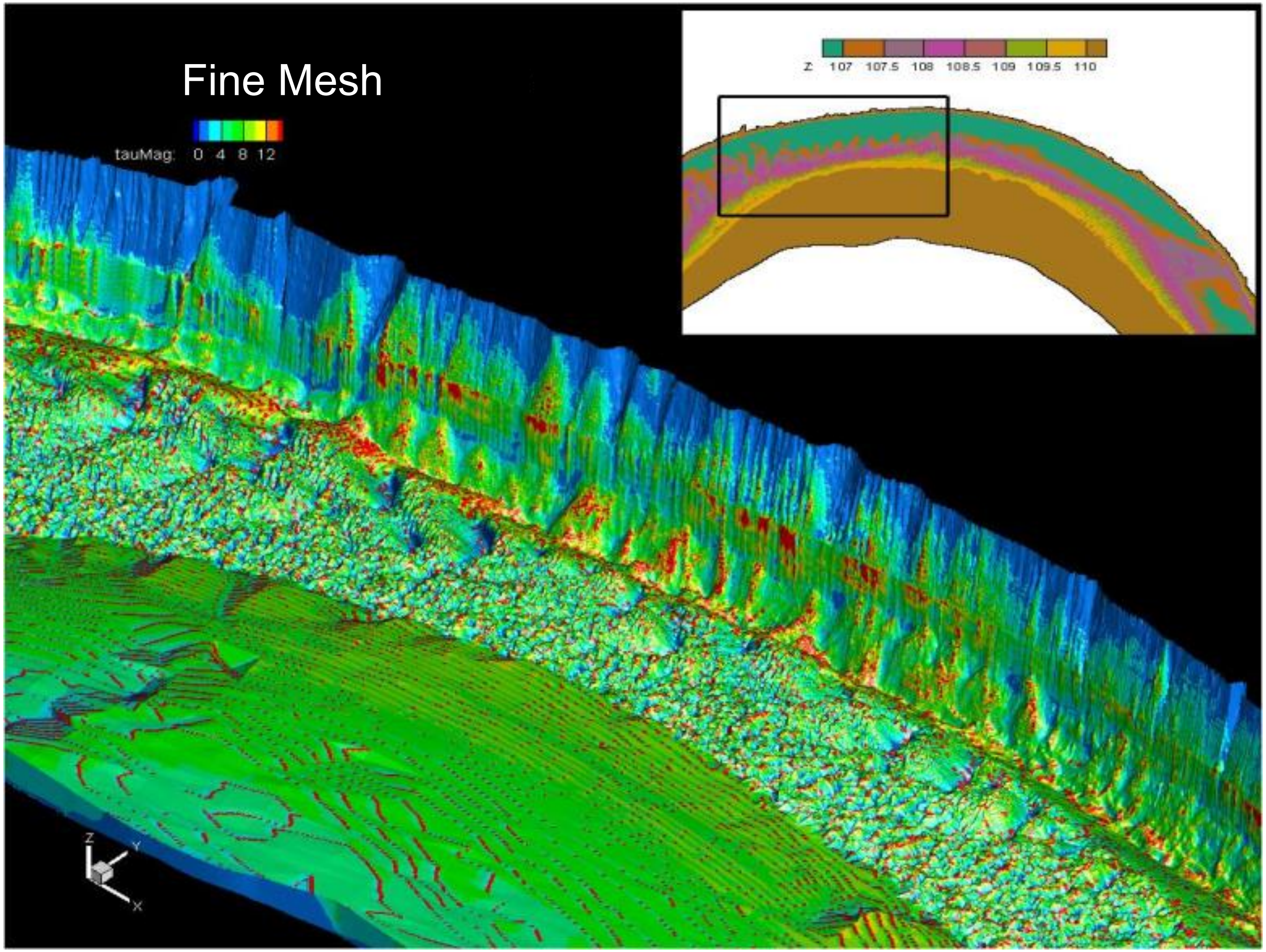

2) NO DUNES

Gutierrez et al. (2013) –JGR-ES

- Figure showing 1D wavelet

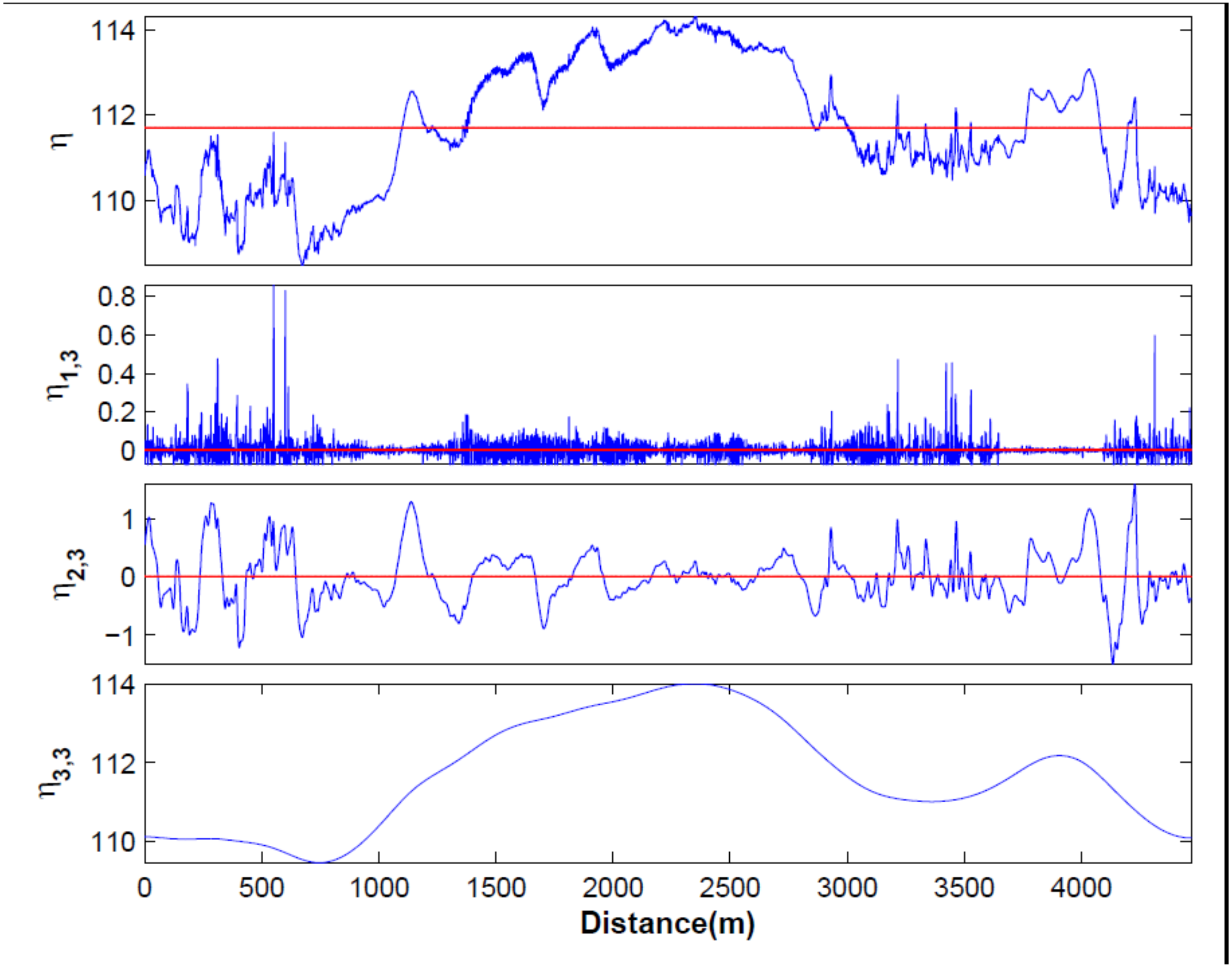

2) NO DUNES

Gutierrez et al. (2013) –JGR-ES

- Figure showing 3D bed – not working

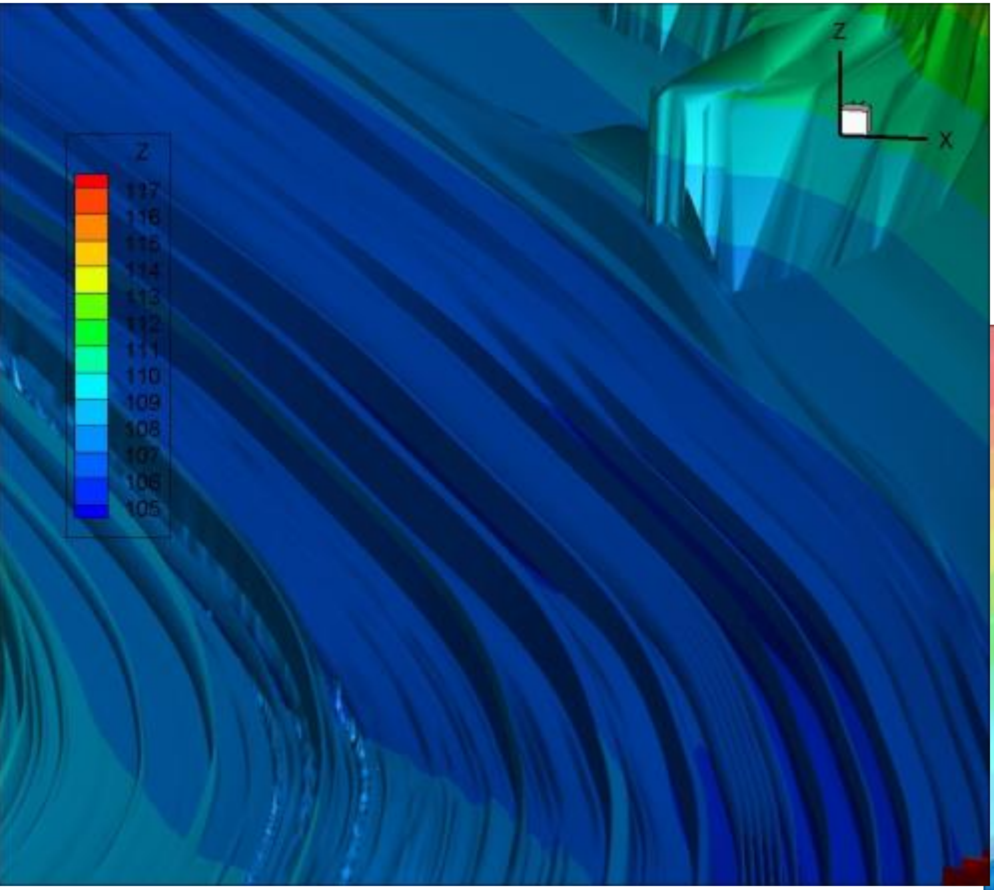

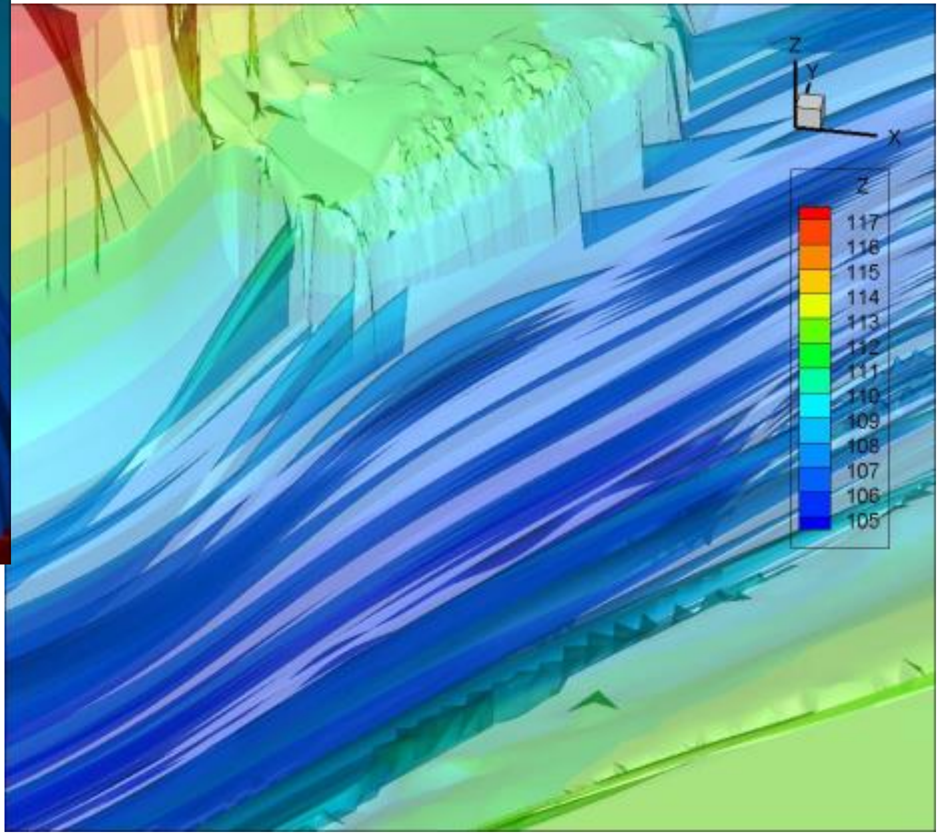

2) NO DUNES

Gutierrez et al. (2013) –JGR-ES

- Figure showing smoothed bed condition

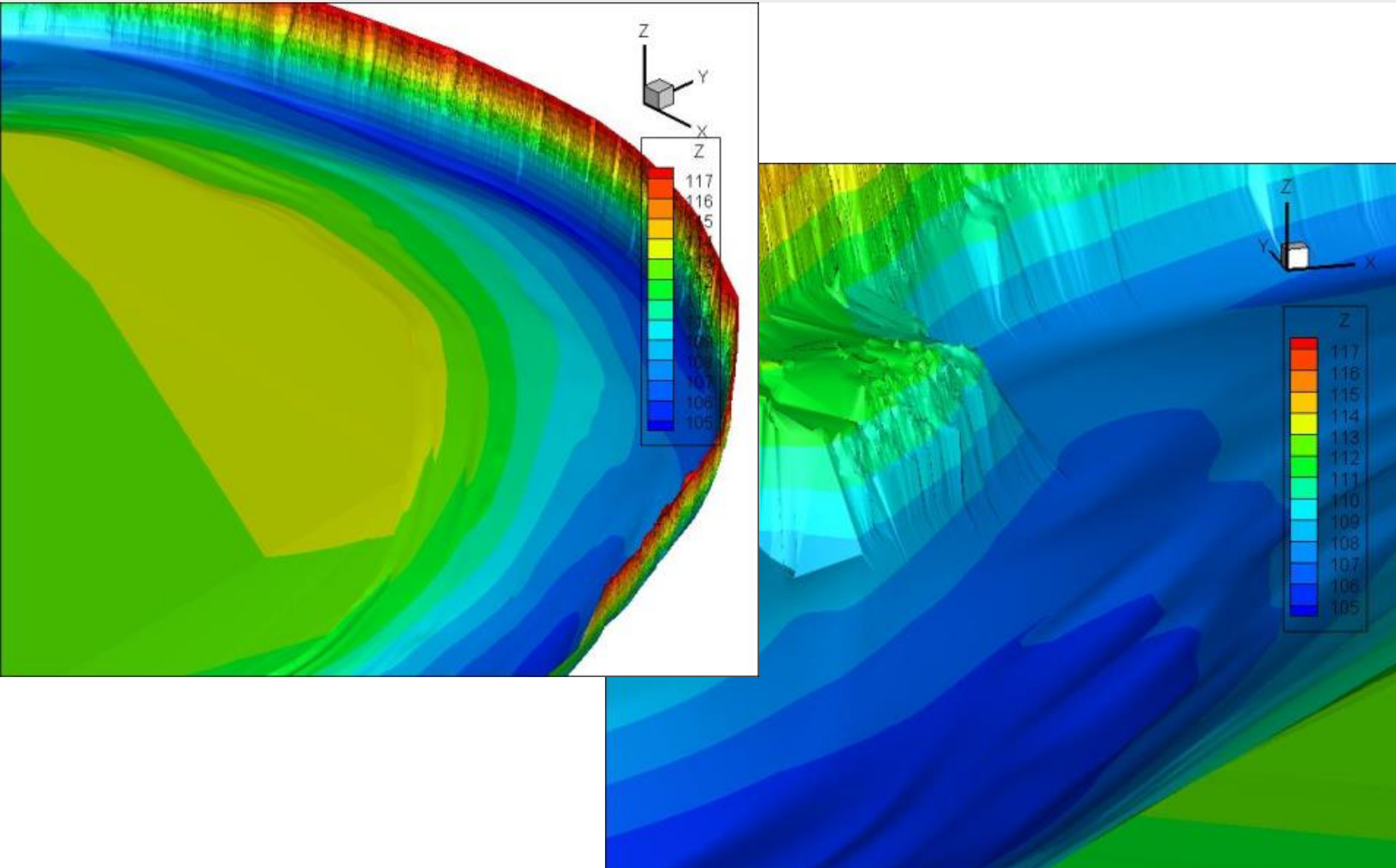

2) NO DUNES

Gutierrez et al. (2013) –JGR-ES

- Figure showing the mesh

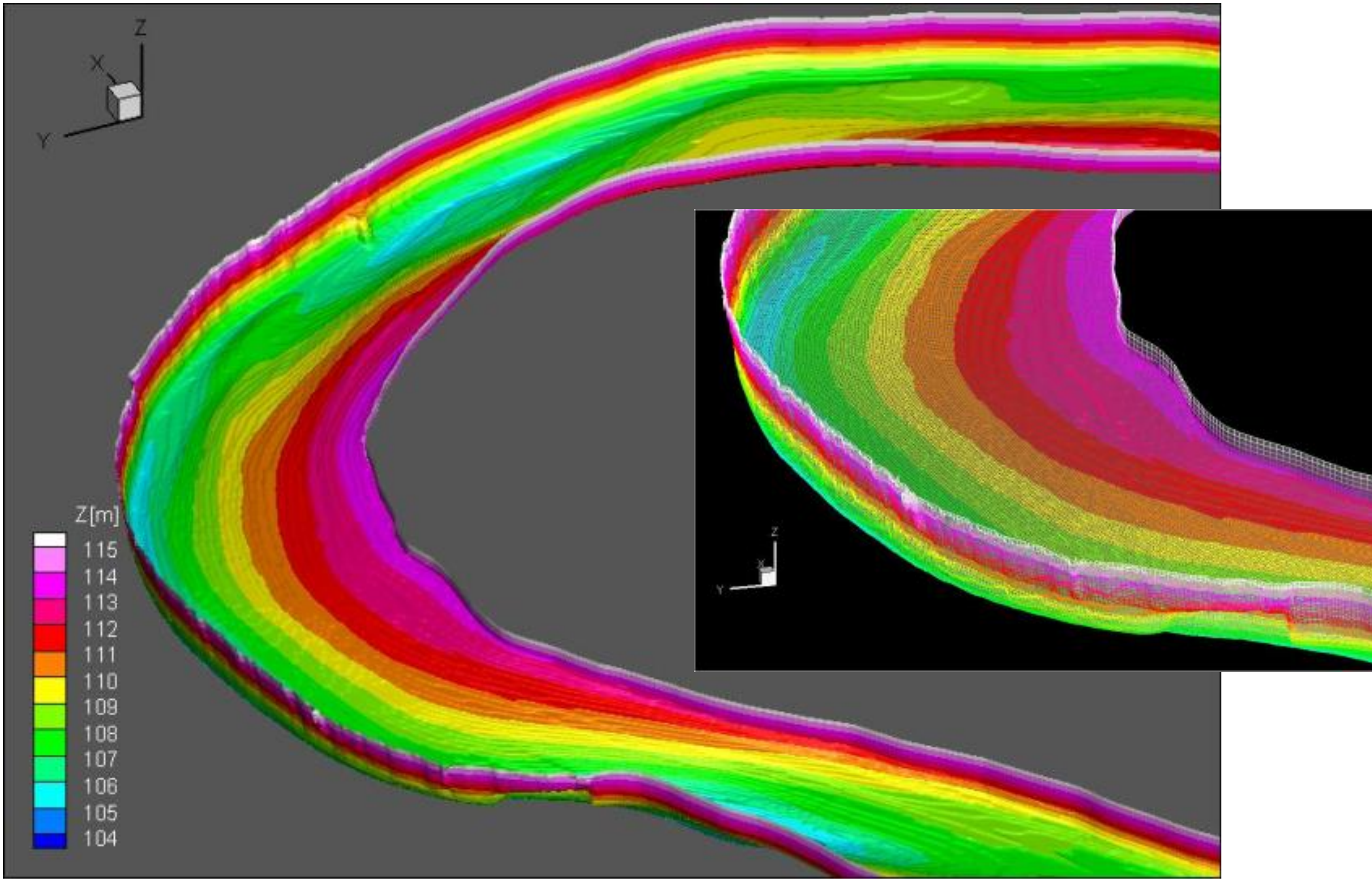

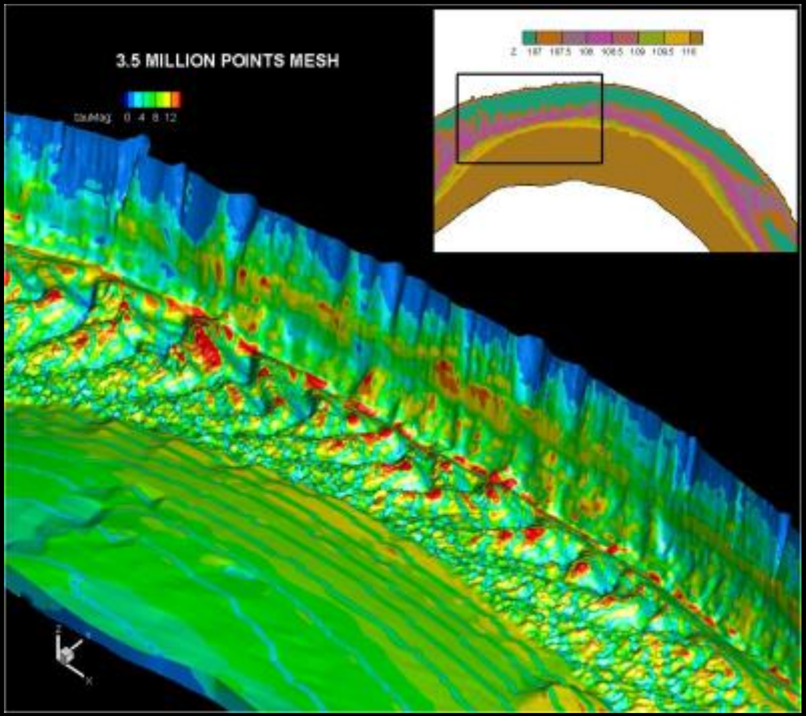
3.5 MILLION POINTS MESH
0 4 8 12

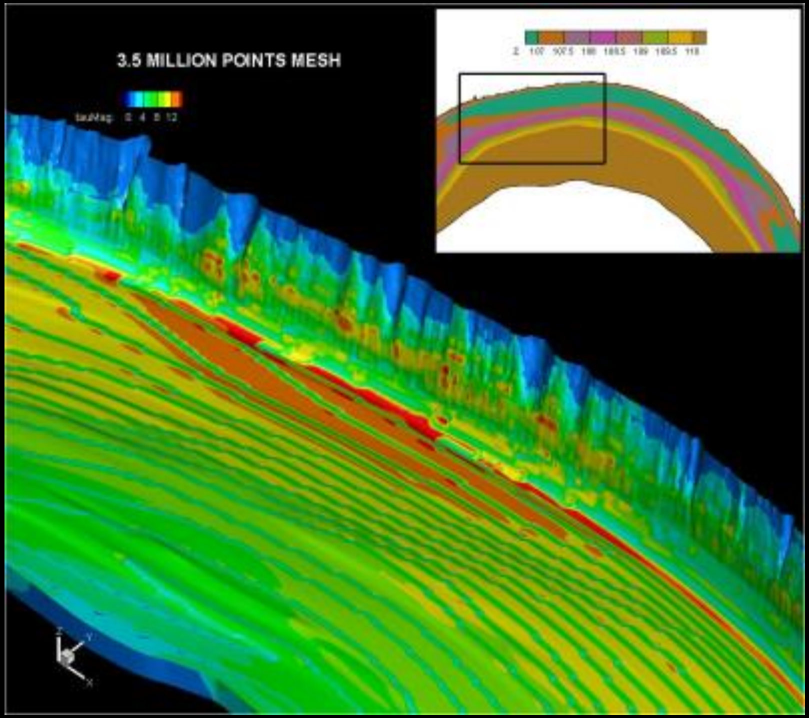
3.5 MILLION POINTS MESH
0 4 8 12

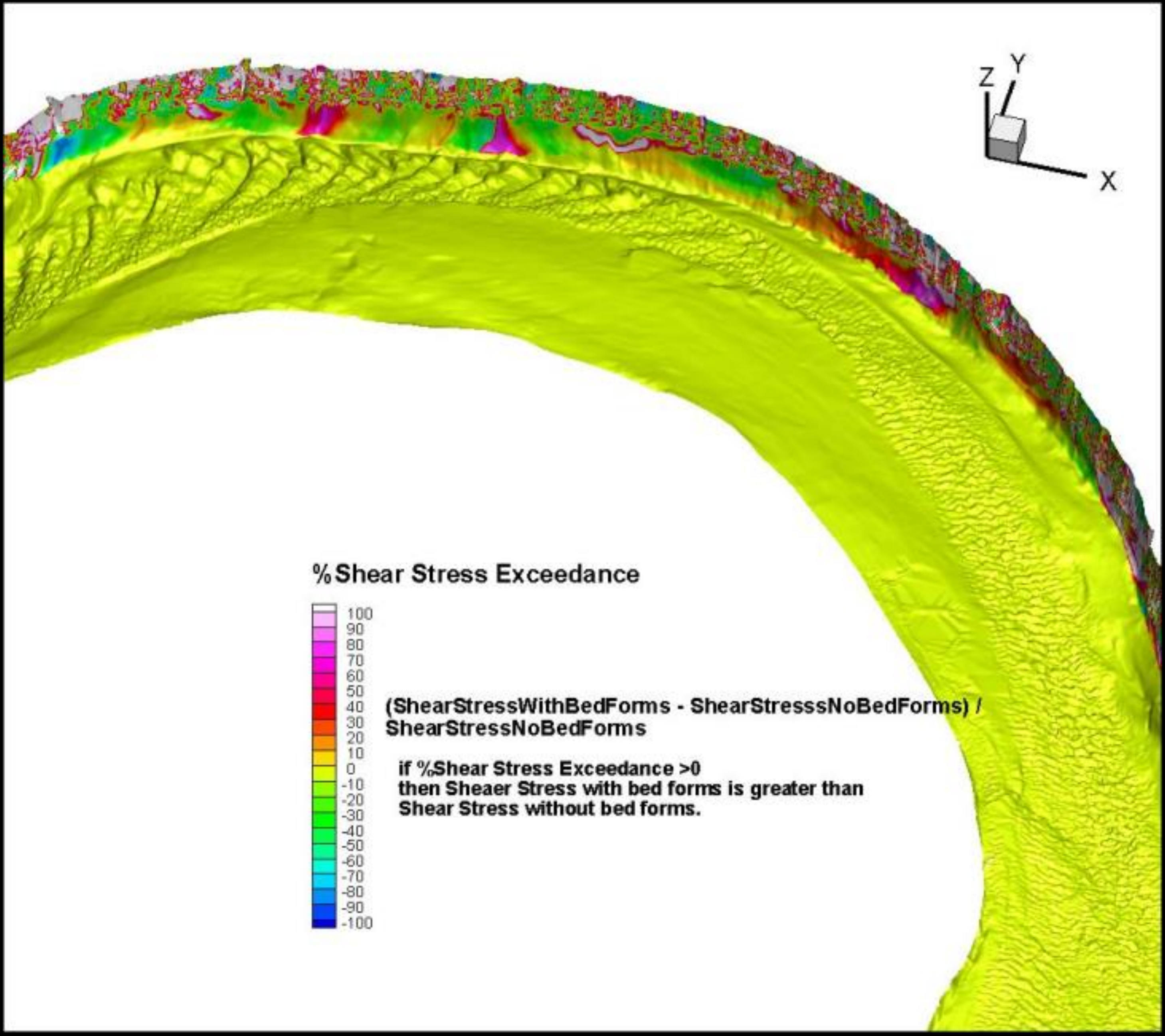

Z
Y
X
% Shear Stress Exceedance
100
90
80
70
60
50
40
30
20
10
0
-10
-20
-30
-40
-50
-60
-70
-80
-90
-100
(ShearStressWithBedForms - ShearStresssNoBedForms) / ShearStressNoBedForms
if %Shear Stress Exceedance >0
then Sheaer Stress with bed forms is greater than
Shear Stress without bed forms.

Steady + unsteady bed morphology

$$\eta(t) = \langle\eta\rangle + \eta'(t)$$

Dunes

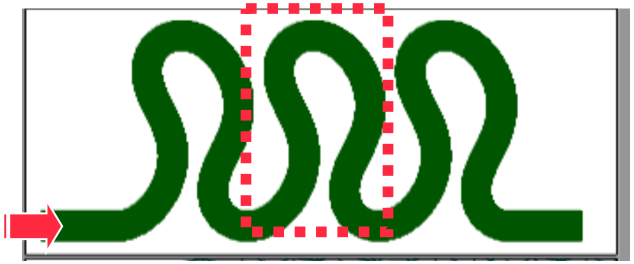

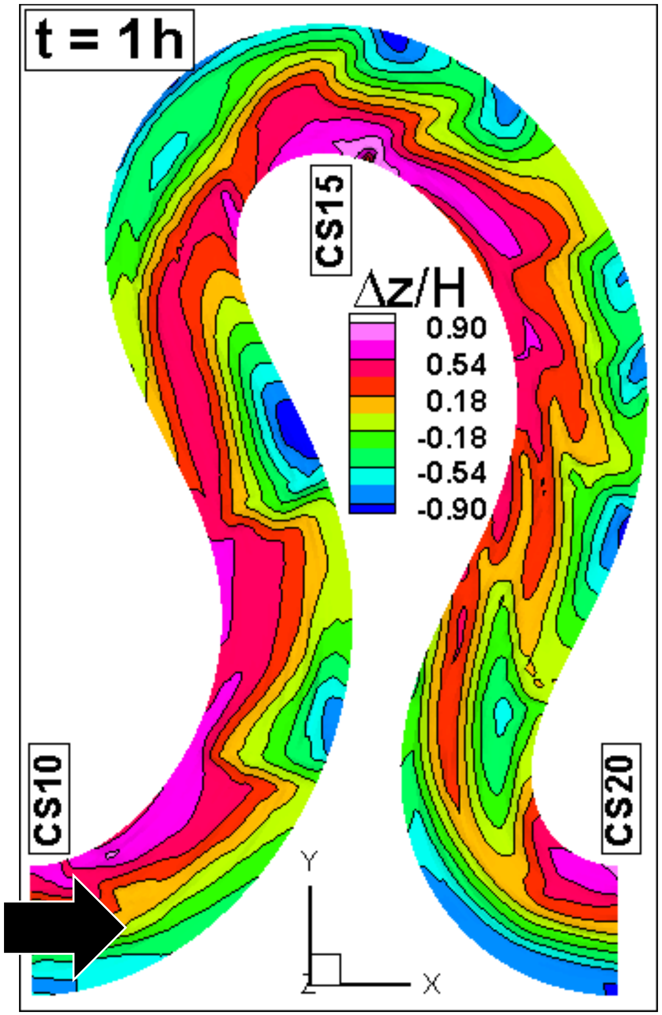

$\langle\eta\rangle$

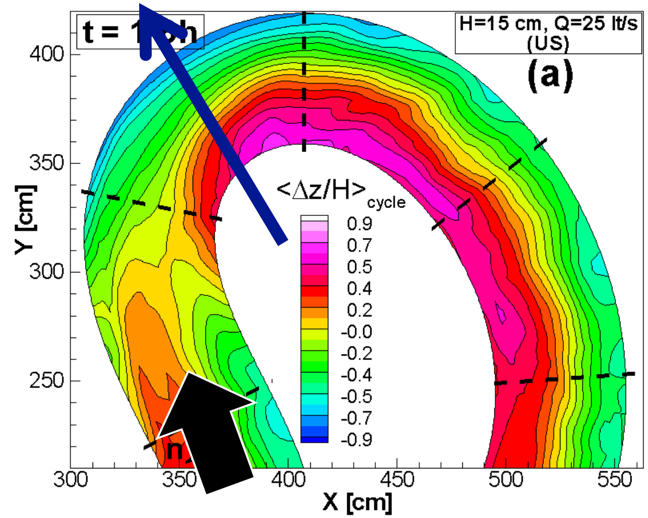

$\eta'(t)$

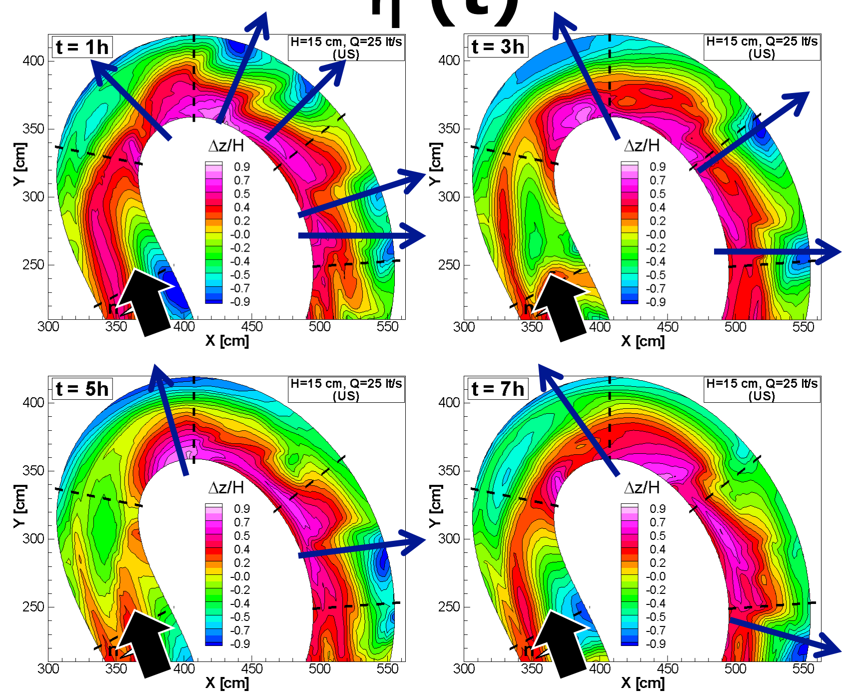

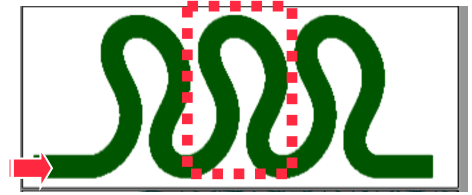

$$\eta(t) = \langle\eta\rangle + \eta'(t)$$

Bed profiles at centerline

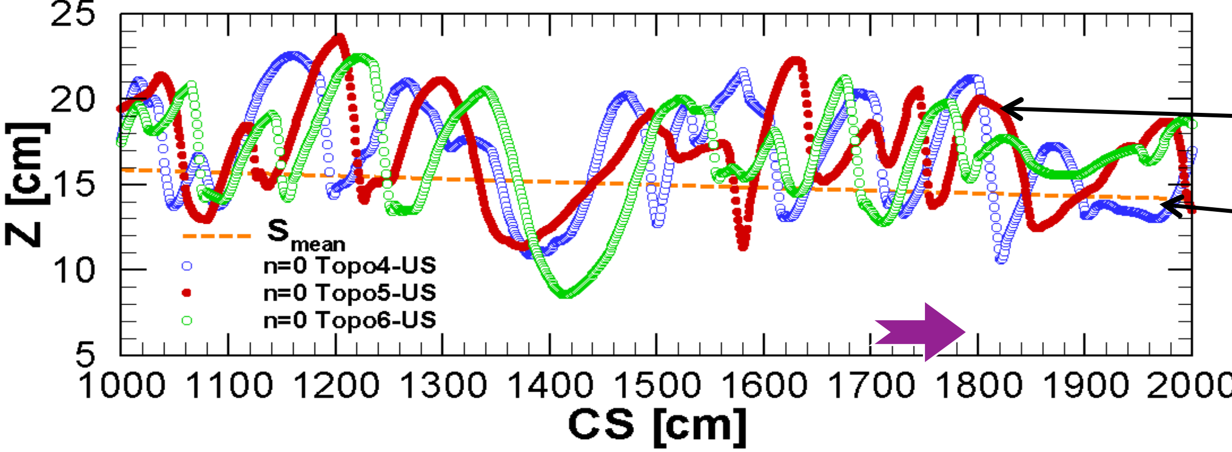

$\eta'(t)$

$\langle\eta\rangle$

$$q_b(t) = \langle q_b\rangle + q_b'(t)$$

Bed load fluxes

q_b'

$\langle q_b\rangle$

$\langle q_b\rangle \sim 9.68E\text{-}07\ m^2/s$

Steady (Point bars)
+ perturbed components (bars)

TOUR OF BEDFORMS IN RIVERS: ALTERNATE BARS

Alternate bars occur in rivers with sufficiently large (> ~ 12), but not too large width-depth ratio B/H. Alternate bars migrate downstream, and often have relatively sharp fronts. They are often precursors to meandering. Alternate bars may coexist with dunes and/or antidunes.

Alternate bars in the Naka River, an artificially straightened river in Japan. Image courtesy S. Ikeda.

BEDFORMS IN THE LABORATORY AND FIELD: ALTERNATE BARS

Alternate bars in a flume in Tsukuba University, Japan: flow turned low. Image courtesy H. Ikeda.

Alternate bars in the Rhine River between Switzerland and Lichtenstein. Image courtesy M. Jaeggi.

BEDFORMS IN THE LABORATORY AND FIELD: MULTIPLE-ROW (LINGUOID) BARS

Linguoid bars in a flume in Tsukuba University, Japan: flow turned off. Image courtesy H. Ikeda.

Linguoid bars in the Fuefuki River, Japan. Image courtesy S. Ikeda.

Designing the experiments: Obtaining β_C and β_R → Sediment transport

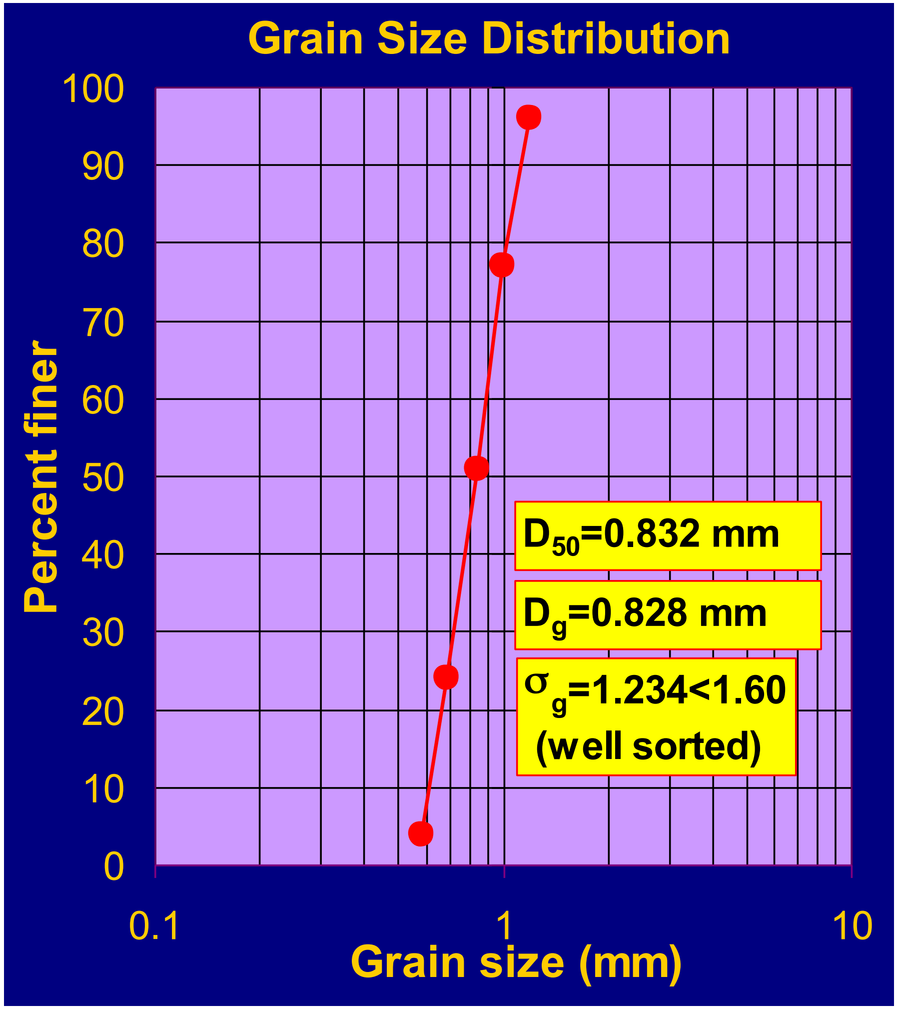

ρ_s=2566.5 Kg/m^3

λ_p=0.4

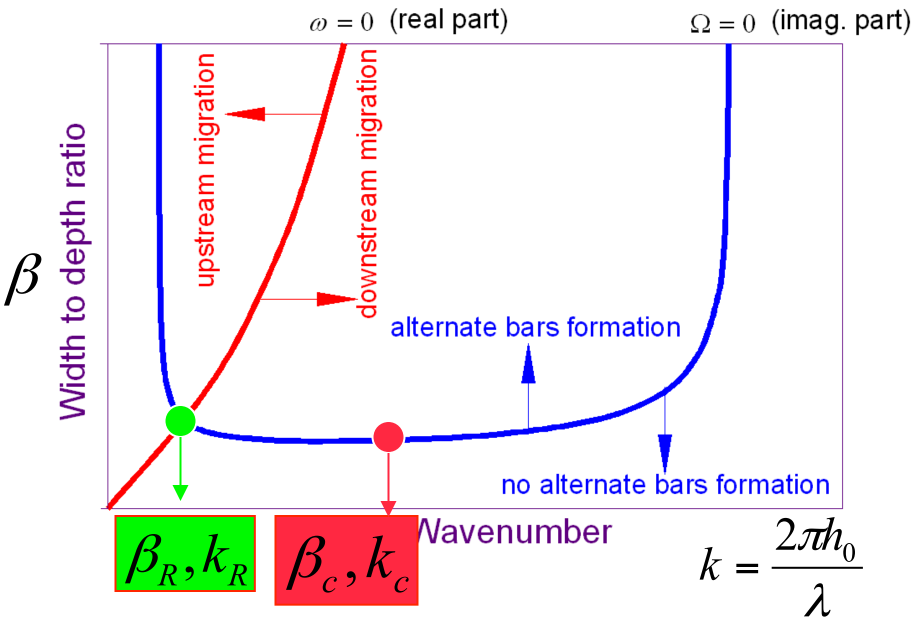

$$q^* = \alpha\left(\phi_s \tau^* - \tau_c^*\right)^{n_e}$$

Free bars regime

Free bars in straight channels

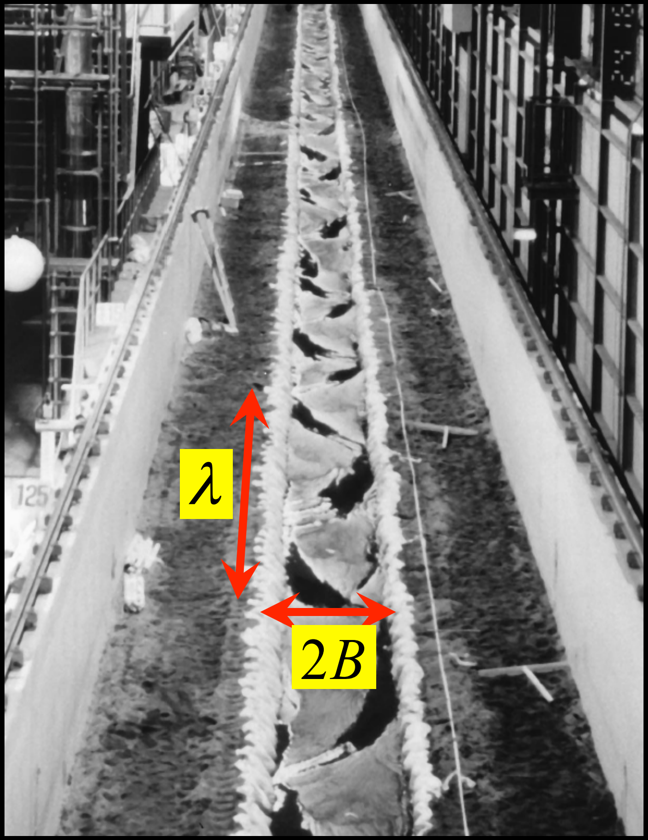

Lisle et al. (1997)

Free bars in HAMC

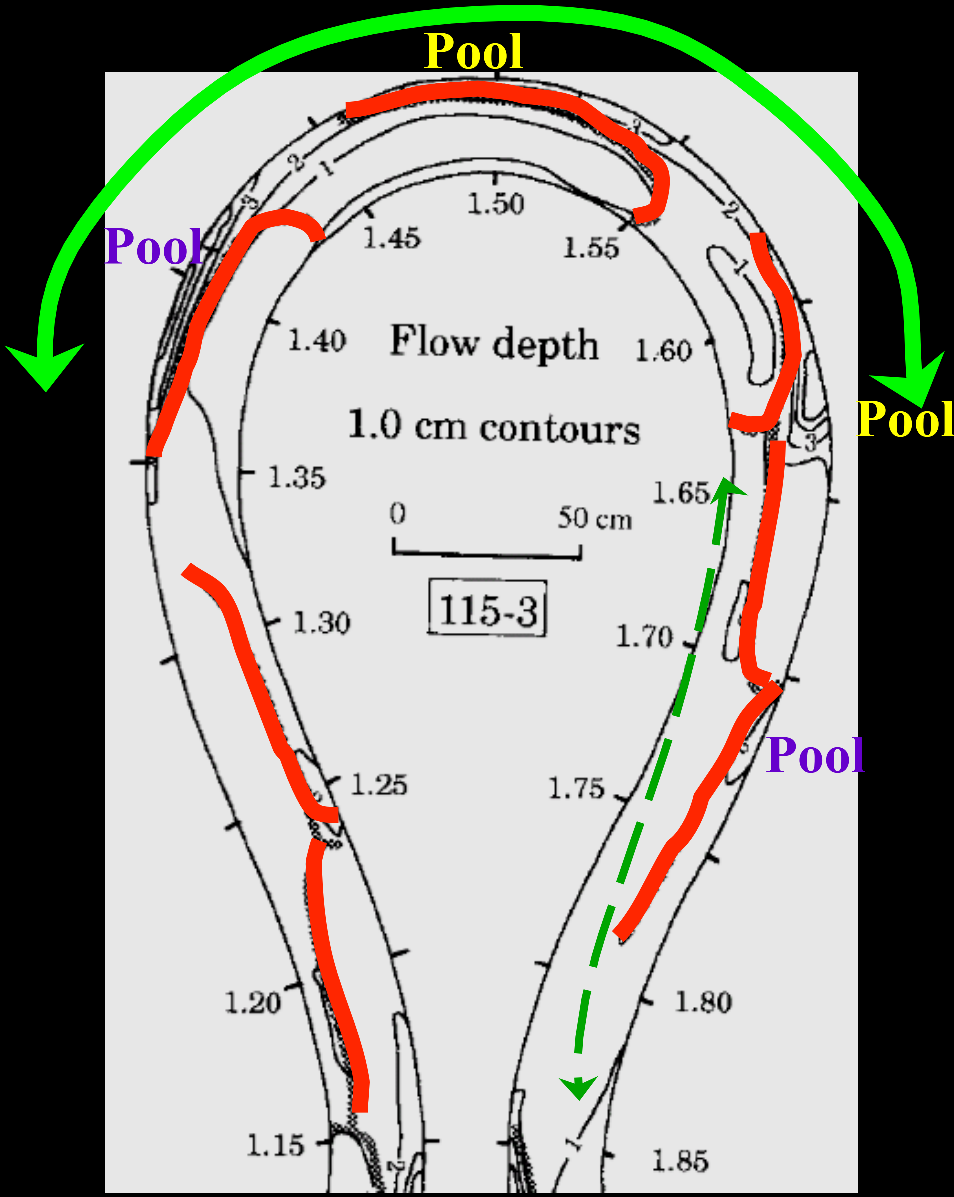

Whiting and Dietrich (1993)

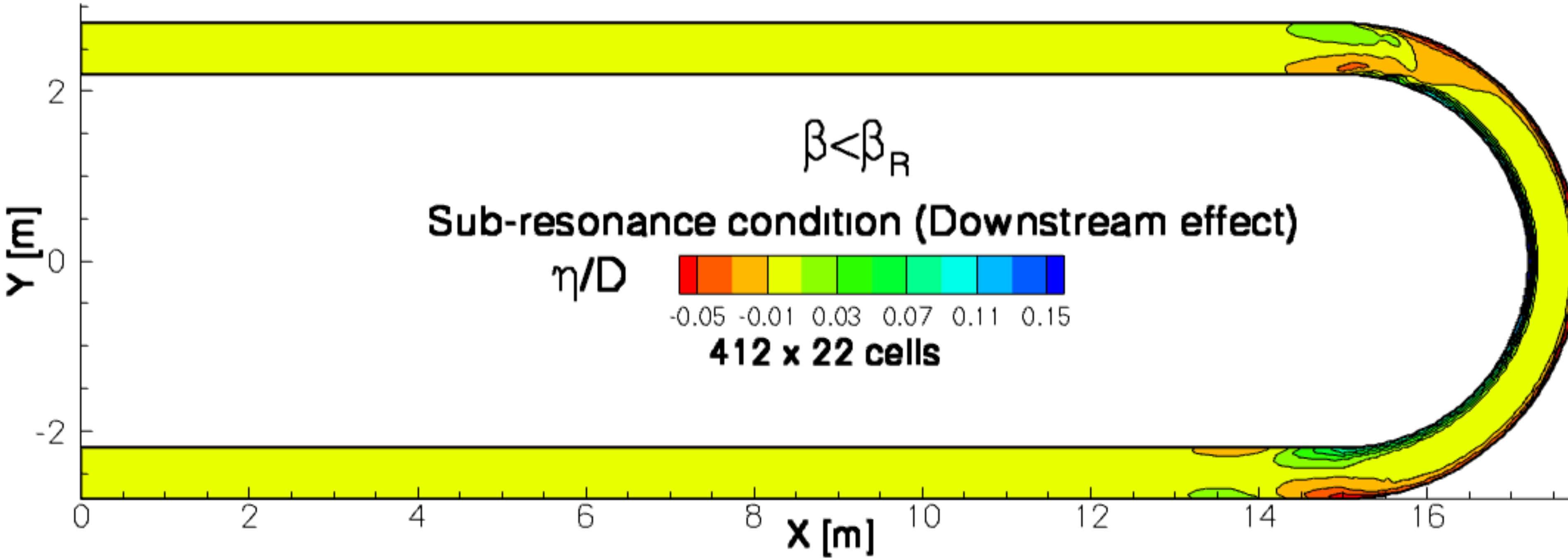
β<β_R
Sub-resonance condition (Downstream effect)
η/D
-0.05 -0.01 0.03 0.07 0.11 0.15
412 x 22 cells
Y [m]
X [m]
0 2 4 6 8 10 12 14 16
2 0 -2

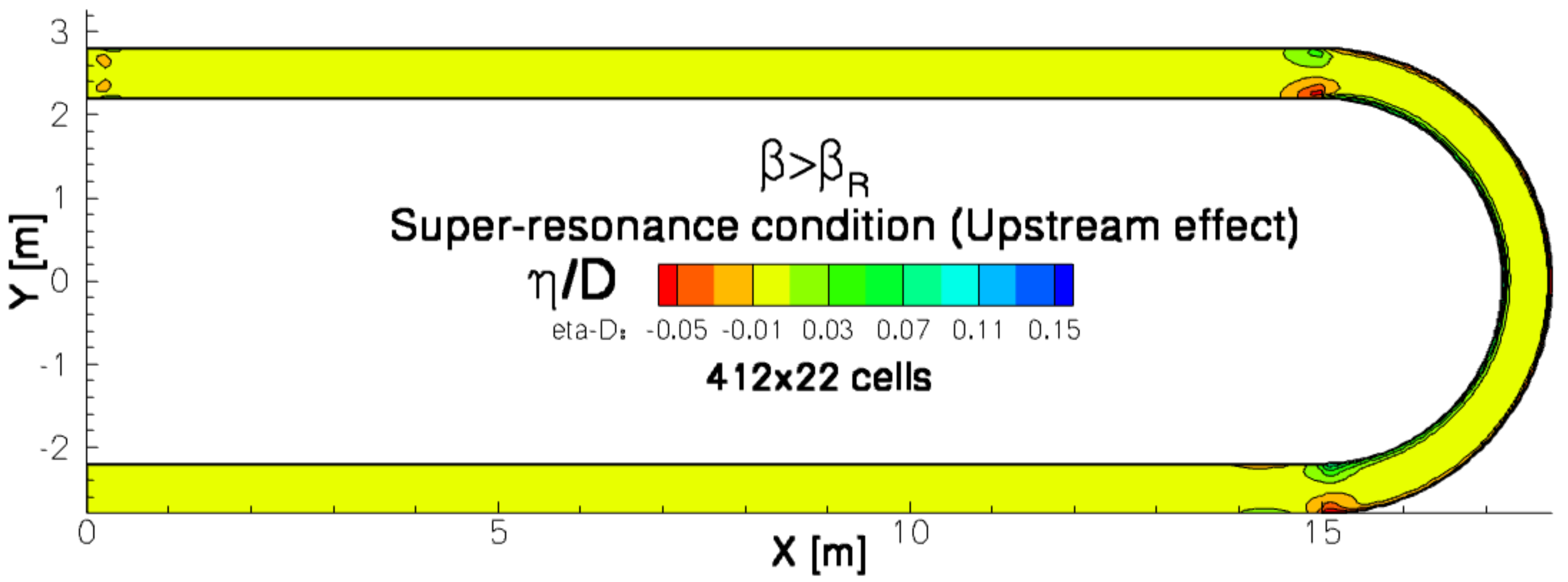
β>β_R
Super-resonance condition (Upstream effect)
η/D
eta-D: -0.05 -0.01 0.03 0.07 0.11 0.15
412x22 cells
Y [m]
X [m]
0 5 10 15
3 2 1 0 -1 -2

Modeling of forced and free bars
Alejandro Mendoza (Postdoc)

Point bars

Free bars

Tools 2D 3D

- Telemac-Mascaret
  http://www.opentelemac.org/
- Mike 21C
  http://mikebydhi.com/Products/WaterResources/MIKE21C.aspx
- Delft 3d
  http://www.deltaressystems.com/hydro/product/621497/delft3d-suite

Bed Morphology

- Telemac-2D
  - Solves St. Venant equations
  - Utilizes FEM in irregular grids
- Sisyphe
  - Computes sediment transport with empirical formulas
  - Applies corrections for bed/bedforms effects and secondary flows when using Telemac-2D

Hooke experiments

FORCED BARS

Hooke experiments

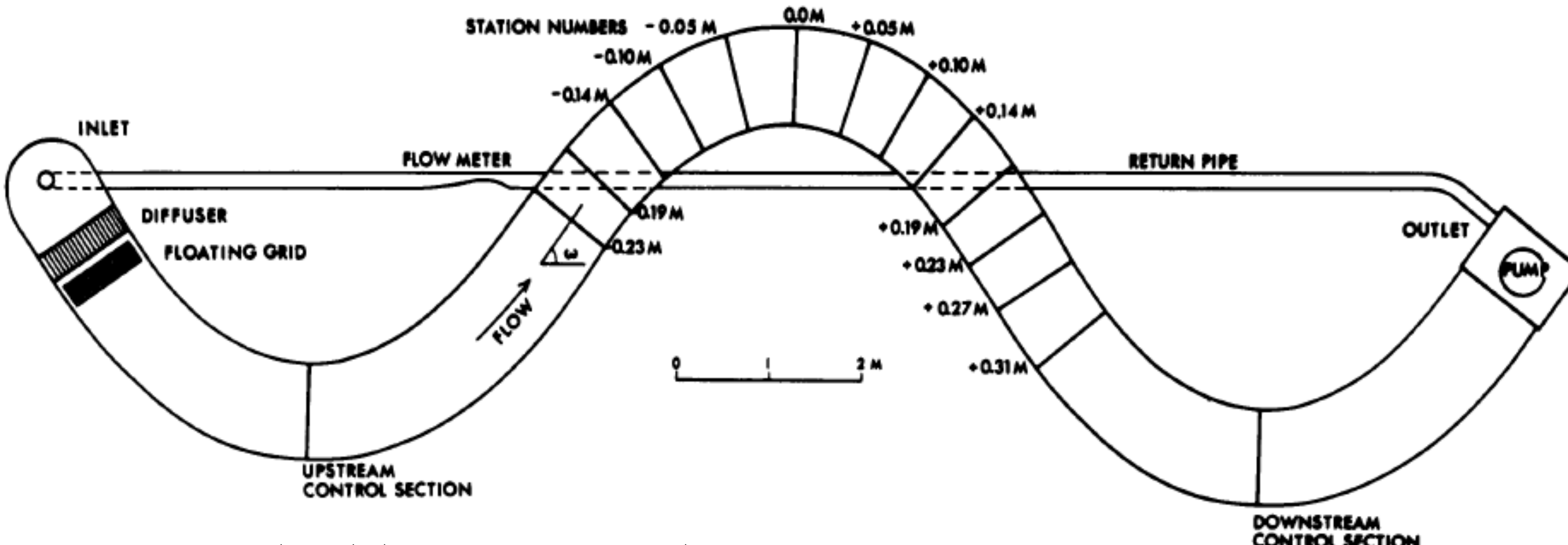

After Hooke (1975) (Journal of Geology)

Experiments

- Q = [10-50.5] l/s
- Recirculated sediment
- diameter = 0.30 mm
- Density = 2700 kg/m3

Mesh and Boundary Conditions

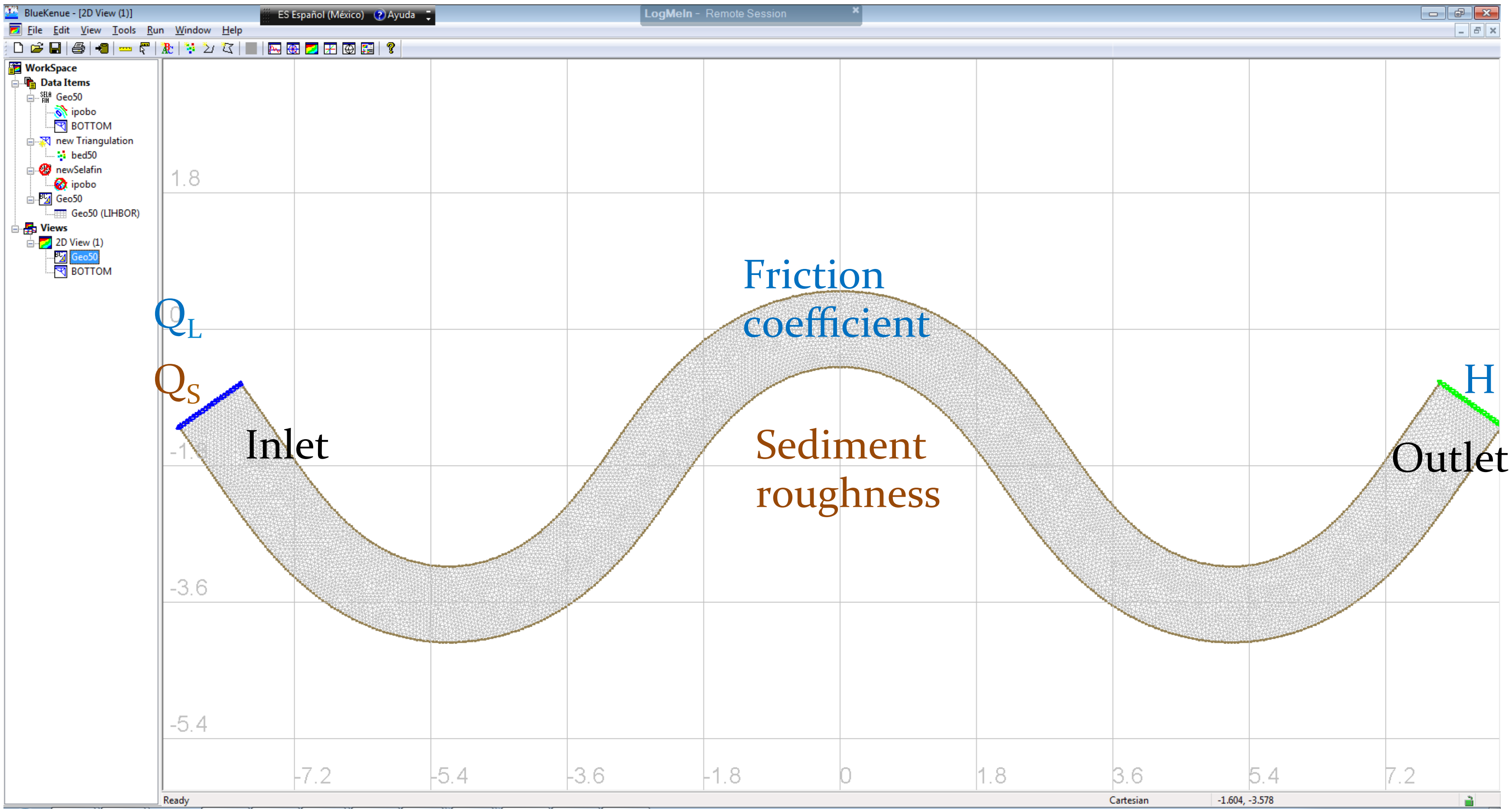

Sediment transport

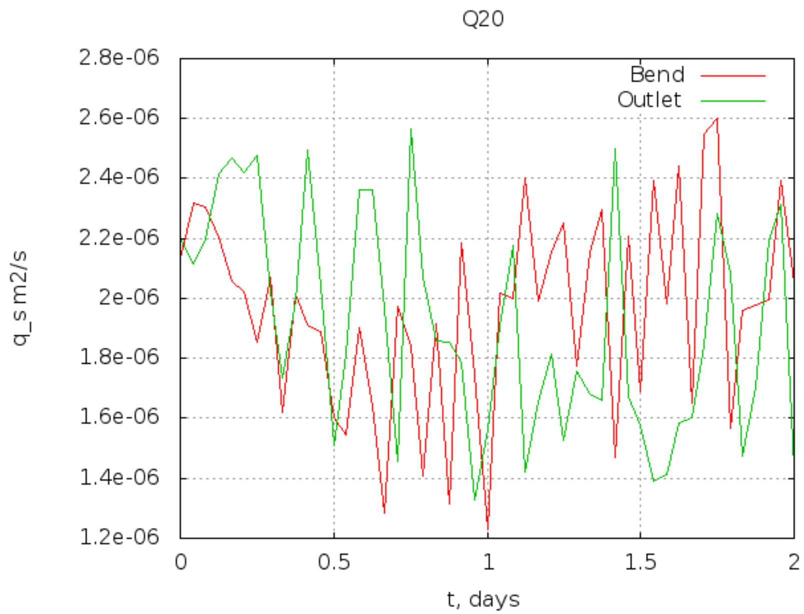

- q_s = 2E-6 m^2/s (from experiments)
- Calibration using different equations
- Roughness of sediment particles
- Use of corrections for bed slope and particle trajectory

Q=20 l/s

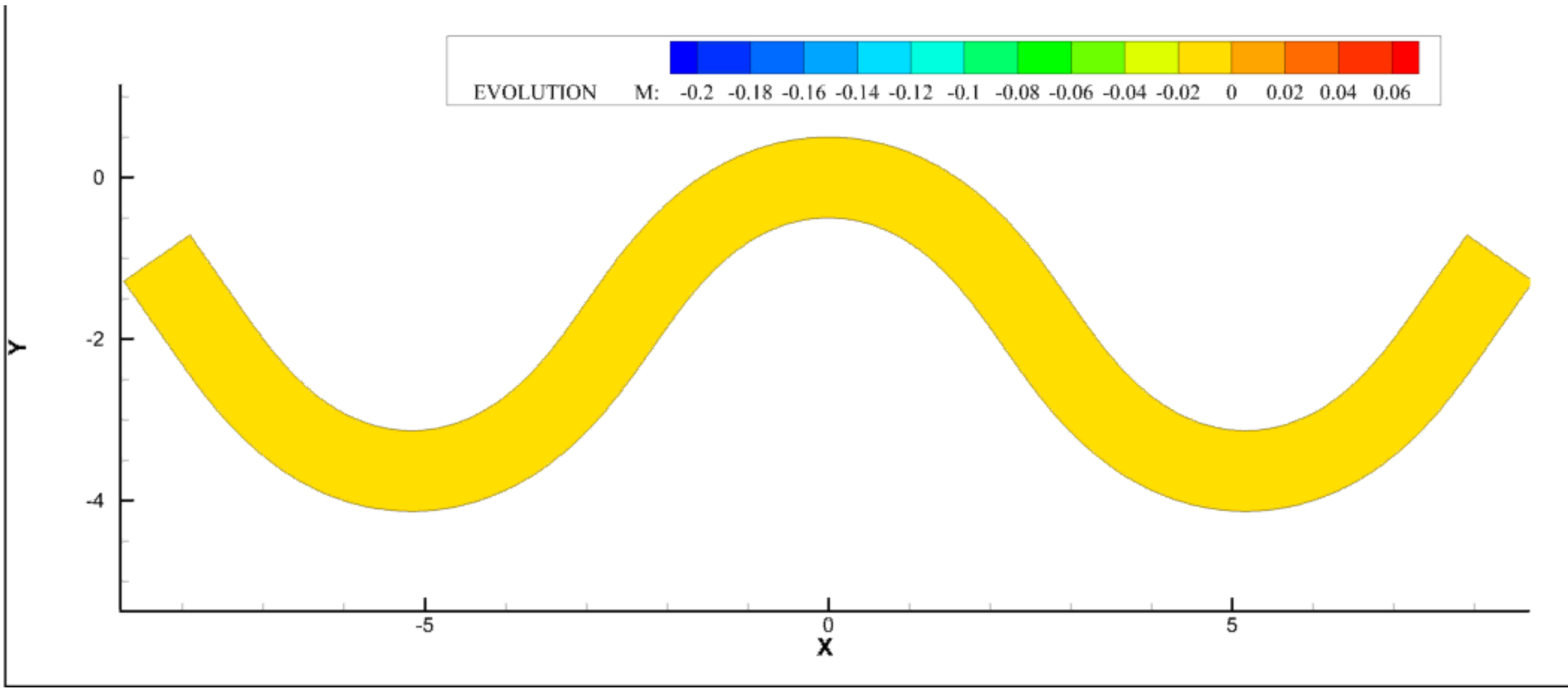
EVOLUTION
M: -0.2 -0.18 -0.16 -0.14 -0.12 -0.1 -0.08 -0.06 -0.04 -0.02 0 0.02 0.04 0.06
Y
0
-2
-4
X
-5
0
5

Q=50.5 l/s

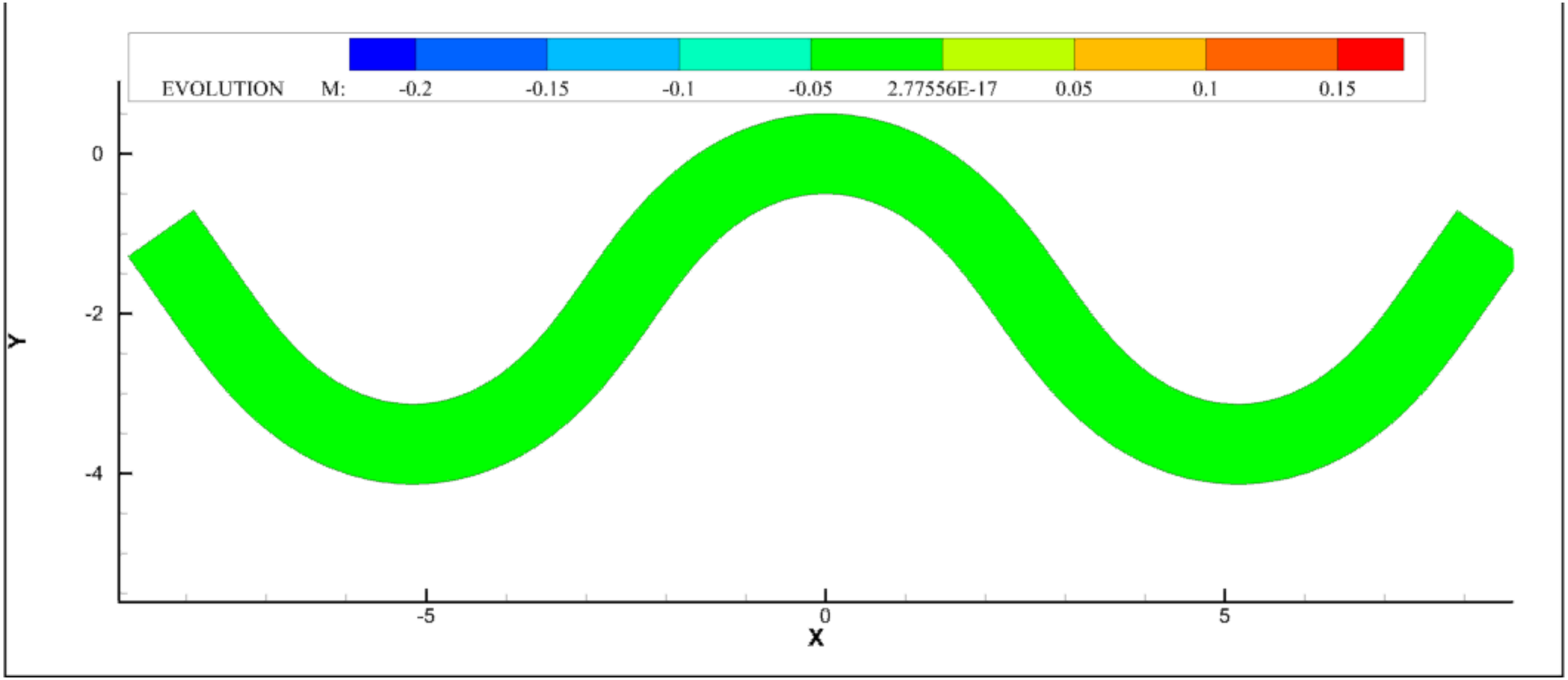

Results for Q=20 l/s

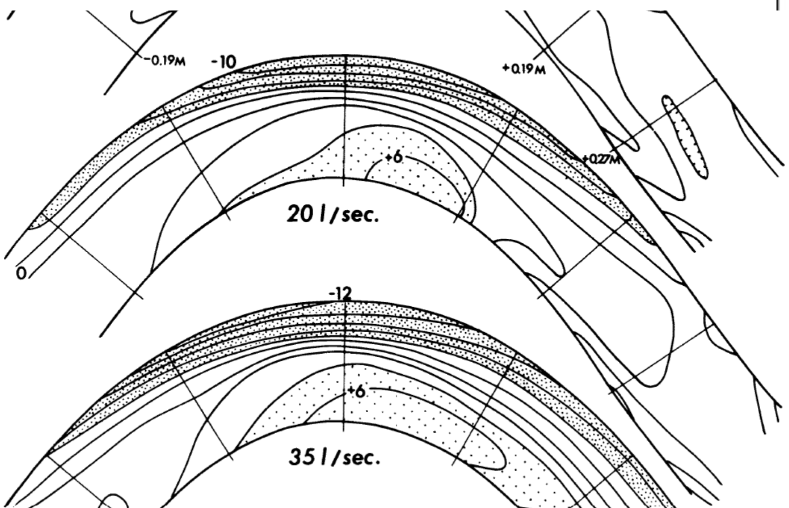

Hooke (1975) (Journal of Geology)

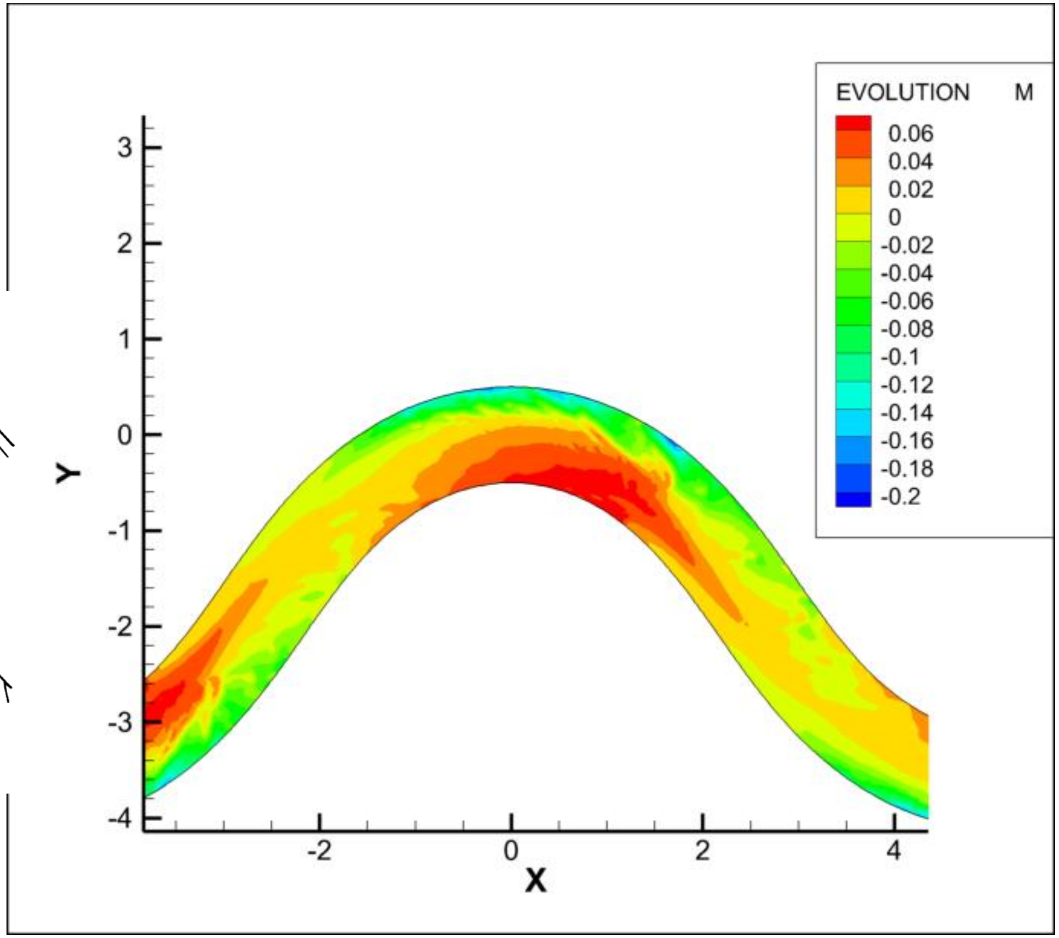

Lanzoni Experiments

FREE BARS

Lanzoni (2000a) WRR

- Development of alternate bars in ripple and/or covered beds
- Flume 55 m long 1.5 m wide
- Sediment recirculation,
- $Qs = 1.05E\text{-}5\ m^2/s$ (converted from $Qs = 94.5$ l/h pores included)
- Sediment characteristics
  - $d = 0.48$ mm
  - $\rho = 2650$ kg/m3
  - $Q = [25\text{-}47]$ l/s

More experiments for free bars

- Modeling is done with Telemac-2D and Sisyphe
- Equation selected was Meyer-Peter and Mueller. Since Telemac computes $\mu = c'_f / c_f$ with c'_f from skin friction calculated with Nikuradse, the sediment transport in Sisyphe was calibrated with $k_s = 3.6 D_{50}$

Sediment recirculation

Q= 30 l/s
Initial perturbation: Bump in the inlet

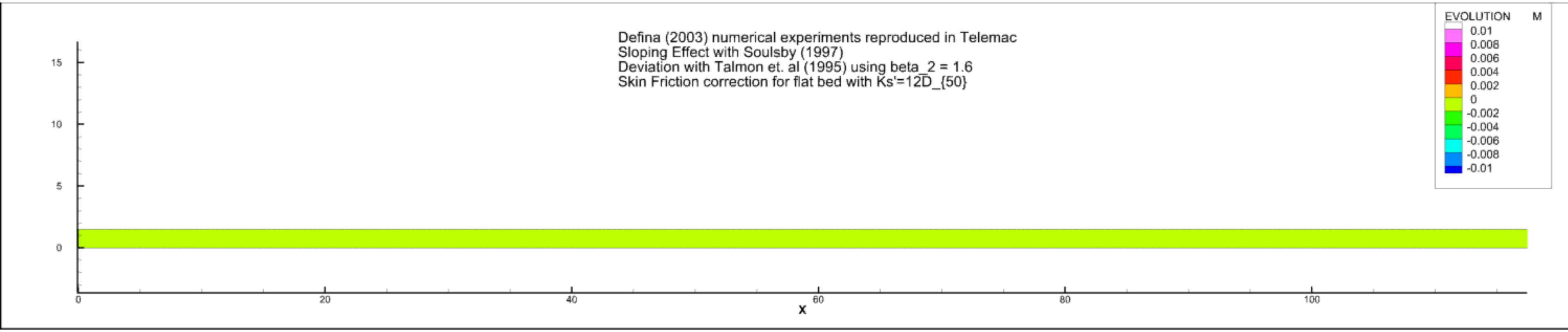

Bed evolution

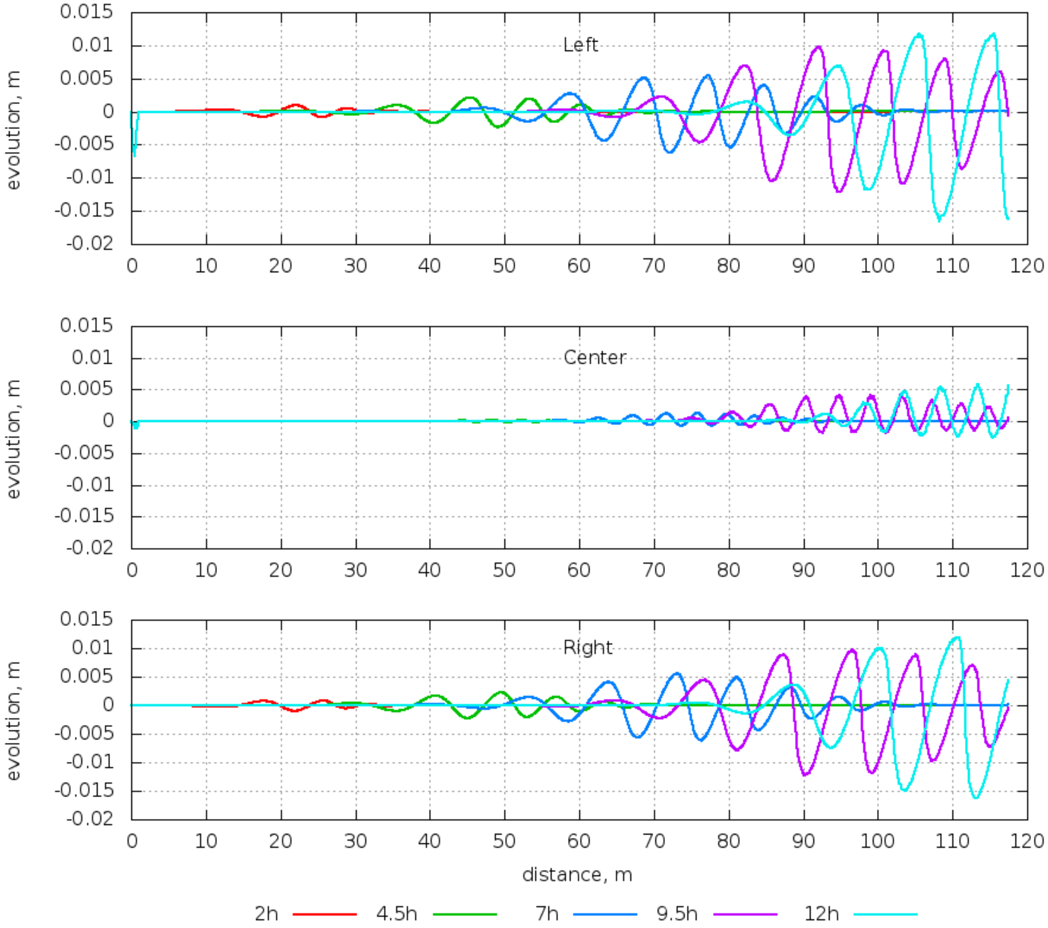

Lanzoni [2000a]
(Table 2, run 1505)
Wavelength = 10.0m
Bar height = 7.7 cm
celerity = 2.8 m/h

Since bars are advected together with the bump, a permanent perturbation is needed

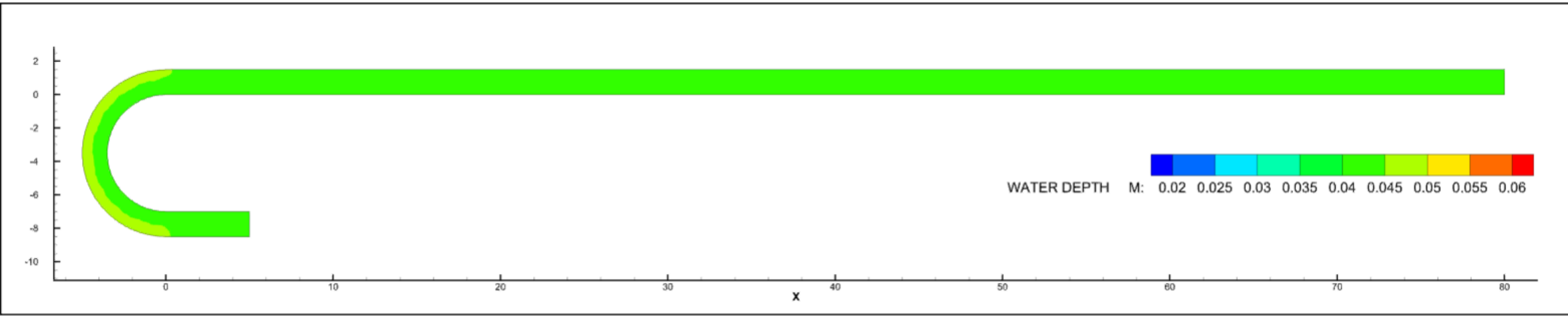

72 HRS SIMULATION

Results

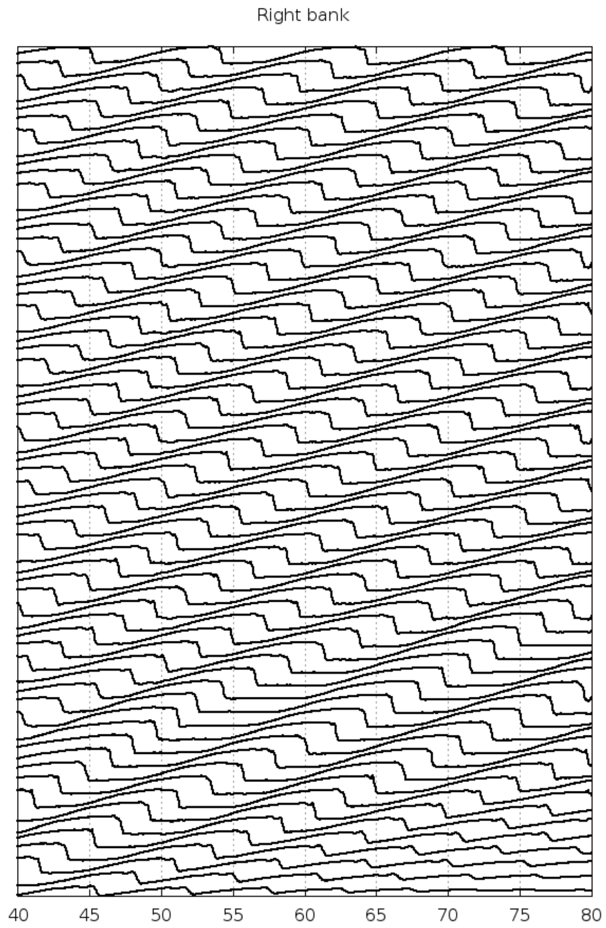

- Evolution of the bed, right bank
- Profiles every 60 min.
- Wavelength 10 m aprox. (Lanzoni measured 10m)
- Celerity 2.2 m/h (Lanzoni measured 2.8 m/h)
- Bar height 8 cm (7.7 from Lanzoni)

Important aspects for bed morphology modeling

- Measurements of sediment transport from field
- Calibrate the sediment equation in order to reproduce measurements

RVR Meander (www.rvrmeander.org)

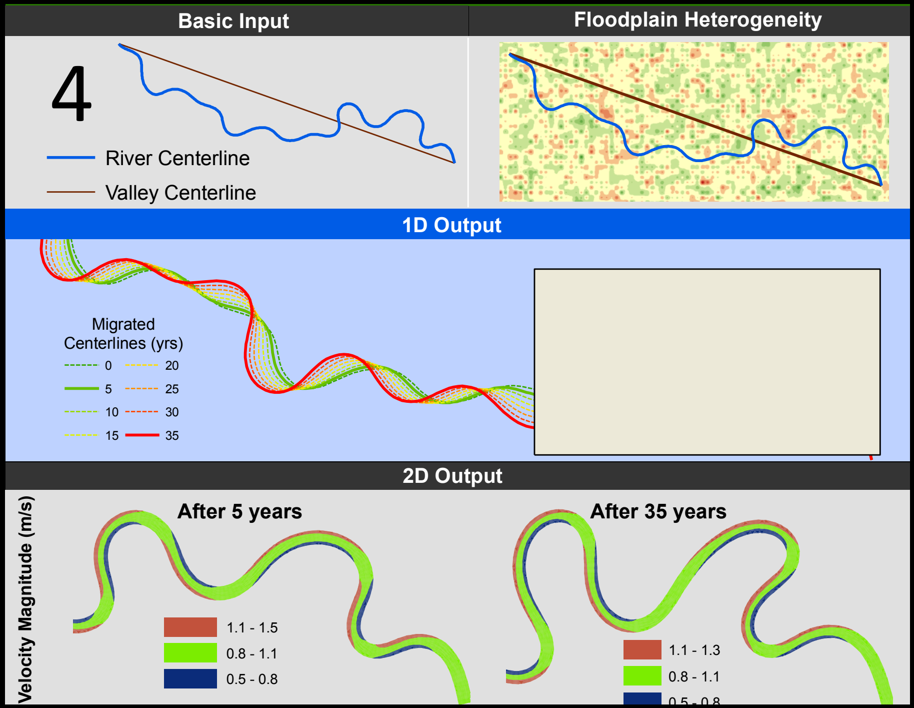

Jorge D. Abad[1], Davide Motta[2], Eddy J. Langendoen[3], Roberto Fernandez[2], Nils O. Oberg[2], Marcelo H. Garcia[2]

[1] Dept. of Civil and Environmental Engineering, University of Pittsburgh

[2] Ven Te Chow Hydrosystems Laboratory, Dept. of Civil and Environmental Engineering, University of Illinois at Urbana-Champaign

[3] USDA-ARS National Sedimentation Laboratory, Oxford, Mississippi

Meandering scales

Somewhere near Detroit

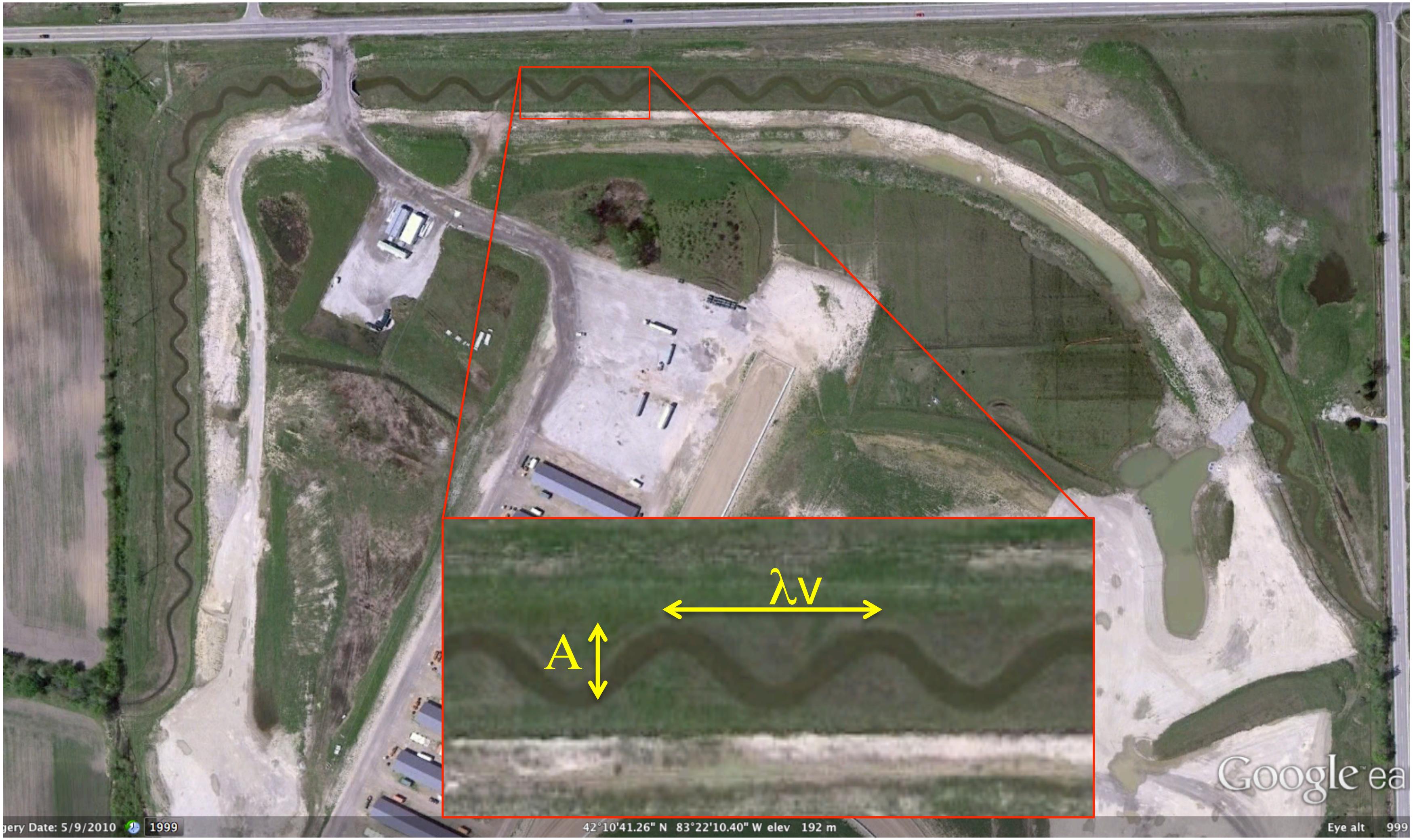

Pictures courtesy
Eddy Langendoen

Meandering scales (λ)

With the ongoing effort in both the United States and Europe to **re-naturalize highly modified streams → more development of GIS Engineering Tools are needed**

Proposed alignments for re-meandering of Trout Creek, Lake Tahoe, California.

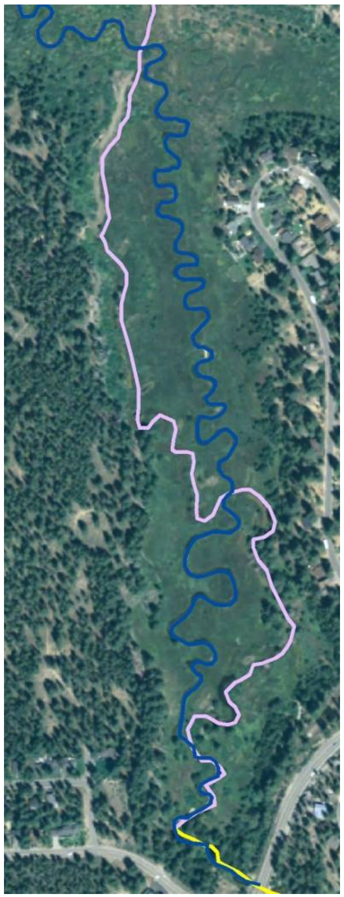

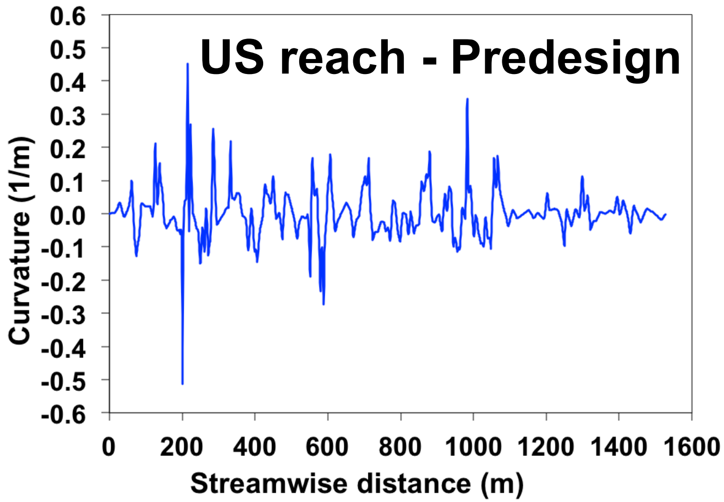

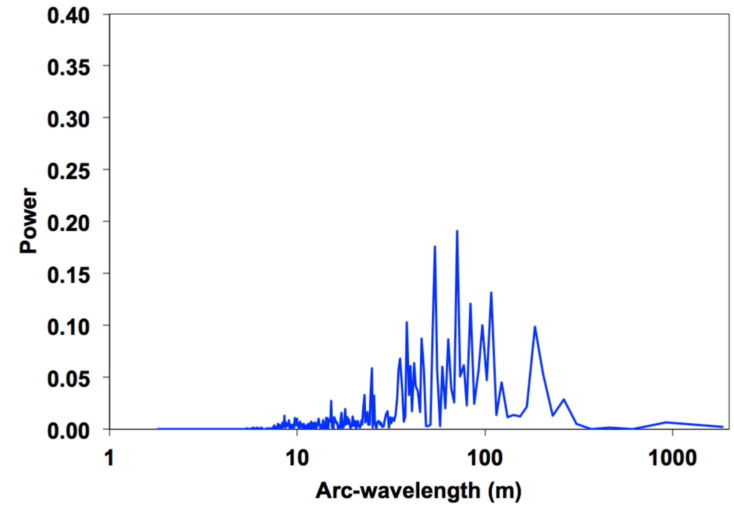

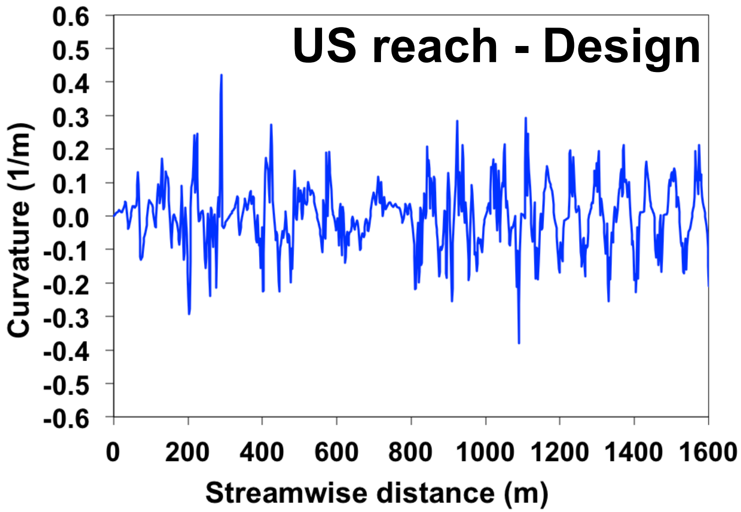

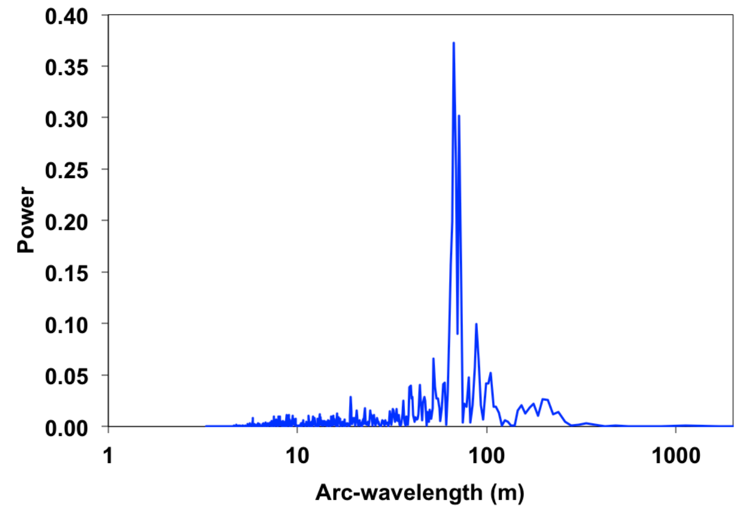

Meandering scales (A)

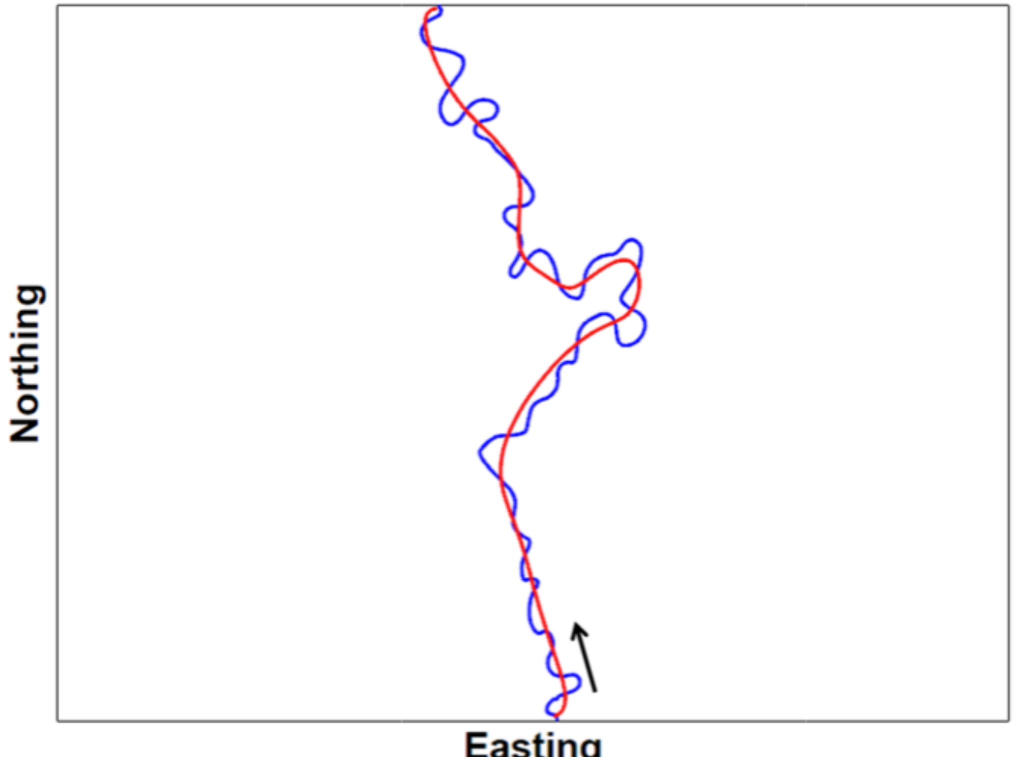

(a) Ucayali–1975–Amplitudes

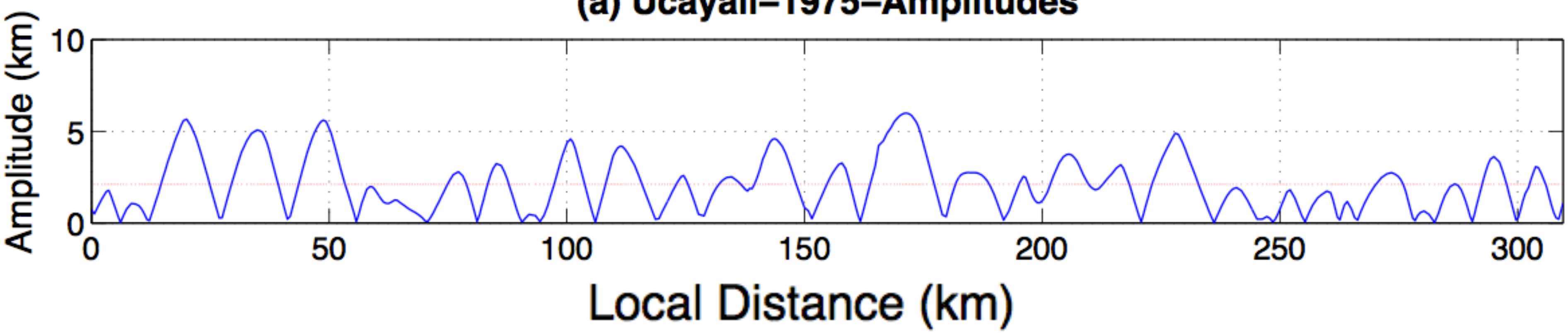

Meandering scales – free?

Near Fargo, ND (Red River)

RVR MEANDER (classical approach)

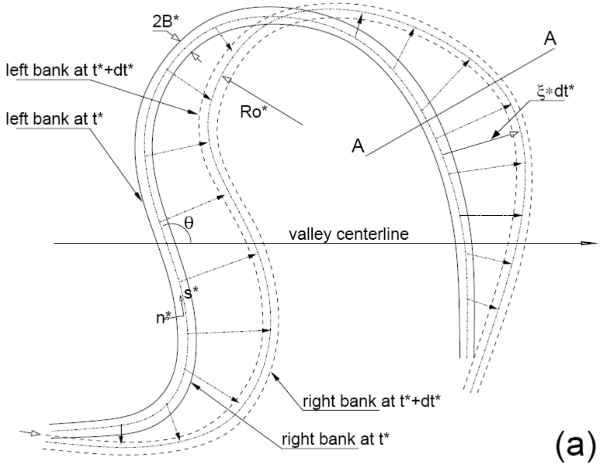

Ikeda et al. (1981)

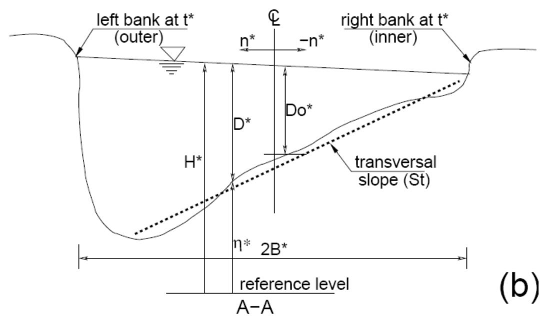

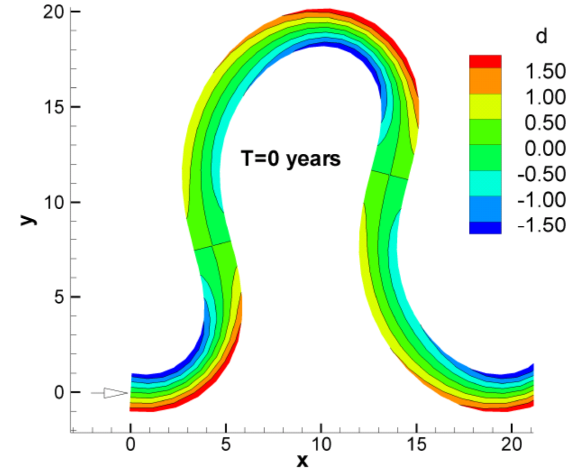

$$\frac{1}{1+n^*C^*}U^*\frac{\partial U^*}{\partial s^*}+V^*\frac{\partial U^*}{\partial n^*}+\frac{C^*}{1+n^*C^*}U^*V^*=-\frac{g}{1+n^*C^*}\frac{\partial H^*}{\partial s^*}-\frac{\tau_s^*}{\rho D^*}$$

$$\frac{1}{1+n^*C^*}U^*\frac{\partial V^*}{\partial s^*}+V^*\frac{\partial V^*}{\partial n^*}-\frac{C^*}{1+n^*C^*}U^{*2}=-g\frac{\partial H^*}{\partial n^*}-\frac{\tau_n^*}{\rho D^*}$$

$$\frac{1}{1+n^*C^*}\frac{\partial (U^*D^*)}{\partial s^*}+\frac{\partial (V^*D^*)}{\partial n^*}+\frac{C^*}{1+n^*C^*}V^*D^*=0$$

$$\frac{\partial \eta^*}{\partial t^*}+\frac{1}{1-\lambda_p}\frac{1}{1+n^*C^*}\left\{\frac{\partial q_s^*}{\partial s^*}+\frac{\partial}{\partial n^*}\left[(1+n^*C^*)q_n^*\right]\right\}=0$$

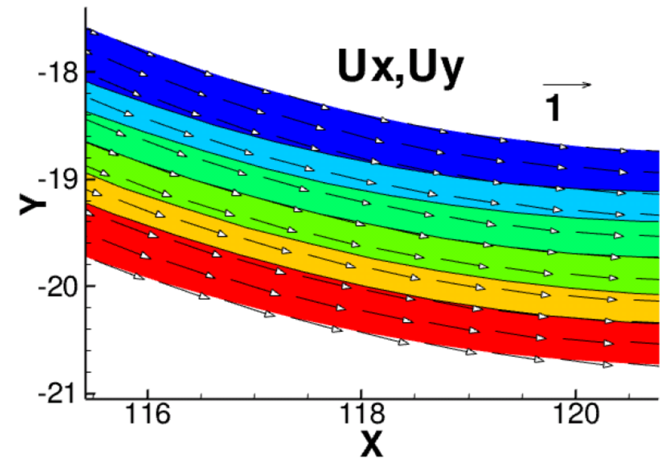

Typical output of linear models

RVR MEANDER (the classical approach)

Classic migration-coefficient method for migration (Ikeda et al. 1981)

$$R^* = E_0 \left(U_b^* - U_{ch}^* \right)$$

The coefficient E_0 is usually obtained via calibration against historic channel centerlines.

Limitations of classic approach based on calibrated migration coefficient:

- it predicts a smooth and "continuous" migration pattern;
- linearity of the expression: it does not explicitly account for local, episodic mass failure mechanisms;
- the formulation does not account for an erosion threshold;
- it does not consider the effect of the bank geometry either;
- it does not consider the impact of the vertical heterogeneity of the bank materials, horizontal could be incorporated changing Eo

Complex planform patterns

Hickin, E. J. (1974). The development of meanders in natural river channels: *American Journal of Science*, 274, 414-442

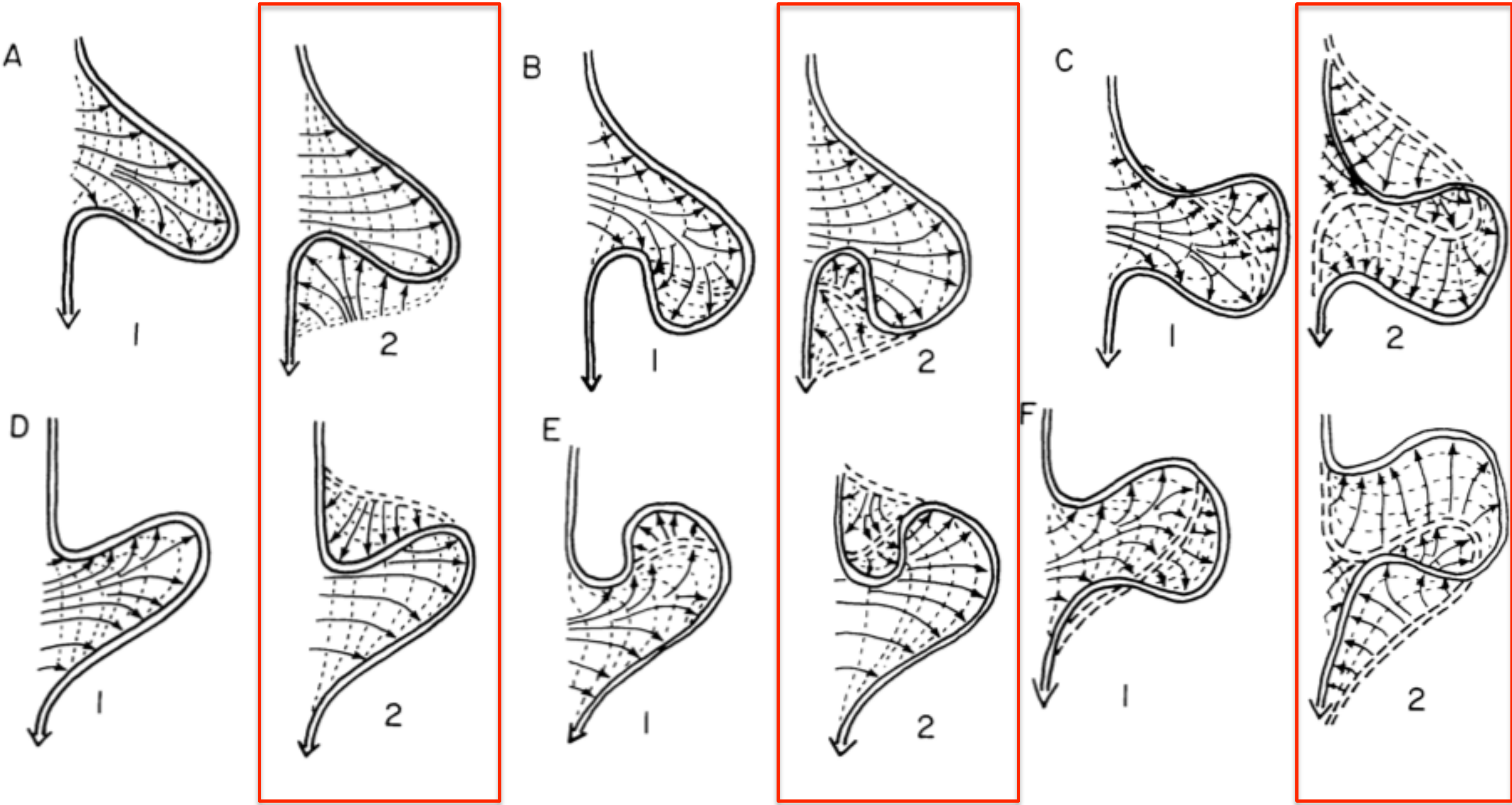

RVR MEANDER (current approach)

The RVR Meander platform merges the functionalities of the first version of MEANDER (Garcia, Bittner, and Nino, 1994) and RVR Meander (Abad and Garcia, 2006) with CONCEPTS (Langendoen and Simon, 2008).

RVR Meander: simplified two-dimensional (2D) hydrodynamic and migration model (Abad and Garcia, 2006), based on migration coefficient approach

CONCEPTS (CONservational Channel Evolution and Pollutant Transport System): one-dimensional (1D) hydrodynamic and morphodynamic model (Langendoen and Alonso, 2008; Langendoen and Simon, 2008; Langendoen *et al.*, 2009)

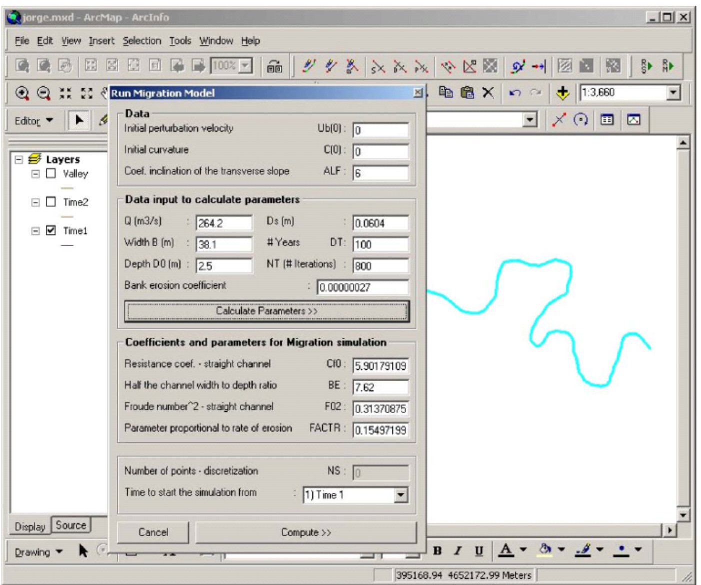

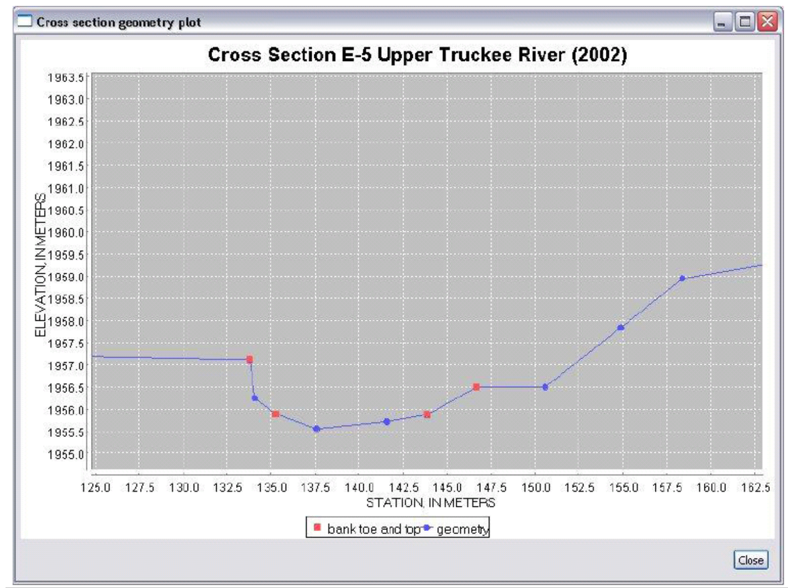

The **new platform**

- ❑ is written in C++ language;
- ❑ is composed of different libraries (preprocessing, hydrodynamics, bank erosion, migration, filtering, plotting, and I/O);
- ❑ stand-alone for Windows and Linux operating systems and interface in ArcGIS-ArcMap.

RVR MEANDER (current approach)

Ikeda et al. (1981)

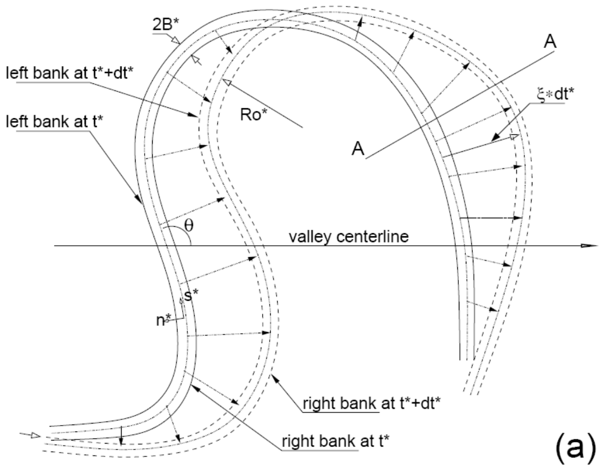

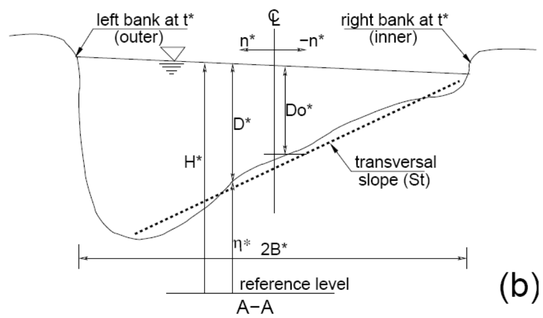

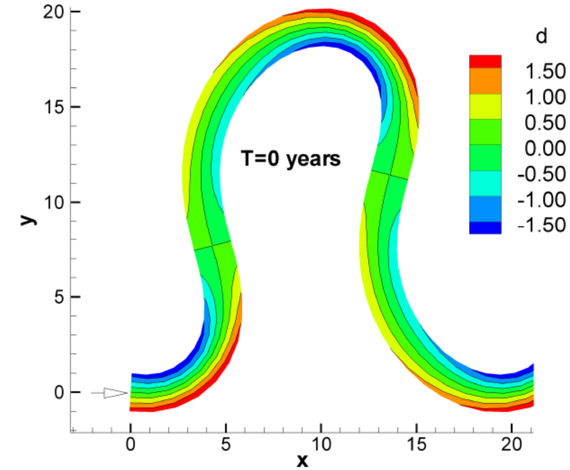

$$\frac{1}{1+n^*C^*}U^*\frac{\partial U^*}{\partial s^*}+V^*\frac{\partial U^*}{\partial n^*}+\frac{C^*}{1+n^*C^*}U^*V^*=-\frac{g}{1+n^*C^*}\frac{\partial H^*}{\partial s^*}-\frac{\tau_s^*}{\rho D^*}$$

$$\frac{1}{1+n^*C^*}U^*\frac{\partial V^*}{\partial s^*}+V^*\frac{\partial V^*}{\partial n^*}-\frac{C^*}{1+n^*C^*}U^{*2}=-g\frac{\partial H^*}{\partial n^*}-\frac{\tau_n^*}{\rho D^*}$$

$$\frac{1}{1+n^*C^*}\frac{\partial (U^*D^*)}{\partial s^*}+\frac{\partial (V^*D^*)}{\partial n^*}+\frac{C^*}{1+n^*C^*}V^*D^*=0$$

$$\frac{\partial \eta^*}{\partial t^*}+\frac{1}{1-\lambda_p}\frac{1}{1+n^*C^*}\left\{\frac{\partial q_s^*}{\partial s^*}+\frac{\partial}{\partial n^*}\left[(1+n^*C^*)q_n^*\right]\right\}=0$$

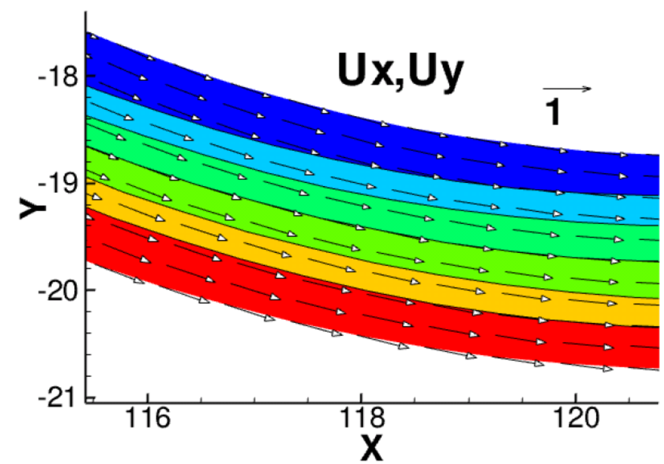

Typical output of linear models

RVR MEANDER (current approach)

Bank erosion

The **hydraulic (fluvial) erosion rate** E^*, in the horizontal direction, is modeled using an **excess shear stress relation**, typical of cohesive material.

Shear stress acting on bank

$$E^* = M^* \frac{(\tau^* - \tau_c^*)}{\tau_c^*}$$

Hydraulic erosion rate

Erosion-rate coefficient

Critical shear stress

Uncertainties on

- ❑ Stress acting on the bank τ^* (from modeling)
- ❑ Critical shear stress τ^*_c (from field)
- ❑ Erosion-rate coefficient M^* (from field)

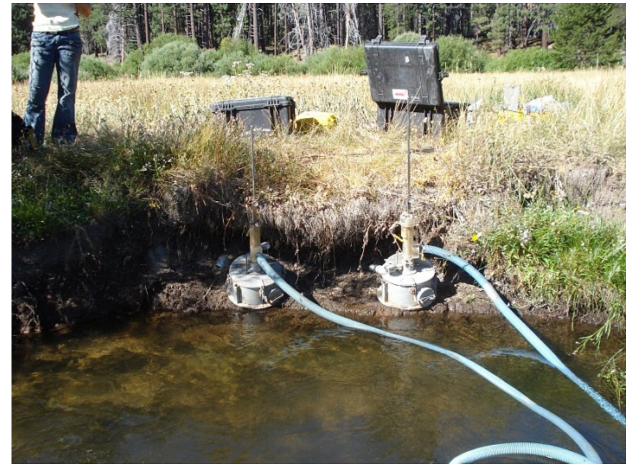

Jet Test for in situ measure of erosion-rate coefficient and critical shear stress.

Cohesive Strength Meter for in situ measure of critical shear stress.

RVR MEANDER (current approach)

Bank materials composed of **fine-grained cohesive sediments.**
Bank erosion: combination of **fluvial shear erosion** and **gravitational mass failure processes**.

Depending on shape of bank profile and physical properties of the bank materials, any one of the following mass failure mechanisms might be observed

- planar
- rotational
- cantilever
- piping or sapping

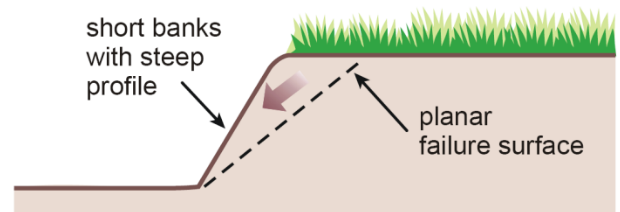

Planar failure

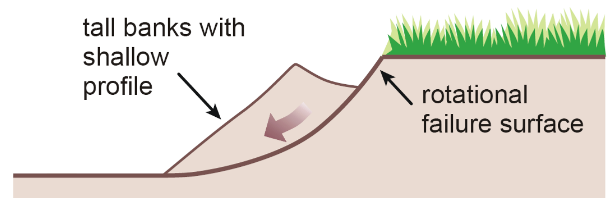

Rotational failure

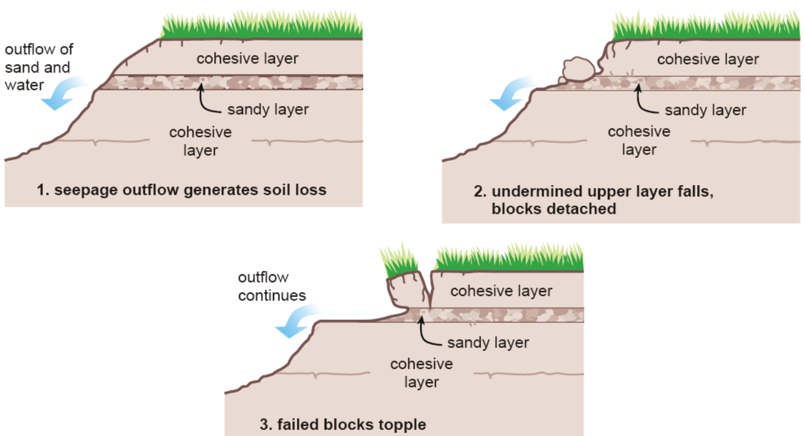

Piping

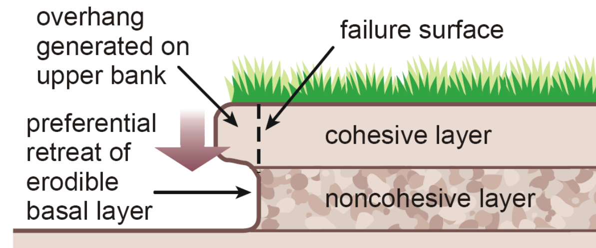

Cantilever failure

Pictures courtesy
Eddy Langendoen

[1] RVR MEANDER: MC vs PB

Motta, D., Abad, J.D, Langendoen, E.J., Garcia, M.H., 2011. *A simplified 2D model for meander migration with physically-based bank evolution*. Geomorphology

Reach of the Mackinaw River in Illinois located in Tazewell County about 15 kilometers upstream of the junction of the Mackinaw River with the Illinois River.

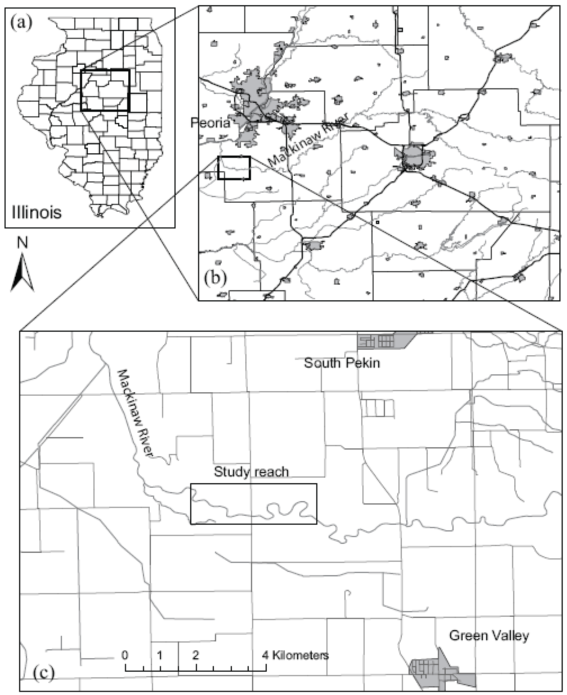

Mackinaw River study reach.

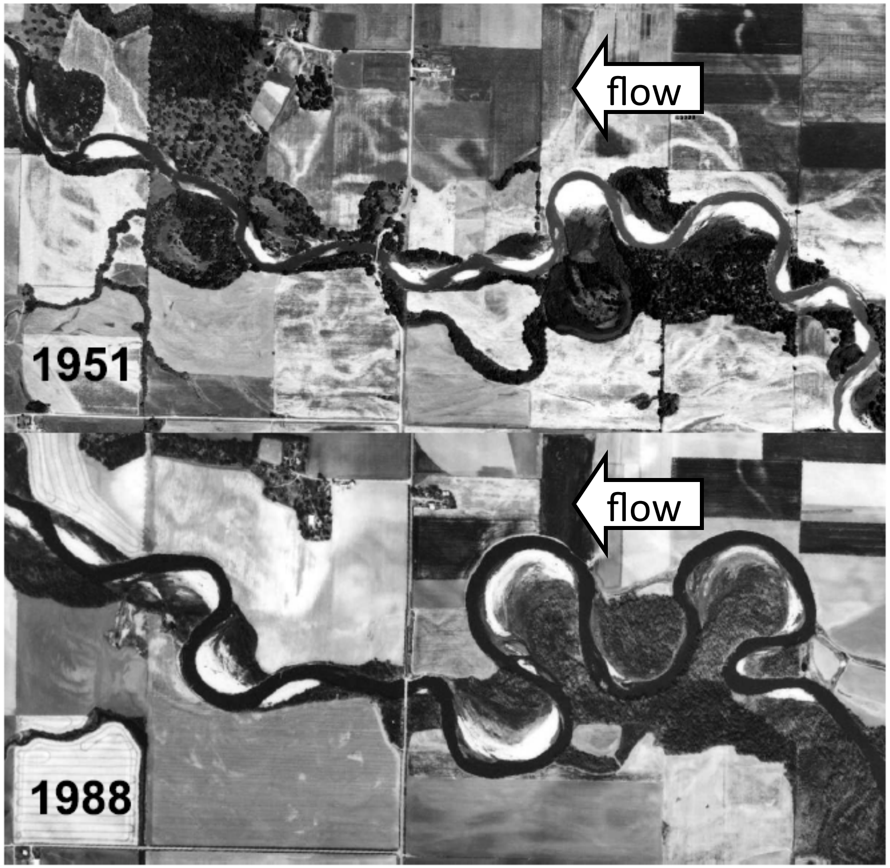

Aerial pictures of the Mackinaw River in the years 1951 and 1988.

[1] RVR MEANDER: MC vs PB

Test for natural river

The proposed approach showed significant improvements over the classic approach in predicting the observed migration in the period 1951-1988, both in terms of

- ❑ **shapes**
- ❑ **prediction error**

❑ **Compound loops are captured by PB**

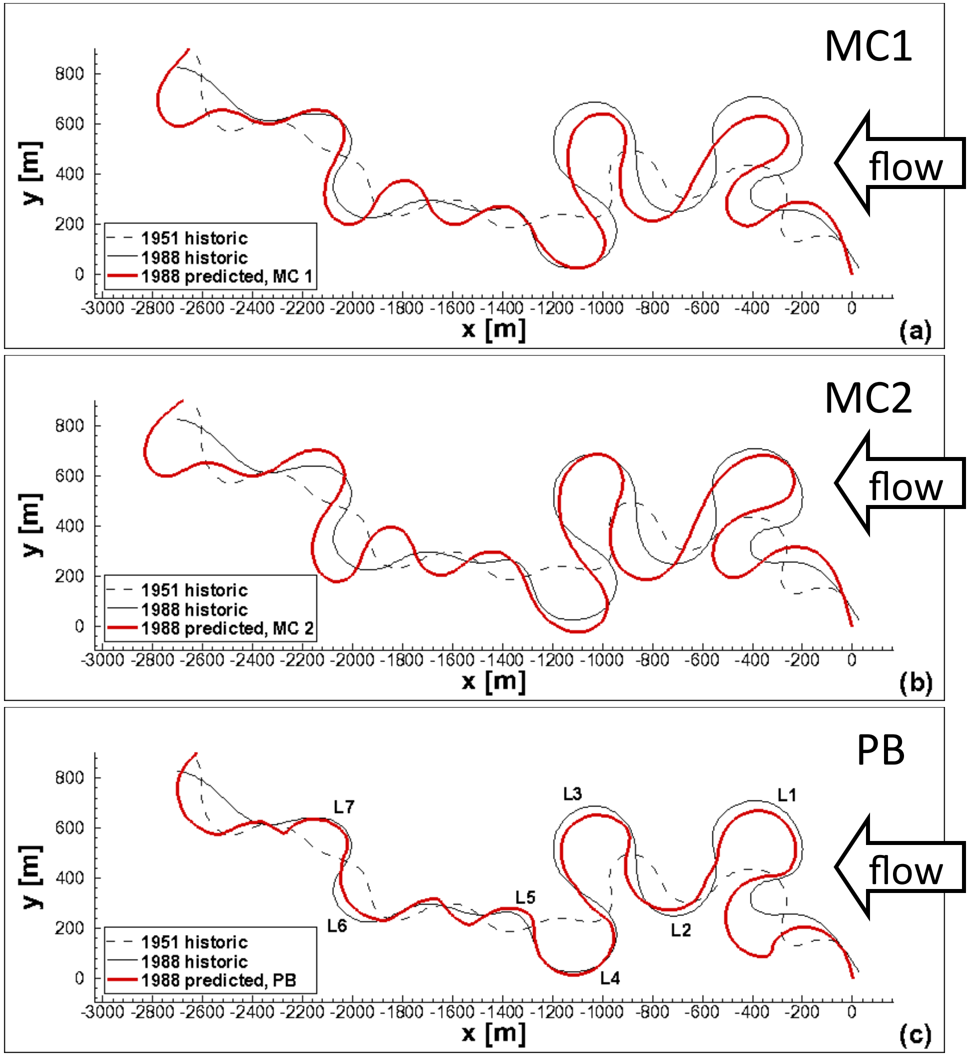

Mackinaw River study reach: historic and predicted centerlines in 1988. Flow is from right to left (Motta et al., 2011).

[2] HORIZONTAL HETEROGENEITY

Motta, D., Abad, J.D, Langendoen, E.J., Garcia, M.H., 2012. The effects of floodplain heterogeneity on meander planform shapes. Water Resources Research

Single realization **All realizations**

$$E^* = M^* \frac{(\tau^* - \tau_c^*)}{\tau_c^*}$$

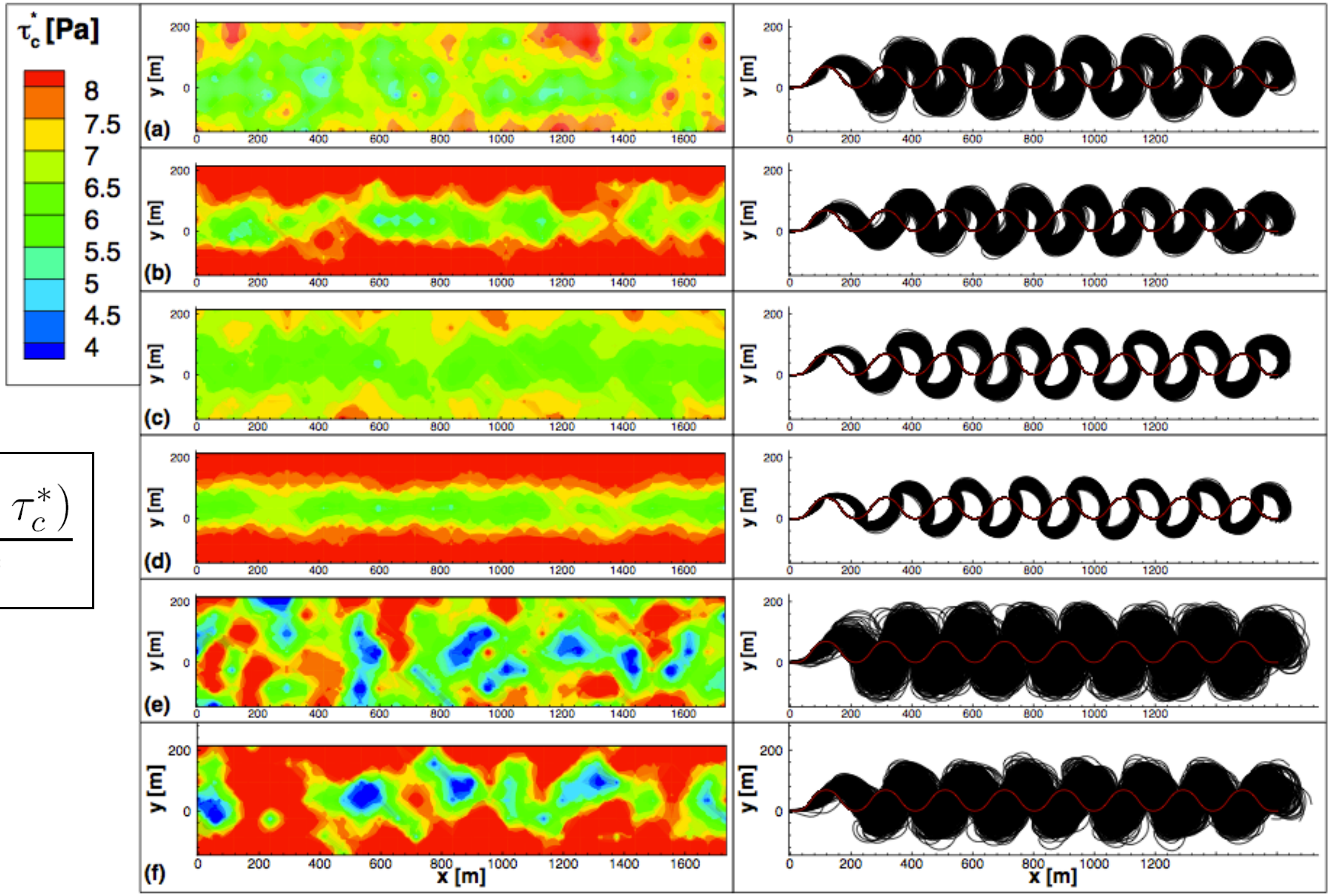

[2] HORIZONTAL HETEROGENEITY

Motta, D., Abad, J.D, Langendoen, E.J., Garcia, M.H., 2012. The effects of floodplain heterogeneity on meander planform shapes. Water Resources Research

Single realization **All realizations**

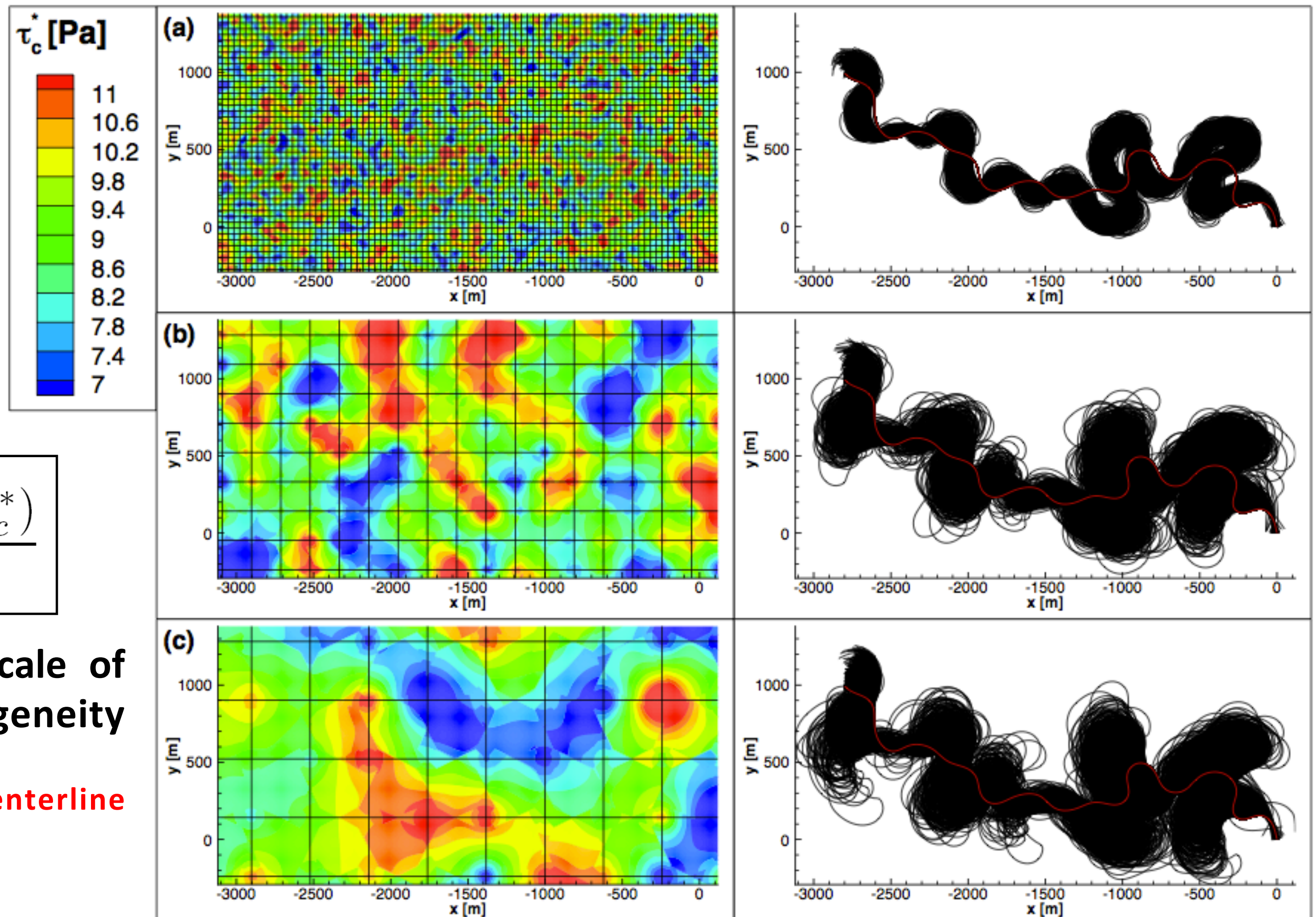

$$E^* = M^* \frac{(\tau^* - \tau_c^*)}{\tau_c^*}$$

Effects of length scale of floodplain heterogeneity

→ the larger the scale

→ more migrated centerline variability

[2] HORIZONTAL HETEROGENEITY

Motta, D., Abad, J.D, Langendoen, E.J., Garcia, M.H., 2012. The effects of floodplain heterogeneity on meander planform shapes. Water Resources Research

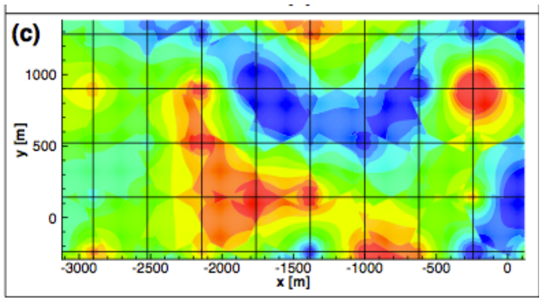

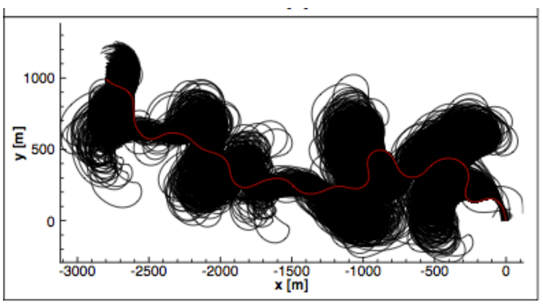

High-frequency meander bends are starting to appear

Single realization **Single realization**

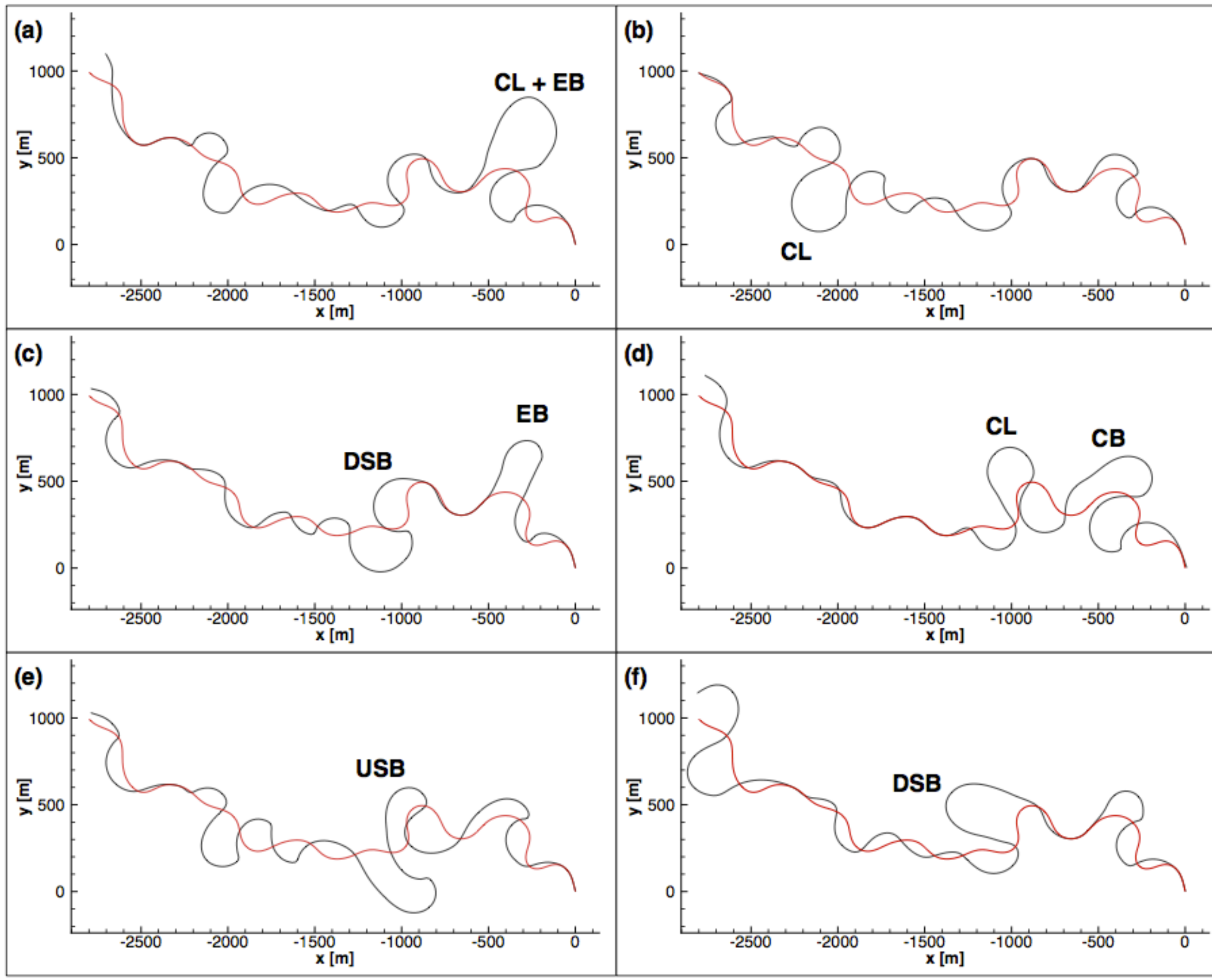

[3] VERTICAL HETEROGENEITY

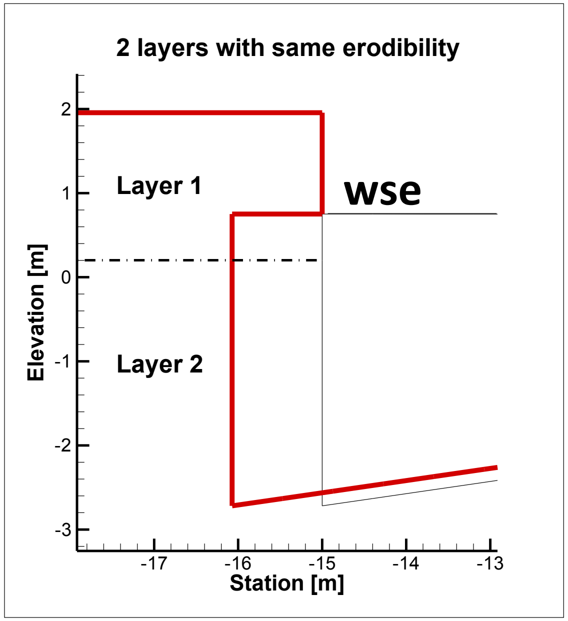

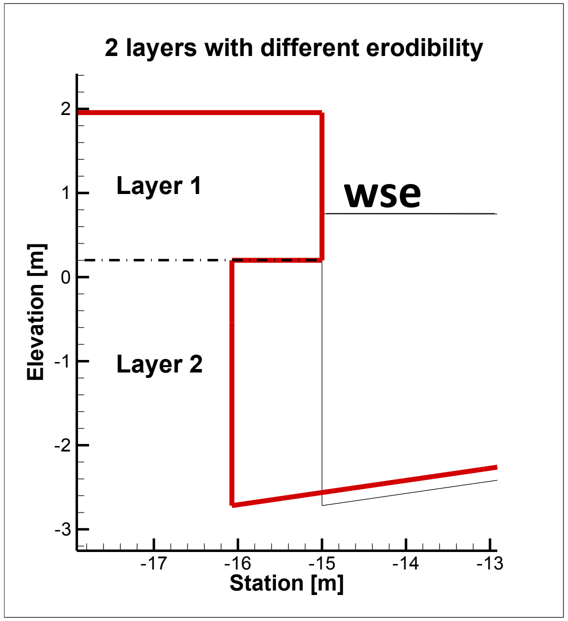

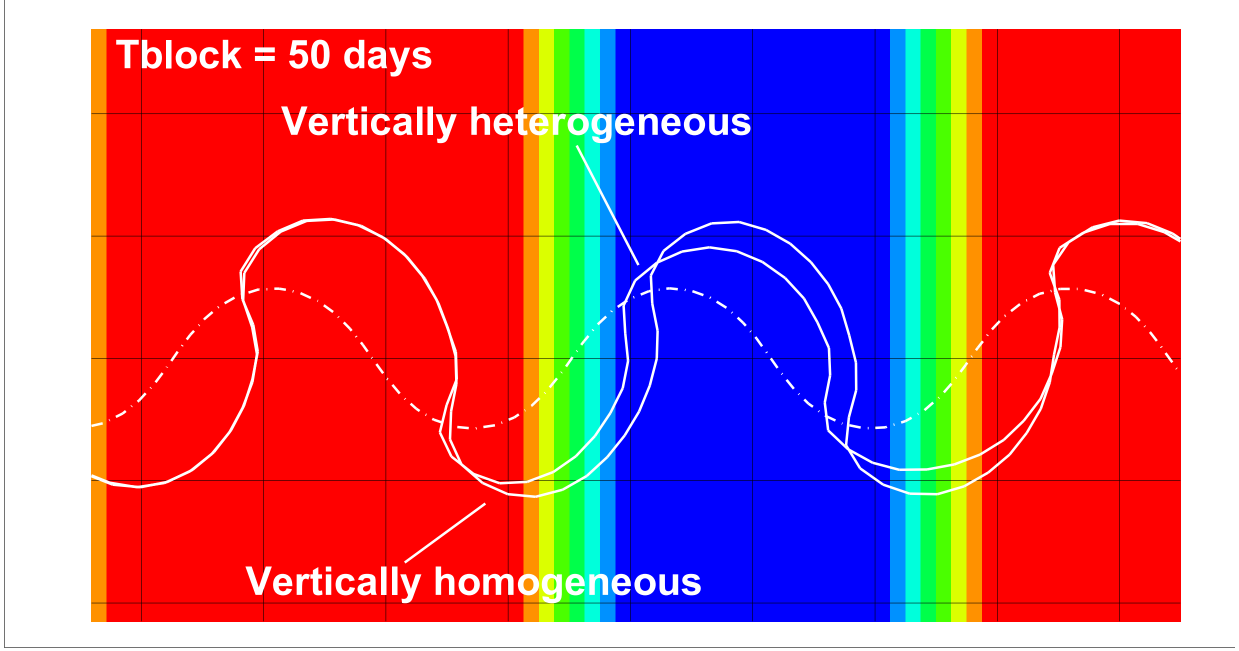

Area of vertical heterogeneity for erodibility

Vertical heterogeneity affects cantilever failure volumes and therefore migration

Homogeneous migrates at higher rates

[3] VERTICAL HETEROGENEITY

Mackinaw River

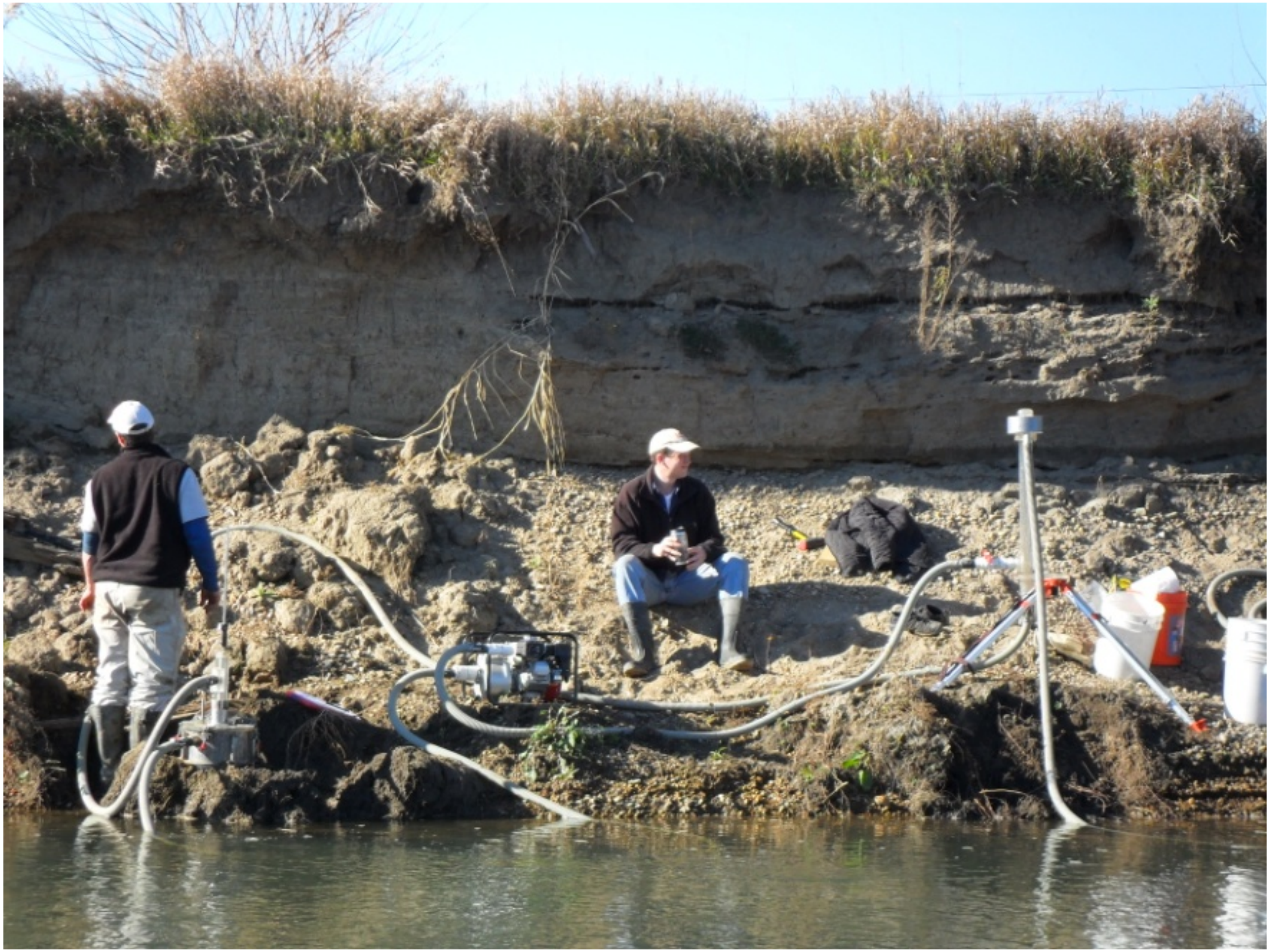

[3] VERTICAL HETEROGENEITY

Motta, D., Abad, J.D, Langendoen, E.J., Garcia, M.H., 2012. Vertical heterogeneity of the floodplain. Journal of Geophysical Research – Earth Surface (in review)

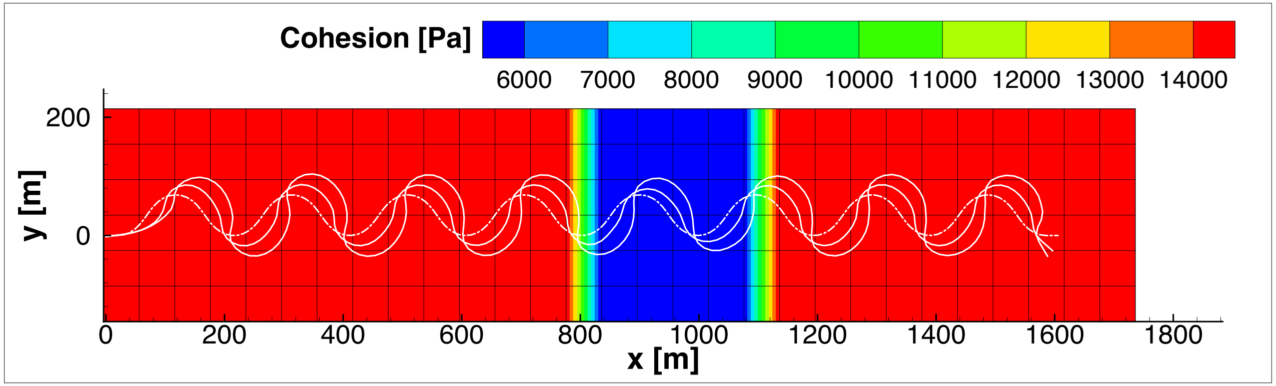

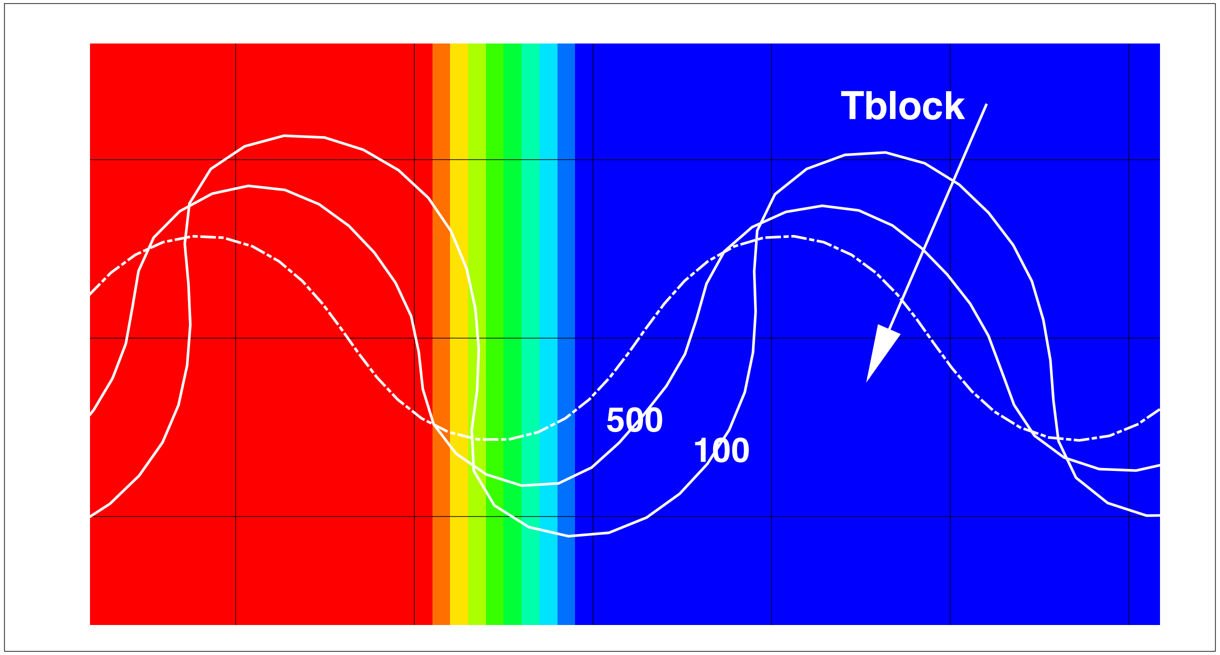

[3] VERTICAL HETEROGENEITY

Motta, D., Abad, J.D, Langendoen, E.J., Garcia, M.H., 2012. Vertical heterogeneity of the floodplain. Journal of Geophysical Research – Earth Surface (in review)

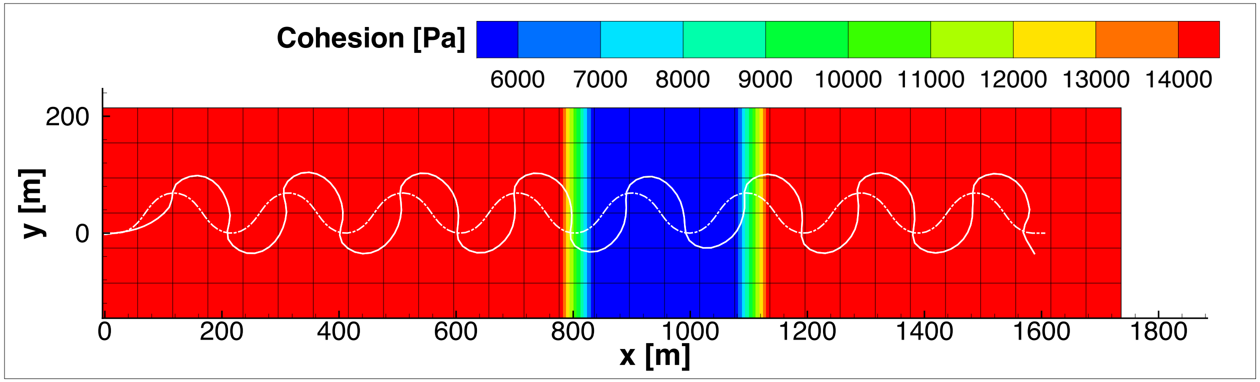

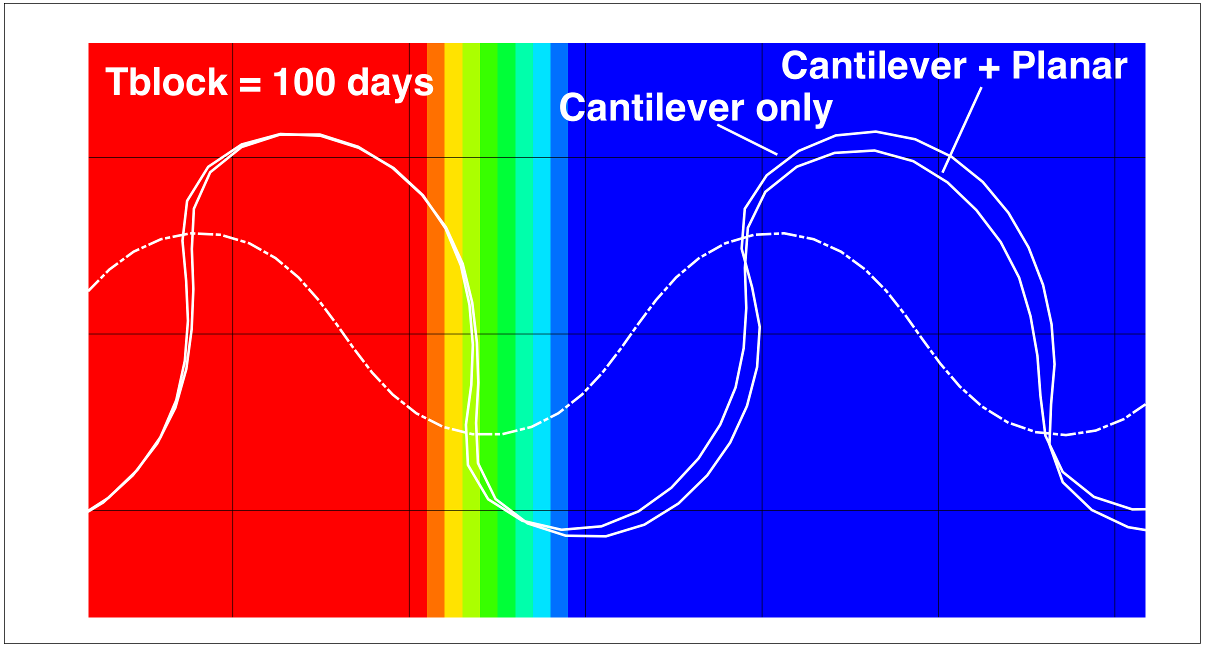

www.rvrmeander.org

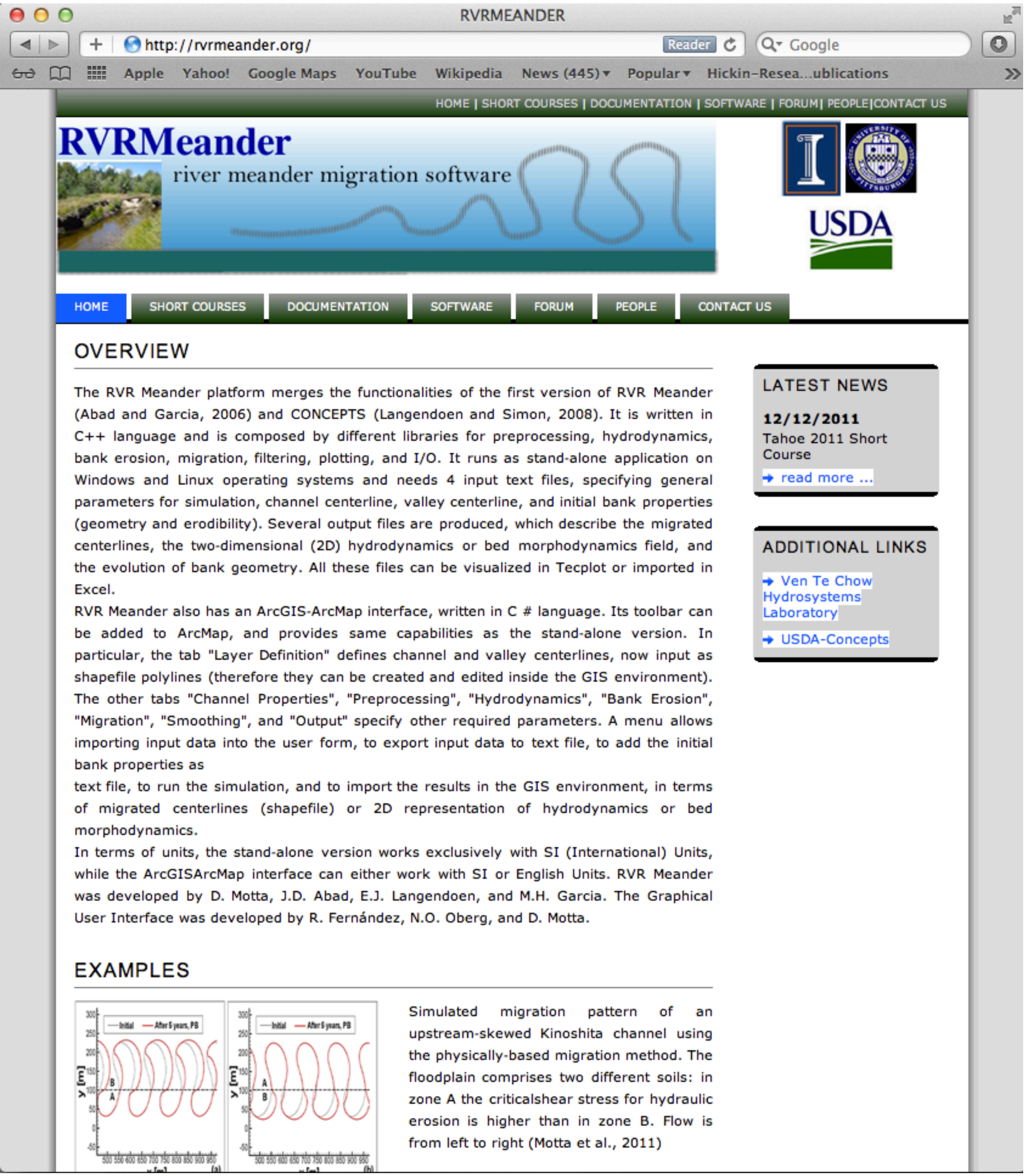

SHORT COURSES

- ❑ River Coastal and Estuarine Morphodynamics, RCEM 2009, Santa Fe, ARGENTINA
- ❑ National University of Engineering, National Congress 2010, Lima, Cusco, PERU
- ❑ River Coastal and Estuarine Morphodynamics, RCEM 2011, Tsinghua University, Beijing, CHINA
- ❑ USDA-FOREST – LAKE TAHOE, Dec 2011, Nevada.
- ❑ UNAM-Mexico, January 2013

www.rvrmeander.org

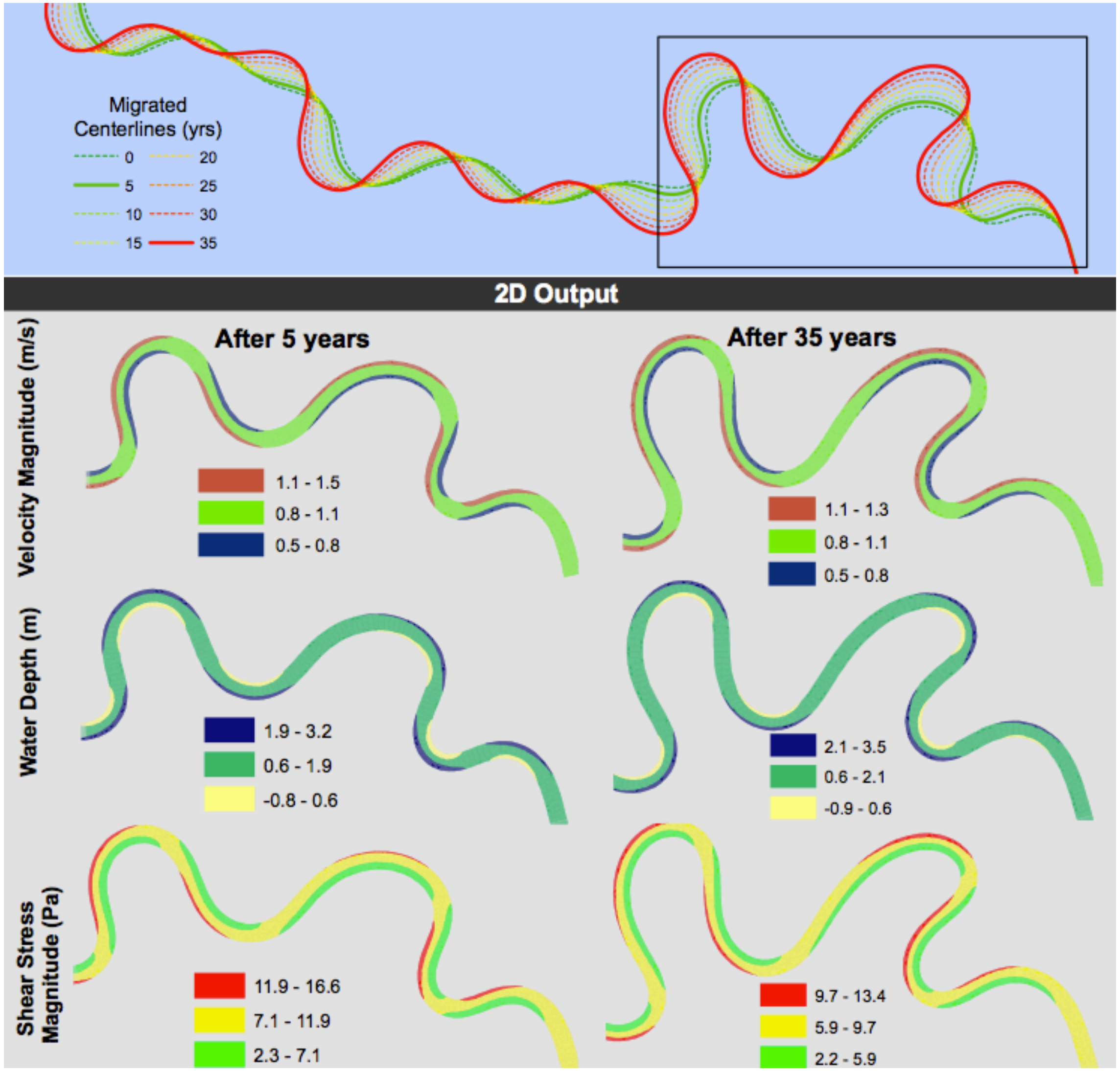

THANKS

RVR MEANDER

Hydrodynamics and bed morphodynamics (contd.)

Linearization

Reach-averaged values — Perturbations

$$(U^*(s^*,n^*), V^*(s^*,n^*), D^*(s^*,n^*)) = (U^*_{ch}, 0, D^*_{ch}) + (U^*_1(s^*,n^*), V^*_1(s^*,n^*), D^*_1(s^*,n^*))$$

$$(\tau^*_s(s^*,n^*), \tau^*_n(s^*,n^*)) = (\tau^*_{s,ch}, 0) + (\tau^*_{s,1}(s^*,n^*), \tau^*_{n,1}(s^*,n^*))$$

$$C^*(s^*) = 0 + C^*_1(s^*)$$

$$C_f(s^*,n^*) = C_{f,ch} + C_{f,1}(s^*,n^*)$$

Dimensionless perturbations of velocity in the streamwise and transverse direction and water depth

$$U_1(s,n) = a'_1(n)e^{-a'_2 s} + n\left(a'_3 C(s) + a'_4 e^{-a'_2 s}\int_0^s C(s)e^{a'_2 s}ds\right)$$

Dimensionless streamwise velocity perturbation

$$V_1(s,n) = \frac{a'_2}{2}e^{-a'_2 s}\left(2\int_1^n U_1(0,n)dn - nU_1(0,n) + U_1(0,1)\right) + \\ + \frac{a'_2}{2}\left(nU_1(s,n) - U_1(s,1)\right) + \frac{a'_5}{2}\left(n^2-1\right)$$

Dimensionless transverse velocity perturbation

$$D_1(s,n) = C(s)n\left(F^2_{ch} + A\right)$$

Dimensionless depth perturbation

Important parameters:

- Sinuosity
- Half width-to-depth ratio
- Froude number
- Friction coefficient

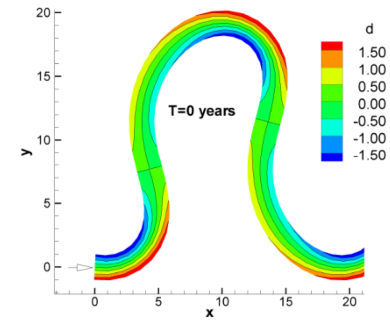

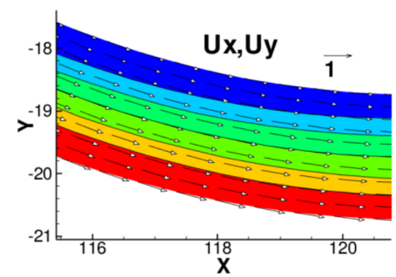

RVR MEANDER

Bank erosion (contd.)

The **cantilever failure** is associated to **overhanging slumps** of mass generated by preferential retreat of highly erodible layers or simply by the erosion of the bank below the water level with respect to its dry portion.

The occurrence of cantilever failure is determined from geometrical considerations, once an **undercut threshold** is exceeded.

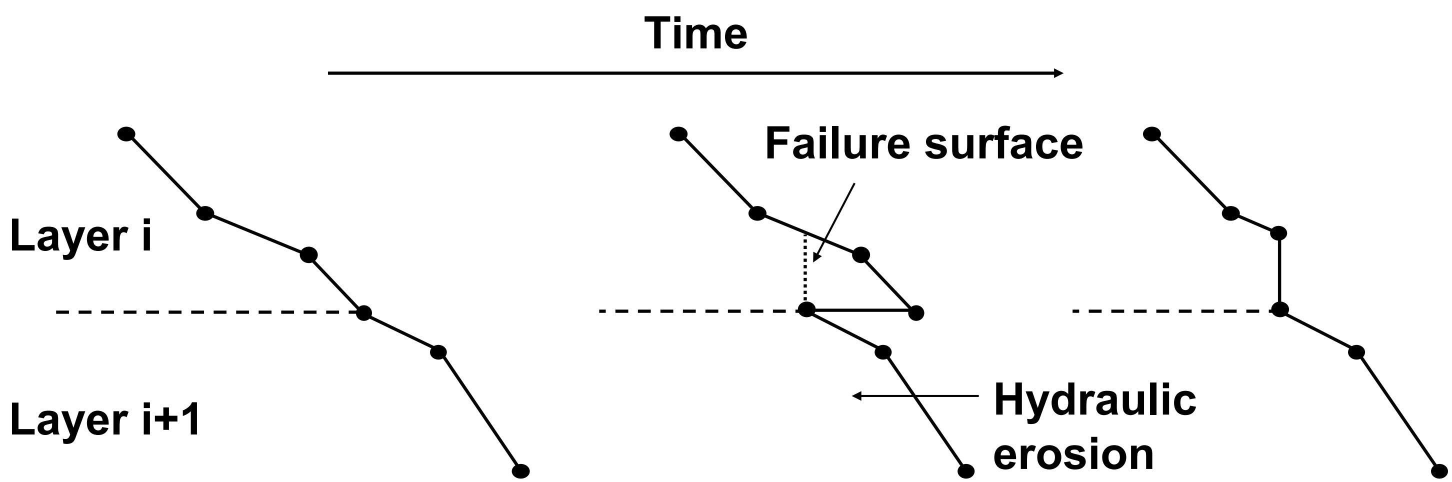

Sketch of cantilever failure.

Bank processes

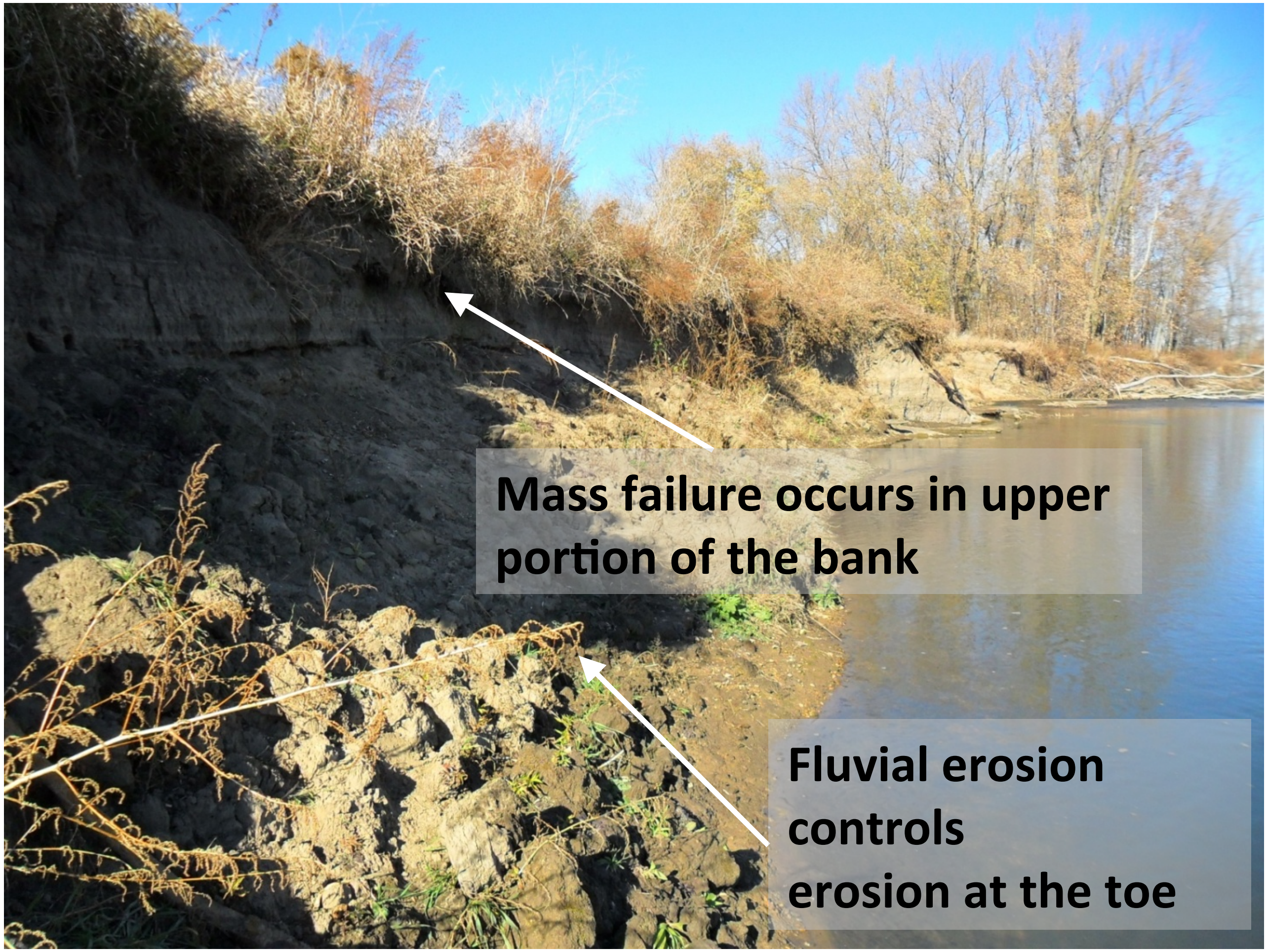

➡ Medium to long-term bank retreat rates are controlled by the process of fluvial erosion at the toe

Bank processes

Bank armoring

➡ Mass failure mechanisms may impact migration rates and shapes through bank toe protection

➡ River scale may affect residence time of slump blocks

Increasing river scale

Bank processes

Bank layering

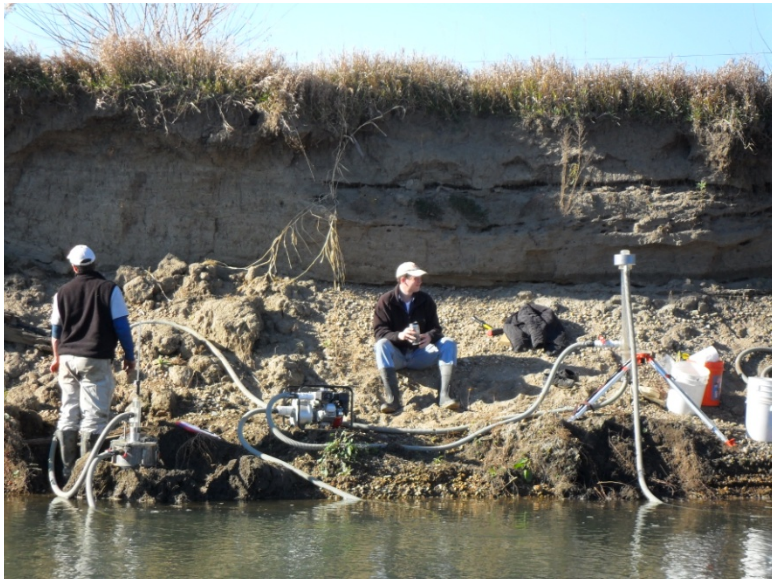

Layering impacts mass failure volumes

⇩

Impacts bank protection

⇩

Impacts migration rates and shapes

➡ Vertical heterogeneity in the floodplain may impact migration rates and shapes